Photophysical Studies of Photon Upconversion via Triplet-Triplet Annihilation in Polymer Systems with Potential Photovoltaic Applications

A Thesis Submitted to the College of

Graduate Studies in Research

in Partial Fulfillment of the Requirements

for the Degree of Master of Science

in the Department of Chemistry

University of Saskatchewan

Saskatoon

By

Philip C. Boutin

Permission to Use

In presenting this thesis in partial fulfilment of the requirements for a Postgraduate degree from the University of Saskatchewan, I agree that the Libraries of this University may make it freely available for inspection. I further agree that permissions for copying this thesis in any manner, in whole or in part, for scholarly purposes may be granted by Professors Timothy L. Kelly and Ronald P. Steer who supervised my thesis work or, in their absence, by the Head of the Department of Chemistry or the Dean of the College of Graduate Studies and Research at the University of Saskatchewan. It is understood that any copying or publication or use of this thesis or parts thereof for financial gain shall not be allowed without my written permission. It is also understood that due recognition shall be given to me and to the University of Saskatchewan in any scholarly use which may be made of any material in my thesis.

Requests for permission to copy or make other use of material in this thesis in whole or part should be addressed to:

The Head
Department of Chemistry
University of Saskatchewan
Saskatoon, Saskatchewan S7N 5C9
Canada

Abstract

The present work reports the study of noncoherent photon upconversion (NCPU) via triplet-triplet annihilation (TTA) in polymer systems. This upconversion mechanism has application in photovoltaic devices through the utilization of sub-band gap photons for potentially enhanced power conversion efficiencies.

First, homomolecular TTA was studied in zinc tetraphenylporphyrin (ZnTPP) in polymer matrices. Here, ZnTPP acts as both the sensitizer and upconverting emitter as TTA yields an S_2 excited porphyrin. Use of poly(methyl methacrylate) (PMMA) as the host polymer demonstrates aggregation-driven upconverted fluorescence (UC) by TTA (TTA-UC). The dye-loading ratio of the precursor solution was varied, controlling the degree of pre-aggregation. Power-dependence studies of the champion film demonstrated that TTA-UC is occurring toward the strong annihilation kinetic limit. A sub-linear dependence of upconverted fluorescence on film thickness was observed in this system.

The ZnTPP study was extended to polymers possessing low glass transition temperatures, representing molecular diffusion-driven TTA-UC. Upconverted fluorescence was not observed in ZnTPP in a polyurethane (PU) matrix, likely due to coordination of the PU to the axial position of the Zn^{2+} ion. Low intensity NCPU via homomolecular TTA was observed in ZnTPP in a poly(ethylene glycol) (PEG) matrix, but the kinetic limit was not determined due to film photodegradation. Dye-loading studies revealed that porphyrin self-quenching was evident at low dye concentrations. Likely reasons for the low upconverted fluorescence intensities realized are this self-quenching and the possibility of

PEG coordination to the Zn^{2+} ion, though it is believed self-quenching is the dominant parasitic effect. Strategies to determine the effect and extent of polymer coordination to the Zn^{2+} ion are discussed.

The study of polymer-based NCPU is extended to a pair of macromolecules, each containing a single ruthenium tris(bipyridine) ($Ru(bpy)_3$) core and multiple pendant arms, which in turn, each contain eight 9,10-diphenylanthracene (DPA) moieties. A power-dependence study of NCPU in this system is reported, and TTA-UC in the weak annihilation kinetic limit was observed. Upconverted fluorescence quantum yields vary linearly with excitation power in both polymers, consistent with the observed kinetic limit. Stern-Volmer experiments have compared the quenching of $Ru(dmb)_3$ phosphorescence (Ph) by monomeric and polymeric DPA. These data show an enhancement in quenching rate constant for the DPA polymer (pDPA). Kinetic analysis of the Ru-DPA polymers has revealed that the energy scheme realized in this system is intrachain TTET from $Ru(bpy)_3$ core to DPA emitter followed by interchain TTA between excited DPA moieties. Low intensity upconverted fluorescence is observed in Ru-DPA containing thin films. Based on the results presented, the requirements of future photophysically-active polymers are discussed with regards to meaningful application in photovoltaics.

Acknowledgements

First and foremost, I wish to thank my supervisors, Drs. Ronald P. Steer and Timothy L. Kelly, for both your academic and your emotional support. I am extremely grateful for your guidance and your patience. I can genuinely say that I am proud of what I have accomplished under your leadership.

Thank you to Dr. K. P. Ghiggino for sending the materials used in Chapter 4 and for collaboration on that work. Without these materials, one can only speculate where my research would have drifted.

I wish to thank various support staff and Kelly/Steer/Paige group members for their assistance with experiments and training: Ted Toporowski & Blair Chomyshen; Dr. Keith Brown; Chelsea Greenwald; Nick Randell; Dr. Sunish Sugunan; Dr. Neeraj Giri; Conie Ponce; Brook Danger. I am also grateful for the thoughtful office discussions I have had with Mahesh Gangishetty, Nick Randell, Kianoosh Poorkazem, and Anindya Ganguly.

I thank my family for encouraging me in my pursuit of happiness. You don't always understand why I am doing what I am doing, but I always feel your support. I appreciate that most of you pretended my lab was exciting.

Finally, I sincerely thank the wonderful Chelsea Greenwald. You have been my pillar of strength through the highs and lows of my research, and believed in me when I did not. For this, I am tremendously grateful.

Contents

Permission to Use i

Abstract ii

Acknowledgements iv

List of Tables viii

List of Figures ix

List of Abbreviations xii

1 Introduction to Triplet-Triplet Annihilation 1

1.1 Energy Limitations in Photoactive Materials 1

1.2 Photophysical Processes 4

1.2.1 Jablonski Diagrams 4

1.2.2 Photoluminescence Quenching 6

1.2.3 Electronic Energy Transfer 8

1.3 Upconverted Fluorescence by Triplet-Triplet Annihilation 12

1.3.1 Fundamental Mechanisms 12

1.3.2 Excitation Power Dependence 15

1.3.3 Spin-Statistics of TTA 16

1.4 Applications of TTA-UC 18

1.5 Material Selection for TTA-UC 21

1.6 Objectives 25

2 Experimental Techniques and Instrumentation 26

2.1 Summary of Equipment Used 26

2.2 Detailed Setup and Implementation of SPEX Fluorolog Spectrofluorometer 27

3 Spectroscopic Studies of ZnTPP in Polymer Matrices 34

3.1 Introduction to ZnTPP-doped Polymer Systems 34

3.2 Solution-Phase and Thin Film ZnTPP 37

3.3 ZnTPP-doped Thermoplastic Polyurethane Films 39

3.4 ZnTPP-doped Poly(methyl methacrylate) Films 41

3.5 ZnTPP-doped Poly(ethylene glycol) Films 48

3.6 Summary and Future Direction 51

4 Spectroscopic and Photophysical Studies of Ru-DPA Polymers 54

4.1 Introduction to Ru-DPA Polymer System 54

4.2 Steady-State Spectroscopy of the $Ru(bpy)_3$-DPA Polymers 58

4.3 Quenching of $Ru(dmb)_3$ Phosphorescence by DPA 61

4.4 Nature of Energy Transfer Processes 65

4.5 Photoluminescence Quantum Yields 67

4.6 Upconverted Fluorescence in Thin Films 71

4.7 Summary and Future Direction 73

5 Overall Summary and Future Work 76

5.1 Overall Scope 76

5.2 ZnTPP-doped Polymer Films 76

5.3 Ru- DPA-containing Polymers 78

5.4 Future Outlook 79

Appendices 81

A.1 Justification of Excitation Power Dependence of Upconverted Fluorescence 82

A.2 Reabsorption Model for SPEX Experimental Setup 85
A.3 Steady-State Spectroscopy of Solution-phase ZnTCPP 88
A.4 Supplementary Experiments for Ruthenium-DPA Polymer System 90
A.5 Mathematical Processing of Ru-DPA Polymer Spectral Data for Quantum Yield Calculations 92

References **112**

List of Tables

2.1 Effect of Neutral Density Filters using the 532 nm Excitation Source . . 30

2.2 Spectral Sensitivity of Hamamatsu H7421-50 Photodetector 32

3.1 Material Properties of Polymers Used 35

3.2 Correction Factors for ZnTPP:PMMA Films 43

3.3 Emission Spectral Data for ZnTPP:Polymer Drop-cast Films 49

3.4 Material Properties of Potential Future Polymers 53

4.1 TTET Rate Constants from $Ru(dmb)_3$ to DPA Moieties 64

4.2 Parameters for Calculation of Sequential Two-Photon Absorption 66

4.3 Summary of QY Results 67

A.1 Diffusion Coefficients of Ru and DPA Containing Species 92

A.2 Summary of Results for TTET Efficiency Calculations in Polymers . . . 95

A.3 Extrapolated Singlet Emission Intensities of Rhodamine 6G Standard . . 98

A.4 Experimental Parameters for the Modelled UC Spectra 102

A.5 Area Correction Factors for Quantum Yield Calculation 104

A.6 Spectral Sensitivity Correction Factors 106

A.7 Upconverted Fluorescence Quantum Yields of Control Monomer Mixtures 108

A.8 Upconverted Fluorescence Quantum Yields of Polymers 109

A.9 Phosphorescence Quantum Yields of Polymers 109

A.10 Phosphorescence Quantum Yields of Control Monomers 110

A.11 Corrected Intensities of Rhodamine 6G Standards 110

A.12 Constants Utilized in Quantum Yield Calculations 111

List of Figures

1.1 Schematic of Bulk Heterojunction and Dye-sensitized Solar Cells 2

1.2 Solar Spectrum and Shockley-Queisser Plot for Theoretical Solar Cell Efficiency Limit 4

1.3 Generic Jablonski Diagram 5

1.4 Förster and Dexter energy-transfer mechanisms. 9

1.5 Schemitic diagram for upconverted fluorescence by heteromolecular triplet-triplet annihilation 12

1.6 Two approaches to TTA-UC application in photovoltaics 18

1.7 Literature examples of TTA-UC applications 20

2.1 Experimental setup of SPEX Spectrofluorometer 27

2.2 Schemiatic of solid state sample holder 28

2.3 Excitation intensity-dependent S_1 fluorescence of 1 mM ZnTPP in DMF 31

2.4 Spectral sensitivity of the GaAs photodetector 31

2.5 Spectral bandwidth-dependent fluorescence of 1.74 μM Rhodamine 6G in $CHCl_3$ 33

3.1 Molecular structures of polymer matrices for TTA-UC in thin films. . . . 35

3.2 Molecular structures of porphyrins studied. 37

3.3 Concentration-dependent S_1 fluorescence of ZnTPP in toluene 38

3.4 Fluorescence of ZnTPP and ZnTPP:PU thin films 40

3.5 Upconverted fluorescence in ZnTPP:PMMA drop-cast film 42

3.6 Absorption, prompt fluorescence, and upconverted fluorescence of ZnTPP:PMMA films with varying dye concentrations 43
3.7 Excitation power-dependent prompt and upconverted fluorescence of a thin film cast from 1% ZnTPP in PMMA 45
3.8 Soret fluorescence in a ZnTPP:PMMA film by direct Soret excitation and by TTA-UC 46
3.9 Thickness-dependent absorption, prompt fluorescence, and upconverted fluorescence spectra in ZnTPP:PMMA films 47
3.10 Variation in prompt and upconverted fluorescence as a function of ZnTPP:PMMA film thickness 47
3.11 Normalized upconverted and prompt fluorescence of ZnTPP:PMMA and ZnTPP:PEG drop-cast films 49
3.12 Absorption, prompt fluorescence, and upconverted fluorescence of ZnTPP:PEG films with varying dye concentrations 50
3.13 Polymers proposed for future TTA-UC thin film studies 53

4.1 Molecular structure of Ru-DPA polymers and control samples 55
4.2 Previously reported data on Ru-DPA polymers, motivating the present TTA-UC studies. 57
4.3 Optical density, phosphorescence, and upconverted fluorescence of Ru-DPA polymers 59
4.4 Excitation power-dependent photoluminescence spectra of Ru-DPA polymers 60
4.5 Double-logarithmic plot of upconverted fluorescence versus phosphorescence in Ru-DPA polymers 61
4.6 Absorption and photoluminescence spectral changes as pDPA is added to $Ru(dmb)_3$ 62
4.7 Absorption and photoluminescence spectral changes as DPA is added to $Ru(dmb)_3$ 63
4.8 Quenching of $Ru(dmb)_3$ phosphorescence by the addition of DPA and pDPA 64
4.9 Energy transfer processes in Ru-DPA polymers 67

4.10 Power-dependent photoluminescence intensities and QYs of Ru2DPA, Ru6DPA, and $Ru(dmb)_3$ 68
4.11 Power-dependent upconverted fluorescence and quantum yield of $Ru(dmb)_3$ + DPA control samples 70
4.12 Upconverted fluroescence spectra in Ru-DPA polymer films 72

A.1 Absorption and upconverted fluorescence of ZnTPP:PEG film for the consideration of reabsorption effects 85
A.2 Schematics of solution-phase absorption and emission spectroscopy for reabsorption considerations 86
A.3 Schematic of thin film absorption and emission spectroscopy for reabsorption considerations 87
A.4 Absorption, prompt fluorescence and upconverted fluorescence spectroscopy of ZnTCPP in DMF 89
A.5 Stern-Volmer plot for the self-quenching of $Ru(dmb)_3$ triplets 90
A.6 Concentration-dependent phosphorescence decays and residual plots of $Ru(dmb)_3$ 91
A.7 Theoretical variation in TTET efficiency from $Ru(dmb)_3$ to DPA moieties 95
A.8 Power-dependent photoluminescence of 1.58 μM Rhodamine 6G in $CHCl_3$ 97
A.9 Fluorescence of 1.58 μM Rhodamine 6G in $CHCl_3$, taken by SPEX and by PTI spectrofluorometers 99
A.10 Phosphorescence spectra and Gaussian fits of Ru2PDA, Ru6DPA and $Ru(dmb)_3$ 100
A.11 Optical density of pDPA, Ru2DPA, Ru6DPA, and $Ru(dmb)_3$ 101
A.12 Upconverted fluorescence and Double-Gaussian fits of Ru2DPA, Ru6DPA, and two control samples containing $Ru(dmb)_3$ and DPA 103
A.13 Modelled data with Gaussian fits for Ru2DPA, Ru6DPA, and two control samples containing $Ru(dmb)_3$ and DPA 105
A.14 Effect of spectral sensitivity on the photoluminescence spectra of Ru2DPA, Ru6DPA, $Ru(dmb)_3$, and control samples made from $Ru(dmb)_3$ and DPA 107

List of Abbreviations

BHJ	bulk heterojunction	Ph	phosphorescence
BODIPY	boron-dipyrromethene	PMMA	poly(methyl methacrylate)
DET	Dexter energy transfer	PS	polystyrene
DMF	*N,N*-dimethylformamide	PU	polyurethane
DOSY	diffusion ordered spectroscopy	QE	quantum efficiency
DPA	9,10-diphenylanthracene	QY	quantum yield
DSSC	dye-sensitized solar cell	RAFT	reversible addition fragmentation chain transfer
EET	electronic energy transfer	Ru(bpy)3	ruthenium tris(bipyridine)
FRET	fluorescence resonance energy transfer	Ru(dmb)3	ruthenium tris(dimethyl bipyridine)
ISC	intersystem crossing	SS	spectral sensitivity
LFP	laser flash photolysis	TTA	triplet-triplet annihilation
MLCT	metal to ligand charge transfer	TTA-UC	upconverted fluroescence by triplet-triplet annihilation
NCPU	noncoherent photon upconversion	TTET	triplet-triplet energy transfer
Nd:YAG	neodymium-doped yttrium aluminum garnet	UC	upconverted fluorescence
PD	power density	ZnTCPP	zinc tetra(carboxyphenyl)porphyrin
PE	polyethylene	ZnTPP	zinc tetraphenylporphyrin
PEG	poly(ethylene glycol)		

Chapter 1

Introduction to Triplet-Triplet Annihilation

1.1 Energy Limitations in Photoactive Materials

One of the first widely-studied photovoltaic technologies focused on the use of crystalline silicon as the photoactive material, with optimization yielding a power conversion efficiency of 25% for a single layer solar cell.[1] Although they have been commercially available for some time, these devices are subject to the high costs associated with the fabrication of single crystal silicon. These cells also lack flexibility and colour variation, which limit their desirability in many niche applications. These limitations have driven the development of new photovoltaic technology. Over the past few decades, organic/polymer solar cells,[2–11] and dye-sensitized solar cells (DSSC)[12–16] have become attractive fields of research. Cell structures are shown in Figure 1.1.

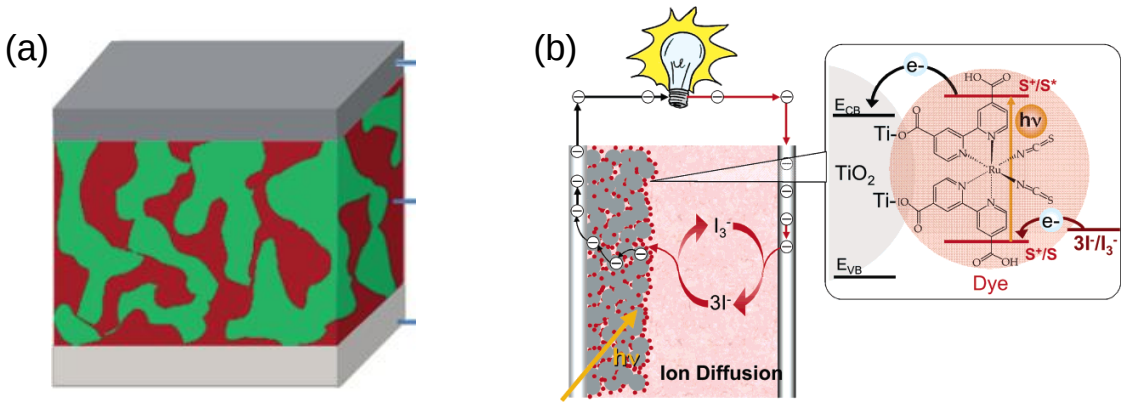

Figure 1.1: *(a) Schematic of a BHJ solar cell, where the active layer is shown as the red/green mixture,*[10] *reproduced with permission by John Wiley & Sons; (b) Schematic of DSSC,*[14] *reproduced with permission by the American Chemical Society.*

Bulk heterojunction (BHJ) solar cells are a type of organic solar cell. These cells generally use conjugated polymers, small molecules, fullerenes, or similar materials blended into a bulk heterojunction as shown in Figure 1.1(a). These cells improve upon planar heterojunctions due to the increased surface area of the donor-acceptor interface. BHJ cells have garnered much attention because they are flexible, cost-effective, and colorful. Despite these desirable traits, champion devices have been limited to efficiencies below 10%.[4;5] The efficiency of these cells must be improved significantly to realize widespread industrial application.

Michael Grätzel introduced the dye-sensitized solar cell (DSSC) in 1991.[12] His cell consisted of a photoactive dye adsorbed onto a colloidal semiconductor, which boasted a high surface area for dye adsorption. This large semiconductor surface area was considered the reason for Grätzel's high cell efficiency as compared a previous model proposed by Gerischer,[17] which utilized a flat semiconductor film. Over the past two decades, devices employing this architecture have seen efficiencies rise above 13%.[13] These cells are also cost-effective and are potentially flexible through the use of polymer-based materials. Though some DSSCs are commercially available, the lack of efficiency in these cells is still a significant obstacle preventing their widespread deployment.

In order to improve efficiency in these photovoltaic devices, the fundamental energy loss mechanisms must be understood. Shockley and Queisser[18] published a report in 1961 that outlined the theoretical efficiency limit of a planar pn-junction solar cell. In this report, they derived a theoretical efficiency maximum of about 33% at a semiconductor band gap of approximately 1.2 eV. This limit considers the Air Mass 1.5 (AM1.5G) solar spectrum absorbed by the cell. This theoretical curve, shown in Figure 1.2(a), approximates the sun as a radiating black body at 6000 K and does not consider the solar radiation absorbed by atmospheric components.

In this calculation, Shockley and Queisser considered the following sources of energy loss: (i) radiative recombination, which puts constraints on the production rate of hole-electron pairs; (ii) radiative losses due to the approximating the solar cell as a black body at room temperature; (iii) vibrational relaxation following absorption of photons with energy greater than the band gap of the semiconductor; and (iv) spectral losses due to transmission of photons with energy less than the band gap of the semiconductor. This limit is an optimistic one, as some potential sources of energy loss were not considered, such as limitations in charge carrier mobility and non-radiative recombination at grain boundaries or defect sites.

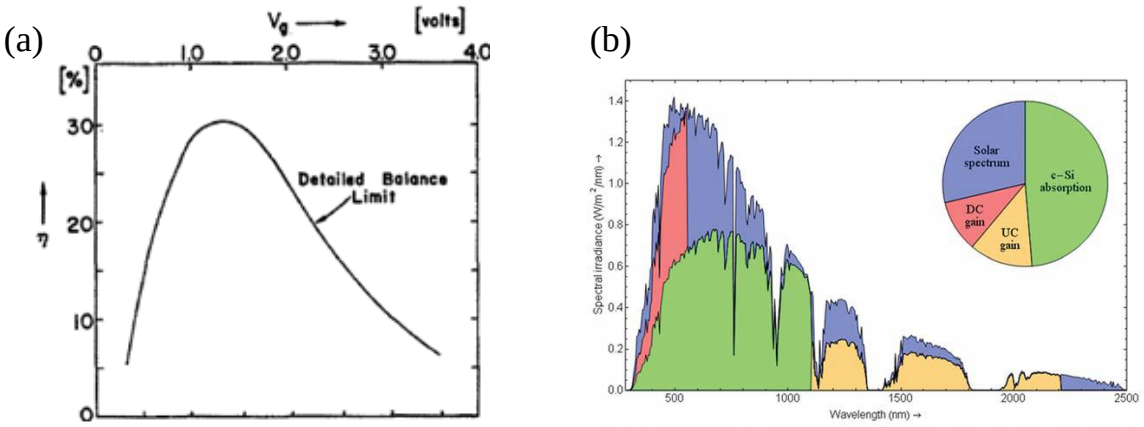

Figure 1.2: *(a) Shockley-Queisser graph for the dependence of theoretical solar cell efficiency as a function of semiconductor bandgap,*[18] *reproduced with permission by the American Institute of Physics; (b) The AM1.5G spectrum, with documentation of regions utilized by first-generation solar cells and those available for enhancement to down- or up-conversion,*[19] *reproduced with permission by the Royal Society of Chemistry.*

This theoretical optimum band gap of 1.2 eV corresponds to a wavelength of about 1000 nm. As shown in Figure 1.2(b), a significant portion of solar radiation is lower in energy than the band gap of Si, which is ≈1100 nm. Analysis of the data in Figure 1.2(a) shows that over 40% of solar radiation is in the near-IR region. It is a significant challenge in modern photovoltaics to make use of this photon-rich IR region. Photon down-conversion,[19], singlet exciton fission,[20;21] multiple-exciton generation,[22] and non-coherent photon upconversion (NCPU)[19;23–25] are proposed methods of potentially circumventing the Shockley-Queisser limit. NCPU is the focus of this thesis, and as such will be described in more detail in Section 1.3.

1.2 Photophysical Processes

1.2.1 Jablonski Diagrams

The electronic and vibrational transitions of interest in a molecule serving as an absorber in a photovoltaic cell can be represented in a Jablonski Diagram. Figure 1.3 builds upon the original depiction[26] to show the processes relevant to the photon upconversion mechanism described in Section 1.3 and analysed in this work.

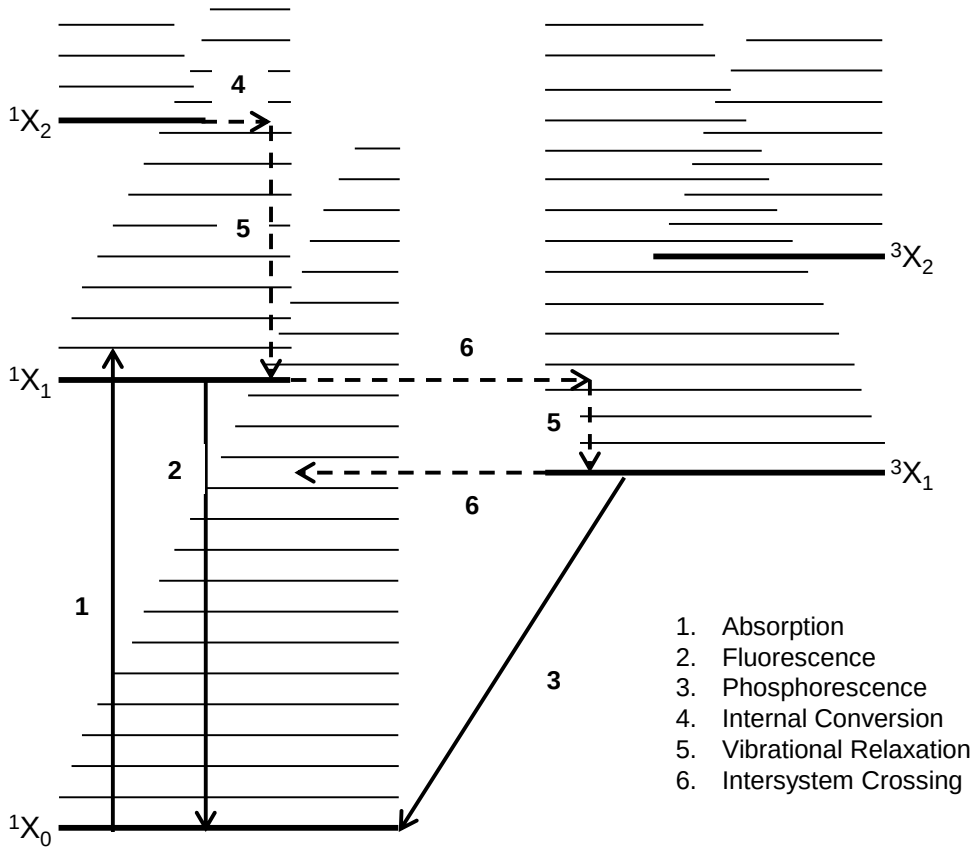

Figure 1.3: *Jablonski Diagram for a generic molecule, X. Both radiative (solid lines) and non-radiative (dashed lines) are shown.*

Processes 1-6 in Figure 1.3 are well studied. Fluorescence (2), in which the initial and final state are of equal spin multiplicity is distinct from phosphorescence (Ph) (3), in which the initial and final states differ in spin multiplicity. These are both radiative relaxation processes. Intersystem crossing (ISC) (6), a radiationless decay process, involves a change in spin multiplicity of a molecule. Here, an electronically excited state relaxes to a lower electronic state by populating a hot vibrational band of the lower state. Internal conversion (4) describes a similar radiationless process in which the initial and final states possess the same spin multiplicity. Vibrational relaxation (5) can occur as an intermolecular or intramolecular process. If a hot vibrational state is populated by photon absorption, the initial vibrational state populated will evolve to a statistically equilibrium distribution of vibrational states at the same total energy by intramolecular vibrational coupling. This process is intramolecular vibrational redistribution and does

not represent a net loss in energy. Vibrational "cooling" can occur through the transfer of vibrational energy from the excited state to the surrounding medium by intermolecular vibrational relaxation. These relaxation processes simply represent a thermal equilibration process between the populated hot vibrational band and the surrounding molecules.

Absorption (1) is only shown in Figure 1.3 from the ground state to the first excited state, though excitation could also occur from the ground state directly to some higher-lying state. Excited state absorption could also occur from the $^1X_1$ state to some higher lying singlet state. Direct absorption from $^1X_0 \rightarrow {}^1X_2$ and subsequent fluorescence are of relevance to the materials utilized in this work. Fluorescence from singlet states higher in energy than the first electronic excited state is a violation of Kasha's rule,[27] which generally states that fluorescence of an electronically excited molecule will only be observed from the lowest excited singlet state. This is because of the dominance of internal conversion from all higher-lying excited singlets to a vibrational state of the lowest excited singlet state at the same total energy. Multiple classes of materials violating Kasha's rule have been identified; the metalloporphyrins described in Section 3.1 are among them.

1.2.2 Photoluminescence Quenching

Photoluminescence quenching occurs in the systems considered in this work both as a requirement for energy transfer (to be discussed) and as a parasitic effect that works to lower the efficiencies of the processes under study. Whether a desired or undesired effect, quenching acts by opening an additional relaxation pathway for an excited chromophore through either collisional deactivation or electronic energy transfer (EET). Though not discussed in the present work, quenching is also possible through electron transfer. If S is an excited chromophore (sensitizer) and Q is a quenching material, the deactivation scheme is as follows:

$$^1S_1 + {}^1Q_0 \rightarrow {}^1S_0 + {}^1Q_1 \tag{1.1a}$$

$$^1S_1 + {}^1Q_0 \rightarrow {}^1S_0 + {}^1Q_0 \tag{1.1b}$$

where schemes (a) and (b) represent the respective cases of EET and collisional deactivation. If the concentration of the ground state quencher is much greater than that of the excited singlet of the sensitizer, the quenching process is kinetically pseudo-first order. Thus, simple kinetic analysis yields the Stern-Volmer equation below, given in two forms.

$$\frac{I_F^0}{I_F} = 1 + k_Q \tau_0 \, [Q] \tag{1.2a}$$

$$\frac{1}{\tau_F} = \frac{1}{\tau_0} + k_Q \, [Q] \tag{1.2b}$$

where I_F^0 and I_F are the fluorescence intensity of the sensitizer in the absence and presence of quencher, τ_0 and τ_F are the unquenched and quenched lifetime of the excited state sensitizer, k_Q is the second order quenching rate constant, and $[Q]$ is the molar quencher concentration. If the sensitizer's excited state is sufficiently short-lived that molecules are essentially static in the sensitizer lifetime, the Perrin quenching sphere model[28] can be used to describe the EET mechanisms described below. Under this model, diffusion is not permitted in the short time frames considered. Thus, the probability of quenching can be described by a step function with respect to some threshold spherical volume, V_Q. A quencher within V_Q of the excited sensitizer has a quenching probability of unity while quencher molecules outside this volume have a quenching probability of 0. Since the sphere is isotropic, one can envision the corresponding radius, r_Q, from excited sensitizer to quencher and the quenching probability, P_Q, as the following piecewise function:

$$P_Q = 1; \quad r_{SQ} \leq r_Q$$
$$= 0; \quad r_{SQ} > r_Q$$

where r_{SQ} is the distance from sensitizer to quencher at the time the sensitizer is excited. In the condition of static quenching, the Stern-Volmer relation is expanded as shown below. In this limit, the quenching ratio is represented by an exponential function of $[Q]$.

$$\frac{I_F^0}{I_F} = exp\left(N_A V_Q [Q]\right) = 1 + N_A V_Q [Q] + \frac{1}{2!}\left(N_A V_Q [Q]\right)^2 + \cdots \tag{1.4}$$

For low quencher concentrations, the quadratic term is negligible and Equation 1.4 is linear. As $[Q]$ is sufficiently increased, however, the quadratic term become non-negligible and the plot of quenching ratio vs. molar quencher concentration diverges from linearity.

1.2.3 Electronic Energy Transfer

Photoluminescence quenching discussed in Section 1.2.2 is a desired effect in many heteromolecular systems. The BHJ solar cell in Figure 1.1 is one such example. Here the active layer is a blend of two compounds, where quenching is a basic principle of operation. In photovoltaics, the pair is often referred to as the electron "donor" and "acceptor", since quenching in these materials is by electron transfer. The present document involves a study of EET systems. Here the active materials are referred to as "sensitizer" and "emitter". The energy pathway includes absorption by the sensitizer, energy transfer from sensitizer to emitter, and photoluminescence of the emitter material.

EET from sensitizer to emitter can be described by the fundamental theories outlined by Förster[29] or Dexter.[30] These transfer mechanisms are shown schematically in Figure 1.4 and described below. In both cases, interaction between the sensitizer and emitter chromophores is a requirement either within a single bifunctional molecule or between

adjacent molecules. In each of these cases, the rate constant for EET is given by

$$k_{EET} = \frac{2\pi}{\hbar} V_{SE}^2 \rho_{SE} \tag{1.5}$$

where V_{SE} contains both the electronic coupling and the Franck-Condon factors for the transition and ρ_{SE} is the density of states. This general expression describes the rate constant as the probability of a transition per unit time, and is expressed in a more useful form in each case presented in this section.

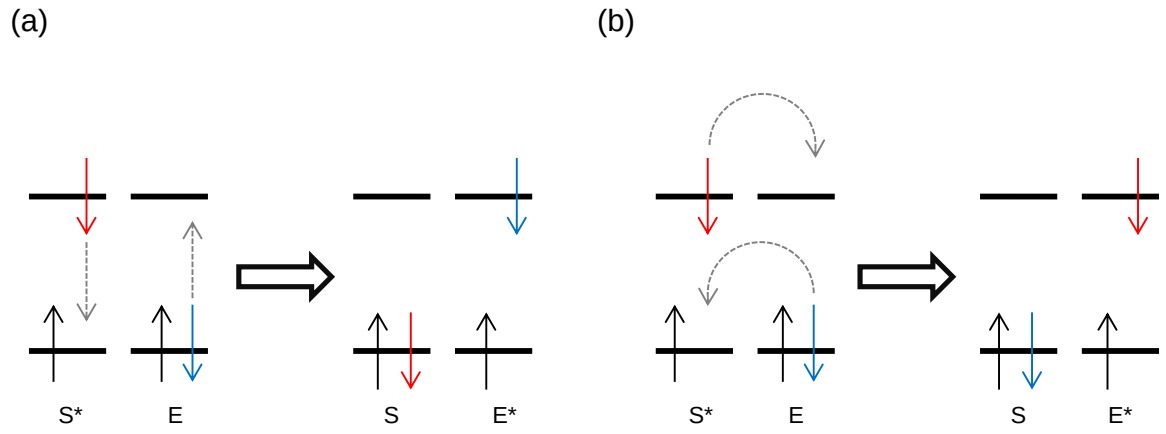

Figure 1.4: *(a) Förster[29] and (b) Dexter[30] energy-transfer mechanisms. S and E are the sensitizer and emitter, respectively.*

Förster Theory

Förster, or fluorescence resonance energy transfer (FRET) theory considers EET resulting from coulombic interactions between the dipoles of the two chromophores. In this case, the dipole-dipole interaction between chromophores is large if both electronic interactions are spin-allowed and dipole-allowed. In other words, FRET is probable between chromophores whose interactions possess large molar absorptivities with oscillator strengths approaching unity. Förster[29] obtained ρ_{SE} from the overlap integral between the normalized photoluminescence spectrum of S^* and the absorption spectrum of E. He also determined V_{SE} by considering the classical interaction energy of the chromophores as point dipoles. From Equation 1.5, he obtained

$$k_{EET}(r) = \frac{\Phi_F\,\kappa^2}{\tau_S\,r^6}\left(\frac{9\,ln\,(10)}{128\pi^5 N_A n^4}\right)J\,(\overline{\nu}) \tag{1.6}$$

Here, Φ_F and τ_S are the unquenched fluorescence quantum yield (QY) and excited state lifetime of the sensitizer, r is the distance between sensitizer and emitter centres, n is the refractive index of the medium, κ^2 is an orientation factor and $J\,(\overline{\nu})$ is the integral of overlap between the emitter absorption and sensitizer normalized fluorescence spectra on an energy scale. κ^2 is determined from the relative orientation of the unit vectors along the transition moments, and is assumed an average value of 2/3 for intermolecular EET in solution, calculated on the assumption of an isotropic distribution of transition moments.

It is clear that the greatest rate constants for FRET are achieved in systems employing a sensitizer with a large fluorescence QY. If the fluorescence QY approaches unity then the non-radiative decay rate constant is sufficiently small to not be competitive with EET. Furthermore, k_{EET} is directly proportional to the degree of overlap between the absorption band of the emitter and fluorescence band of the excited sensitizer. In other words, the rate constant can be controlled by the careful consideration of electronic properties through the functionalization of materials.

Though the rate constant has a $\frac{1}{r^6}$ dependence, it is realistic for FRET to occur over considerable distances on a molecular scale. To this end, the Förster distance, R_0 has been defined as the distance in which the EET has an efficiency of 50%. Here, the efficiency is defined as the rate constant for EET over the sum of the EET, radiative and non-radiative rate constants. R_0 is defined as the distance in which $k_{EET}=k_r+k_{nr}=1/\tau_S$ and Förster distance and EET efficiency are calculated as follows:

$$R_0^6 = \Phi_F\,\kappa^2\left(\frac{9\,ln\,(10)}{128\pi^5 N_A n^4}\right)J\,(\overline{\nu})\,; \quad k_{EET} = \frac{R_0^6}{\tau_S\,r^6} \tag{1.7}$$

$$\eta_{EET}(r) = \frac{1}{1 + \left(\frac{r}{R_0}\right)^6} \tag{1.8}$$

R_0 values of 2 to 4 nm are common, though values of 10 nm are known, verifying the occurrence of efficient FRET over large distances. The theory is oversimplified in large molecules whose dimensions approach R_0. This is due to the consideration of the classical interaction between two point dipoles, leading to limited quantitative accuracy in larger molecules.

Dexter Theory

Dexter, or electron exchange theory, best describes the case in which one or both of the electronic energy transitions is forbidden, resulting in negligible dipole interactions. Here, Dexter energy transfer (DET) is controlled by electron exchange between molecules as per Figure 1.4(b). Thus, molecular orbital overlap is required. In this case, $J(\overline{\nu})$ is used to determine the density of states as in FRET theory, but here V_{SE} is determined by the extent of orbital overlap between excited sensitizer LUMO and emitter HOMO. Here the rate constant for EET falls off exponentially as the distance between sensitizer and emitter is increased due to the decrease in molecular orbital electron density far from the nucleus. Dexter[30] determined that the rate constant could be calculated by

$$k_{EET} = KJ\left(\overline{\nu}\right) exp\left[-\frac{2R_{SE}}{L}\right] \tag{1.9}$$

where R_{SE} is the distance between the S^* and E centres, L is the sum of the van der Waals radii of S^* and E, and K is a constant. Thus, efficient electron exchange occurs when the two chromophores are in close proximity and possess a large overlap integral.

The special case of DET presented in this work involves the annihilation of two triplet states into a ground-state singlet and an excited singlet whose energy is approximately double that of the triplet state. The detailed mechanism and application of this triplet-

triplet annihilation (TTA) is introduced in the following section.

1.3 Upconverted Fluorescence by Triplet-Triplet Annihilation

TTA as a means of realizing delayed fluorescence was first reported many decades ago.[31;32] Its reappearance over the past decade, as evidenced by the surge of recent reviews,[23–25;33;34] has been driven by the potential applications described in Section 1.4. The past decade of research has spanned the synthesis of suitable sensitizer-emmiter materials,[35–41] excitation power dependence,[42–44] fundamental kinetics and mechanics,[45–53] diffusion rates,[54;55] upconverting polymer films,[56–67] and upconverting nanoparticles.[68–70]

1.3.1 Fundamental Mechanisms

The most commonly utilized energy mechanism for realizing upconverted fluorescence via heteromolecular TTA is depicted in Figure 1.5. Homomolecular TTA follows a similar mechanism involving two molecules of the same compound.

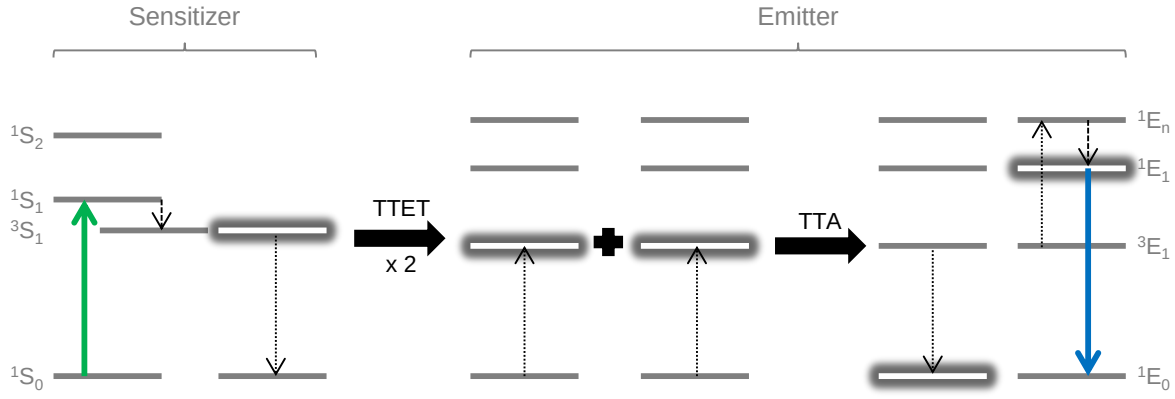

Figure 1.5: *General energy mechanism for heteromolecular TTA Here the solid pathways represent radiative processes while the dotted and dashed processes represent intermolecular and intramolecular non-radiative processes, respectively. The emphasized states represent the highlights of the energy-transfer processes. Here S and E represent the sensitizer and emitter species. TTET represents triplet-triplet energy transfer.*

In Figure 1.5, the sensitizer material absorbs radiation and is excited into the S_1 state.

It then undergoes subsequent ISC to the T_1 state. This triplet sensitizer can undergo TTET to an emitter molecule, populating the T_1 state of the emitter. If two triplet emitter molecules meet, they can undergo TTA, which produces a ground-state emitter singlet and an S_1 emitter. This singlet-excited emitter undergoes subsequent fluorescence.

Figure 1.5 outlines the general requirements for achieving efficient TTA via the most widely realized mechanism. The sensitizer material requires a high oscillator strength and undergoes efficient ISC from the singlet to triplet manifold. This sensitizer must possess a relatively long-lived triplet state so that deactivation by the triplet can occur primarily by triplet-triplet energy transfer (TTET) to the emitter species. Generally, the sensitizer requires efficient absorption of radiation followed by fast, efficient ISC to a long-lived triplet state - an effective pooling of energy in the sensitizer's triplet manifold.[71]

With noted exceptions,[47;50;53] TTET requires an emitter species with triplet energy level below that of the sensitizer to promote guided energy flow from sensitizer to emitter. This emitter requires a long-lived triplet state with a negligible probability for ISC. An efficient fluorescing state in this molecule must uphold the energy relation $2 \times {}^3E_1 \geq {}^1E_1$ so that the reorganization of energy involved in the annihilation process can populate this excited singlet state. In this context, upconverted fluorescence refers to the high energy of fluorescence from the emitter singlet relative to that absorbed by the sensitizer. The reaction scheme for this energy mechanism is as follows:

$$ {}^1S_0 + h\nu_{ex} \rightarrow {}^1S_1 \tag{1.10a} $$

$$ {}^1S_1 \rightarrow {}^3S_1 \tag{1.10b} $$

$$ {}^3S_1 + {}^1E_0 \rightarrow {}^1S_0 + {}^3E_1 \tag{1.10c} $$

$$ {}^3E_1 + {}^3E_1 \rightarrow {}^1E_0 + {}^1E_1 \tag{1.10d} $$

$$ {}^1E_1 \rightarrow {}^1E_0 + h\nu_{em} \quad ; \quad h\nu_{em} > h\nu_{ex} \tag{1.10e} $$

This mechanism is the most general for realizing upconverted fluorescence, though Schmidt and co-workers[47] have demonstrated upconverted fluorescence in a system with ${}^3E_1 > {}^3S_1$, which they determined was entropy-driven TTET. Baluschev[49;50] reported the above mechanism alongside that shown in Scheme 1.11, which was suggested to correspond to the cases of emitter triplet energy level below and above, respectively, that of the sensitizer. The authors stated that in the absence of TTET from sensitizer to emitter, upconverted fluorescence could be realized through TTA between two sensitizer triplets and subsequent singlet energy transfer from a higher lying sensitizer singlet state to an excited emitter singlet state.

$$ {}^1S_0 + h\nu_{ex} \rightarrow {}^1S_1 \tag{1.11a} $$

$$ {}^1S_1 \rightarrow {}^3S_1 \tag{1.11b} $$

$$ {}^3S_1 + {}^3S_1 \rightarrow {}^1S_0 + {}^1S_2 \tag{1.11c} $$

$$ {}^1S_2 + {}^1E_0 \rightarrow {}^1S_0 + {}^1E_1 \tag{1.11d} $$

$$ {}^1E_1 \rightarrow {}^1E_0 + h\nu_{em} \tag{1.11e} $$

Baluschev's proposed mechanism has been met with criticism[51;52] due to the extremely short lifetime of the proposed upconverted state in his sensitizer and the low potential for singlet energy transfer to the emitter within this lifetime. Steer and co-workers[53] discredited the proposed mechanism through detailed kinetic analysis and calculations based on FRET theory. The alternative mechanism involves complexing of the triplet sensitizer by a ground-state emitter molecule. This forms a triplet exciplex, which is capable of annihilation with another triplet sensitizer in a three center process capable of producing an excited emitter singlet. This mechanism is shown below.

$$^1S_0 + h\nu_{ex} \rightarrow {}^1S_1 \tag{1.12a}$$

$$^1S_1 \rightarrow {}^3S_1 \tag{1.12b}$$

$$^3S_1 + {}^1E_0 \rightarrow {}^3[S_1 \cdots E_0]^* \tag{1.12c}$$

$$^3[S_1 \cdots E_0]^* + {}^3S_1 \rightarrow {}^1E_1 + {}^1S_0 + {}^1S_0 \tag{1.12d}$$

$$^1E_1 \rightarrow {}^1E_0 + h\nu_{em} \tag{1.12e}$$

Schemes 1.10 and 1.12 represent the commonly accepted mechanisms for achieving upconverted fluoresence by heteromolecular TTA. The present work will utilize Scheme 1.10, where the triplet energy of the sensitizer is greater than that of the emitter. Though it is controversial as a heteromolecular model, Scheme 1.11 is of relevance to the present work. Scheme 1.11(a-c) represents the pathway utilized for homomolecular TTA, in which sensitizer and emitter are of the same species.

1.3.2 Excitation Power Dependence

Kinetic analysis for the excitation power dependence of TTA-UC is detailed in Appendix A.1. It is shown that upconverted fluorescence varies quadratically and linearly with emitter triplet concentration in the weak and strong annihilation kinetic regimes, respectively. Since emitter triplet concentration varies linearly with excitation power density in the materials studied, one obtains an excitation power dependence of upconverted fluorescence that varies from quadratic to linear as the system moves from the weak to strong annihilation kinetic regime. Power-dependence studies have become a key component in characterizing and verifying upconverted fluorescence, as evidenced by a number of reports.[36–38;40;42–44;46;53;55–59;61;65;67–70;72–88] These reports demonstrate the general relation described mathematically in Appendix A.1 and based on a 2012 report from Castellano and co-workers.[43] In the weak annihilation kinetic regime, the majority

of emitter triplets are decaying by some first or pseudo-first order relaxation pathway. This region can be deemed one of low triplet concentration. Due to this low concentration of triplets, any one ground-state molecule is likely not in close proximity to a triplet molecule. For TTA to occur, two adjacent ground-state molecules must be triplet-sensitized. The pair of one-photon excitations required is the reason for the quadratic dependence on excitation power in this region.

The strong annihilation limit can be viewed as one of high triplet concentration. Thus a ground-state emitter is likely within close proximity to a triplet molecule for DET. Thus, triplet sensitization of the ground-state molecule can result in TTA with the nearby triplet. Here TTA is possible through absorption of a single additional photon, and upconverted fluorescence varies linearly with excitation power in this limit.

1.3.3 Spin-Statistics of TTA

Also detailed in the Appendix is the method for determining QYs of upconverted fluorescence and of TTA. The TTA-UC mechanisms presented in Section 1.3.1 are concerned only with annihilation resulting in an excited singlet emitter. Though Nickel[89] concluded that the singlet state product of TTA is the highest excited singlet state that is energetically available, the singlet is only one of three possible product states. Of interest in the present section is f, the probability that TTA yields an excited singlet molecule. Historically, this probability has been equal to the factor of 1/9 determined by spin statistics,[90–94] though Schmidt and co-workers[45;46] have demonstrated that perhaps this limit is not a strict rule. The spin-statistical limit is based on the encounter complex formed between a pair of excited triplet molecules. From the tensor product of the initial spin states of the molecules,[45] this encounter complex can have singlet, triplet, or quintet multiplicity.[90–94] The spin multiplicity of the encounter complex has a direct effect on the states produced in the annihilation event.

$$^3X_1 + {}^3X_1 \rightleftharpoons {}^{1,3,5}[X\cdots X]^* \rightarrow {}^1X_0 + {}^1X_1 \quad (1.13a)$$

$$\rightarrow {}^1X_0 + {}^3X_2 \quad (1.13b)$$

$$\nrightarrow {}^1X_0 + {}^5X_1 \quad (1.13c)$$

One degenerate singlet complex exists along with three degenerate triplet complexes and five degenerate quintet complexes, for a total of nine possible states. The spin-statistical limit is surpassed by considering energy recycling in annihilation steps (b) and (c). The higher-lying triplet produced in Scheme 1.13(b) would likely undergo rapid internal conversion to the $^3X_1$ state and be available for the next annihilation event. Thus, annihilation from the triplet encounter complex represents a recycling of energy in the formation of a ground-state singlet and the reproduction of an excited triplet state. The energy loss in this process would be equal to the energy of one triplet state of the annihilating molecules. This loss is significant in the system, but is half that which is predicted by spin statistics due to the reformation of an excited triplet molecule.

Now consider the quintet encounter complex shown in Figure 1.13(c). Bachilo and Weisman[92] and Levin *et al.*[93] state that the quintet encounter complex cannot undergo an annihilation event. This is because the excited quintet state is almost always at sufficiently high energies such that $2 \times E\,(^3X_1) < E\,(^1X_0) + E\,(^5X_1)$. Thus the energy of the annihilating triplets is insufficient for the formation of an excited quintet molecule. The quintet encounter complex will simply dissociate back into the pair of excited triplets. This pathway represents a return to the initial state without significant loss. When recycling events are considered, Schmidt and co-workers[45] demonstrated that the theoretical limit is over 40%.

1.4 Applications of TTA-UC

Theoretical[19;22;23;33;95–97] and experimental[88;98–104] studies of upconversion-enhanced solar cells have been reported. From this preliminary work, proof in principle of upconversion-enhanced photovoltaics has been achieved. Strategies for realizing significant upconversion-enhanced efficiencies for industrial application have been proposed from these proof in principle studies. Two distinct approaches to utilizing NCPU in photovoltaics exist, as depicted in Figure 1.6.

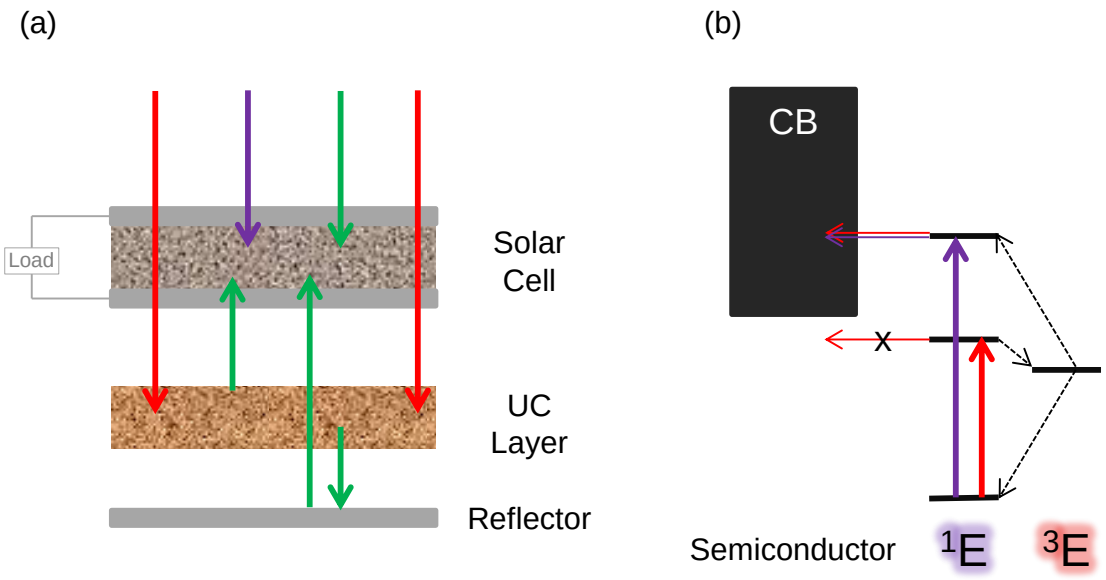

Figure 1.6: *Schematic of TTA-UC applications in photovoltaics through (a) absorption of upconverted fluorescence; and (b) electron injection from the annihilation-excited state. For clarity, (a) is shown in expanded view while actual model contains only an electronically insulating layer between active layers. The diagram in (a) is based on those described in the literature.*[19;23;33]. *In (b), E represents the emitter species.*

Figure 1.6 provides a cartoon of the two distinct and separate approaches of TTA-UC in photovoltaics. The literature reports of UC-driven photovoltaic devices have utilized the application depicted in Figure 1.6(a). Here, the UC-active material is employed as an auxiliary layer, constructed behind the solar cell. As incident light reaches the solar cell, high-energy photons are absorbed and only those photons which transmit through the

active layer will reach the UC-active layer. These sub-band gap photons are absorbed and upconverted by the auxiliary layer, then subsequently emitted at higher energy. Through the use of reflectors, these upconverted photons are directed back to the active layer, where they can now be absorbed by the primary cell. Cells utilizing this structure must be comprised of transparent electrodes to allow the passage of light through the primary cell to the auxiliary layer.

The schematic examples contained in de Wild's review[19] also make reference to the utilization of an UC-active layer *within* the cell structure. The original authors of this report[104] describe the most successful cell structure as that in which the UC-active auxiliary layer is situated directly above the dye-adsorbed semiconductor layer, separated by a thin transparent semiconductor layer. This allows for swift absorption of upconverted photons by the dye in a system that is comparable to that described above.

In Figure 1.6(b) the UC-active material is an active material within the cell. This model is distinct from the application in (a), in which the active solar cell harvests the upconverted photons from the UC-active material contained in an auxiliary layer. In the model shown in Figure 1.6(b), the excited state of the annihilator species is situated above the conduction band of the semiconductor such that electron injection is kinetically favourable. Here, the direct excitation results in occupation of an excited state which is lower in energy than the conduction band edge of the semiconductor. TTA, however, results in occupation of an excited state which is higher in energy than the conduction band edge. The result is TTA-UC induced electron injection - a mechanism with direct application in DSSCs. This TTA-induced electron injection could also be achieved by utilizing the UC-active material as a supplementary dye. A recent report[105] demonstrated enhanced efficiency of a DSSC when zinc tetrakis(carboxyphenylporphyrin) (ZnTCPP) was added to the model dye (N719), owing to electron transfer from ZnTCPP to N719 en route to electron injection into the semiconductor. Although this report focused on direct excitation of ZnTCPP and did not give consideration to TTA-UC processes, it

serves as a reasonable analogy for an application of TTA-UC in DSSCs. The Morandeira group[73] and Steer and Paige[106] groups have demonstrated TTA-UC on a zirconia surface, which was unquenched due to zirconia's high-lying conduction band. These reports demonstrate a higher-lying excited state occupied by TTA-UC in molecules bound to a semiconductor, a concept with direct potential for application in DSSCs.

In addition to the photovoltaic applications considered below, TTA-UC also has application in photocatalysis,[107–109] photochromic displays,[110;111] and biological imaging.[69;112;113] Some examples from the literature are shown in Figure 1.7.

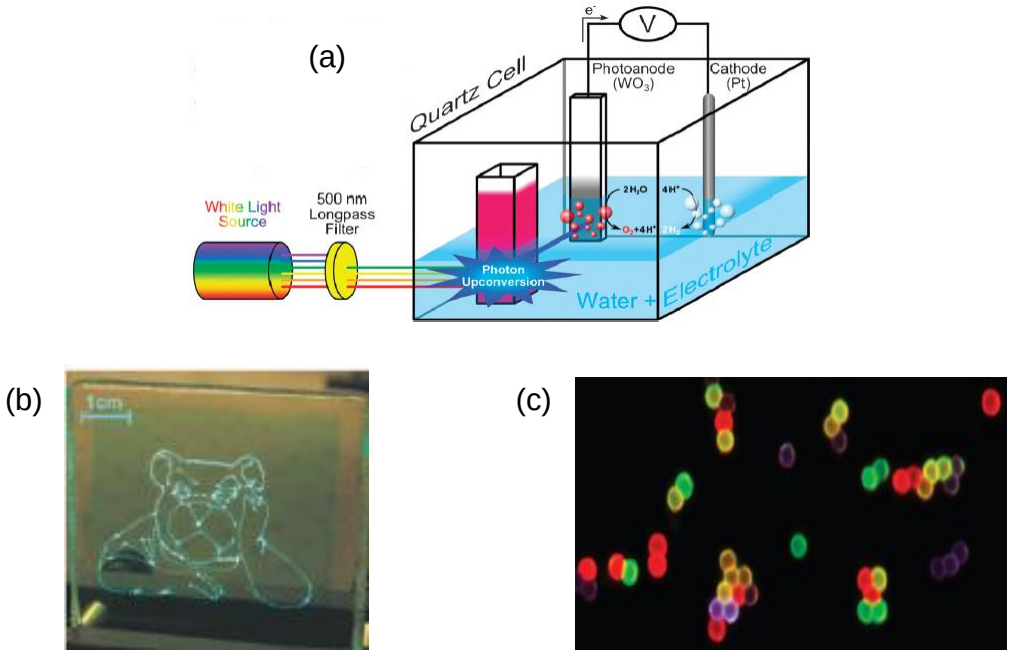

Figure 1.7: *Applications of TTA-UC in: (a) photocatalysis,[107] reproduced with permission by the Royal Society for Chemistry; (b) photochromic display,[110] reproduced with permission by the Institute of Physics; (c) biological imaging,[113] reproduced with permission by Nature Publishing Group.*

Castellano and co-workers[107] demonstrated photoactivity in a photochemical cell utilizing sub-band gap photons by TTA-UC. This was achieved by selecting an emitter material whose fluorescence wavelength was slightly above the band gap edge of the photoanode, WO_3 in this report. In this way the application is very similar to the photovoltaic applications discussed previously. UC-powered photochemistry is an attractive

application due to the low energy requirements of the excitation source. Situating the UC-active material near the photoanode allows for long-wavelength excitation through the majority of the photochemical cell. This reduces the risk of photochemical changes in the photochemical cell materials.

Eliminating the requirement of short-wavelength excitation sources is also an asset in the application of TTA-UC to photochromic display. Baluschev and co-workers[110] demonstrated transparent, flexible polychromic displays by depositing NCPU-active materials in an arranged manner in a polymer matrix. Through the utilization of TTA-UC materials, a long-wavelength excitation source can be used, reducing the risk of photodegradation of the polymer materials.

Biological imaging of cell tissues utilizing NCPU has also been reported.[69;113] If an UC-active material can be bound to the cell (as a nanoparticle in the references discussed here), the cell can be imaged via long-wavelength excitation sources that have no effect on the host cell. This notion is especially attractive in photodynamic therapy of cancer cells.[69;114] Once an UC-active material can be bound to the cancer cells, long-wavelength excitation sources can be used for therapy. The low-energy excitation source will not be damaging to the host cells. TTA-UC will produce high-energy photons in the vicinity of target cells that can potentially destroy these cells. This manner of therapy would be less invasive that the current methods, which require an excitation source of sufficient energy to damage the target cells. These high-enery sources are equally damaging to cells besides the intended targets.

1.5 Material Selection for TTA-UC

The requirements of sensitizer and emitter materials are described in Section 1.3.1. Heteromolecular TTA-UC will be achieved by the most commonly utilized Scheme 1.10

in the present work. The sensitizer must possess a high oscillator strength in the visible to near-IR region of the spectrum and must undergo efficient ISC into a relatively long-lived triplet state. For guided energy flow, the emitter species must have a triplet energy level slightly below that of the sensitizer. This triplet state must be long-lived, since bimolecular TTA is generally a diffusion-controlled process. The emitter must possess a singlet state at an energy level slightly less than the sum of the two triplets in order for TTA to occupy this excited singlet. The excited singlet state of the emitter must have a high fluorescence QY. The requirements for sensitizer and emitter have been fulfilled in general by metallated macrocycles and aromatic hydrocarbons, respectively.

Homomolecular TTA uses a single species as both sensitizer and emitter. This species requires a high oscillator strength and efficient ISC to a long-lived triplet state as described for the sensitizer component. This species must also possess a fluorescent singlet state with energy slightly less than double the triplet energy. This is required for TTA to produce an upconverted fluorescent state. Zinc tetraphenylporphyrin (ZnTPP) has been identified as a suitable candidate for homomolecular TTA studies.[53;60;106;115] The discussion of homomolecular TTA in ZnTPP is continued in Chapter 3.

A detailed summary of the sensitizer-emitter pairs utilized in heteromolecular TTA-UC studies is given in recent review articles[24;25;33] and is briefly introduced here. Though non-metal triplet sensitizers including 2,3-butanedione,[77] fullerenes,[85] and boron - dipyrromethene (BODIPY),[40;116] have been reported, the majority of triplet sensitizers employed in TTA studies have consisted of transition metal complexes with π-conjugated organic ligands. This extended π system red-shifts the spectral features of the sensitizer.[25] Common organometallic triplet sensitizers are bipyridine derivatives utilizing ruthenium,[37;42;74–76;117–120] iridium,[121;122] or rhenium[123] centres and metalloporphyrin derivatives.[36–38;43–47;49;50;53–65;68–70;72;73;78–80;83;84;86–88;94;98;100;101;106;107;115;124–135]. Zhao has also demonstrated TTA sensitized by other platinum-based macrocycles.[41;136;137]. The heavy metal centres in these sensitizers promote efficient ISC due to enhanced spin-orbit

coupling. Several near-IR triplet sensitizers have been reported, owing to the highly tunable ligand systems in these sensitizers.[37;38;40;45;118;119;138]

Common emitters reported in the literature include various derivatives of napthalene,[128] anthracene,[41–44;49;50;54–59;65;68;70;72;74–76;78;80;83;84;107;117–120;123;124;128;129;131;132;134;135] perylene,[38;40;41;47;53;69;79;116;125;126] rubrene,[38;45;46;87;88;98;100;101;127] anthanthrene,[85] pyrene,[83;121;136] tetracene,[86] phenylene,[62–64] and coumarin.[53;137] Further studies have utilized well-known blue-emitting polymers poly(phenylenevinylene),[94] and polyfluorene[50;56;61;64;130;133]. Most of these common emitter materials are aromatic hydrocarbons with low ISC efficiency and flourescent S_1 states. The majority of these sensitizer-emitter systems have been realized by mixing the two components in solution.

Thin film Systems

Practical applications of TTA-UC in photovoltaics require thin film systems as opposed to the solution phase. Heteromolecular TTA-UC via suitable sensitizer-emitter pairs has been reported in polymer matrices of poly(ethyleneoxide/epichlorohydrin),[57;58] poly(methyl methacrylate) (PMMA),[85;129;135;139] cellulose acetate,[59] poly(ethylene glycol) (PEG),[40] and a variety of commercially available thermoplastic polyurethane (PU) materials.[55;57;58] Additionally, recent studies have demonstrated sensitized TTA-UC on polymer glasses.[65;66] These significant literature reports outline two separate and distinct environments for TTA-UC that vary with the material properties of the host polymer.

Castellano and co-workers[58] provided a detailed temperature-dependent study of heteromolecular TTA-UC in polymer films of low glass transition temperature. A polymer above its glass transition temperature is in a "rubbery" state, allowing for diffusion of the embedded molecules. Thus polymers exhibiting low glass transition temperatures allow for molecular diffusion-driven TTA-UC. Castellano's study confirmed this result by

demonstrating how fluorescence via TTA-UC was suppressed below the glass transition temperature of the host polymers. Furthermore, TTA-UC was enhanced considerably with increasing temperature up to some threshold, when irreversible breakdown of the host polymer occurs. The effect of temperature on TTA-UC fluorescence is consistent with Stokes-Einstein behaviour in this system, where diffusion coefficients are directly proportional to temperature and inversely proportional to the viscosity of the host material. Thus, fluorescence via TTA-UC increases substantially with temperature in a rubbery material up to the threshold temperature at which the polymer breaks down.

The literature reports of fluorescence via TTA-UC in a PMMA matrix[60;85;129;135;139] represent a different class of TTA-UC. PMMA is below T_g at ambient temperature, preventing significant molecular diffusion in the film. Thus, fluorescence via TTA-UC in this system provides evidence of pre-aggregation of the involved species and exciton migration through the aggregates. This is followed by TTA at molecular orbital overlap distances, also provided by the aggregates. Low yields of upconverted fluorescence via TTA-UC in PMMA matrices have been reported in heteromolecular[85;129;135;139] and homomolecular[60;106] TTA-UC systems.

These thin film studies realize TTA-UC by casting a film from solution of a sensitizer-emitter mixture. In addition to these heteromolecular films, TTA-UC has been reported in sensitizer-emitter macromolecules.[62;74;120;140] In these macromolecular systems, sensitizer and emitter and covalently bound together. Structures for covalently bonding sensitizer and emitter moieties into a copolymer have recently been proposed,[33] but have yet to be realized experimentally.

1.6 Objectives

This work will set out to advance the knowledge of TTA-UC in polymer systems. Chapter 2 describes the general experimental methods used and details the custom-modified SPEX Fluorolog Spectrofluorometer that was designed for the study of TTA-UC systems. Homomolecular TTA in ZnTPP-doped polymers is studied in Chapter 3. In this chapter, two distinct classes of polymers are employed in order to study TTA-UC that is driven by molecular diffusion and pre-aggregation of dye molecules, respectively. Chapter 4 describes the study of two photophysically active polymers containing a ruthenium tris(bipyridine) ($Ru(bpy)_3$) core and multiple 9.10-diphenylanthracene (DPA)-containing pendant arms. Heteromolecular TTA-UC is demonstrated within these polymers in solution and the solid phase. The nature of the energy-transfer mechanisms involved in this system are studied through a combination of calculation and experiment utilizing control samples consisting of ruthenium tris(dimethyl bipyridine) ($Ru(dmb)_3$) and DPA moieties. A detailed summary of results and suggestions for future work are given in the body chapters 3 and 4. Chapter 5 provides the overall conclusions of the two projects.

Chapter 2

Experimental Techniques and Instrumentation

2.1 Summary of Equipment Used

Absorption spectroscopy was performed on a Cary 6000i spectrophotometer operating in dual beam mode. A PTI Quantamaster spectrofluorometer was used for routine photoluminescence spectroscopy. Spin-cast films were obtained through the use of a WS-650 Series Spin Processor from Laurell Technologies Corporation and thickness measurements were obtained using an AlphaStep D Profiler and software from KLA Tencor. Diffusional information on the polymeric materials studied in Chapter 4 was obtained by diffusion ordered spectroscopy (DOSY) on a 500 MHz Avance NMR Spectrometer provided by Bruker.

Photoluminescence decay experiments were performed using an Edinburgh Instruments LP920 laser flash photolysis system, as described in the literature.[85] Briefly, a flash-lamp-pumped frequency-doubled ns Tempest 300 neodymium-doped yttrium aluminum garnet (Nd:YAG) laser was used as the 532 nm excitation source. Photoluminescence was focused onto a Czerny-Turner grating monochromator (TMS300) and detected using an LP900 photomultiplier. Data was acquired via L900 software supplied by Edinburgh Instruments.

The majority of steady-state spectroscopic experiments were performed using a cus-

tom built laser-excited spectrofluorometer. The sample chamber and emission double monochromator are of Jobin-Yvon SPEX origin, reconditioned by Olis, Inc. The photodetector is a thermo-electrically cooled, single-photon counting photomultiplier supplied by Hamamatsu, chosen for its sensitivity out into the red region of the visible spectrum. In lieu of an excitation monochromator, a laser excitation system has been designed and implemented with a bias toward the study of upconverted fluorescence in solution and the solid phase. This experimental setup was based on a previous model described in the literature[53] and is described in detail in the following section.

2.2 Detailed Setup and Implementation of SPEX Fluorolog Spectrofluorometer

A schematic of the custom-modified SPEX spectrofluorometer designed for the study of upconverting systems is shown in Figure 2.1. The double-monochromator and photodetector have been used as received from the manufacturer, utilizing the standard SPEX internal optics. The double-monochromator has a linear dispersion of 1.8 nm per mm slit opening and the photodetector is a solid-state GaAs single photon counter (Hamamatsu model H7421-50). The manufacturer of this photodetector claims that it responds with excellent linearity up to its saturation limit of 1.6 million counts per second.

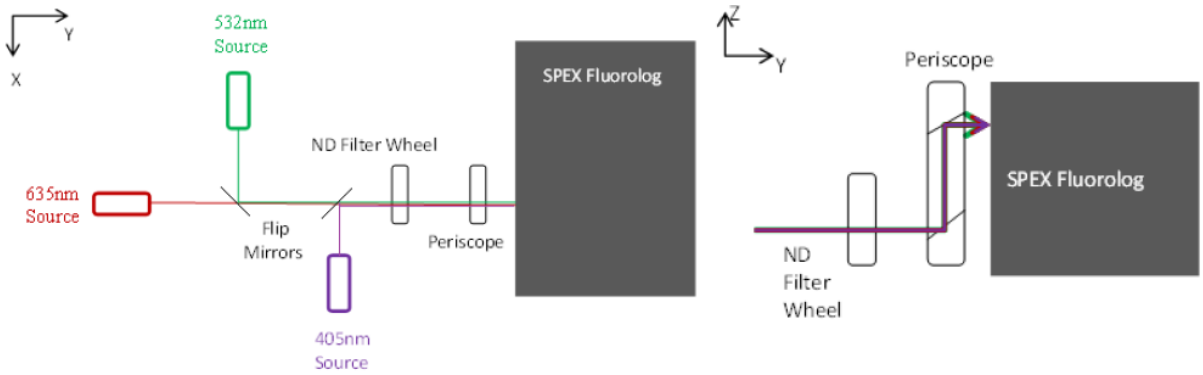

Figure 2.1: *Experimental setup of SPEX Spectrofluorometer.*

The manufacturer-provided sample holder in the SPEX apparatus was designed for a

1 cm × 1 cm cuvette. Since molecular oxygen is a known triplet quencher,[141] solution-phase upconverted fluorescence spectroscopy was performed in a custom-made 1 cm × 1 cm quartz cuvette with an attached bulb that can easily be connected to a vacuum line to facilitate degassing of the solution. Because the standard high-vacuum cuvette is 1 cm × 1 cm and excitation occurs at approximately the center of the solution, the photoluminescence must pass through 0.5 cm of solution before it can reach the detector. For samples with a small Stokes' shift and large optical density, reabsorption effects are non-negligible. The reabsorption correction method utilized for this apparatus is described in Appendix A.2 for both solution and solid phase. A solid-state sample holder was designed and implemented to facilitate the study of TTA-UC in thin films. This sample holder is shown in Figure 2.2.

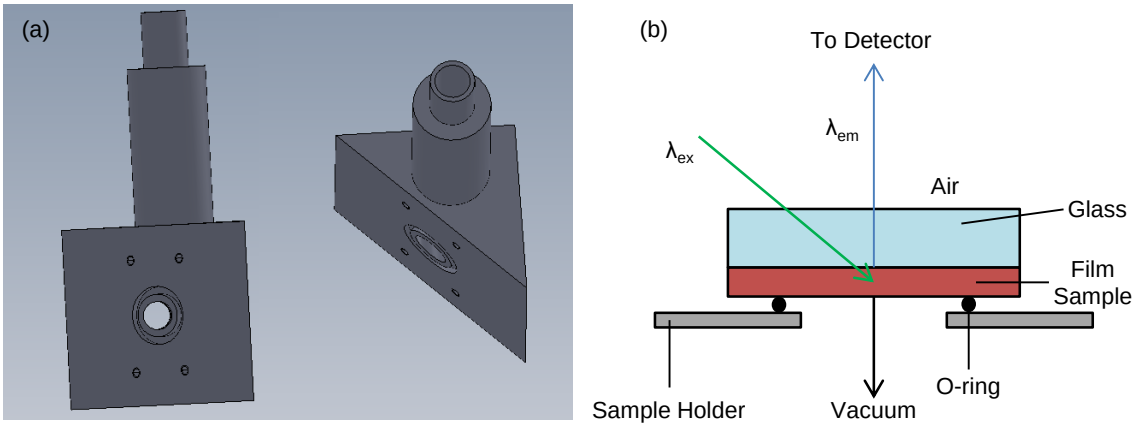

Figure 2.2: *(a) Solidworks schematic of custom designed solid state sample holder; (b) Cartoon depiction of excitation of a thin film sample.*

The solid state sample holder was designed to facilitate upconverted fluorescence measurements of thin films in vacuum, and was a modified version of a brass triangular sample holder reported in the literature.[85] The top of the holder is epoxied to brass piping, which is attached to the existing vacuum system. The film is deposited on a glass slide which is mounted sample side into the vacuum chamber, as shown in Figure 2.2(b). A rubber O-ring is situated around the sample to form an air-tight seal with the glass to maintain vacuum. The apparatus is capable of maintaining pressure below 5 mTorr for a thin film sample. Slide holders have been fabricated to accommodate round slides

1″ in diameter or rectangular slides with a 1″ width and length of at least 0.75″. The backside of the sample holder includes a slide of non-reflective glass held into place with epoxy, allowing the incident photons which pass through the sample to exit the holder, eliminating backside reflection as a source of laser scatter. To further reduce laser scatter, the SPEX internal optics are rotated upon front-face illumination and a notch filter is incorporated into the emission path length prior to the monochromator. This notch filter is easily substituted as appropriate.

The laser excitation sources currently in operation are a 635 nm diode, a 532 nm frequency-doubled Nd:YAG, and a 405 nm diode with nominal powers of 5 mW, 24 mW, and 8 mW, respectively. The benefit of a three-laser system in upconverted fluorescence studies in metalloporphyrins is the ability to observe Soret (blue) emission via NCPU and verify its source by swiftly changing excitation sources to observe Soret emission via direct excitation. The excitation sources were chosen for the model system of homomolecular TTA in ZnTPP, but can easily be substituted as the model system requires. The lasers were aligned individually such that each passes through a pair of neutral density filters before passing through the center of the sample. Flip mirrors have been installed to facilitate rapid changes between laser sources without realignment. Neutral density filters are situated on a pair of wheels such that the excitation power delivered to the sample can be modified with a turn of either filter wheel. A detailed list of normalized apparent excitation powers is outlined in Table 2.1. The values in Table 2.1 are specific to the 532 nm excitation source, and the relative effect of the density filters on each laser is wavelength-dependent. Thus the power must be measured *in situ* in the sample chamber for each laser. In addition, *in situ* measurements will account for fluctuations in an excitation source through time.

The ability to do excitation power-dependent emission spectroscopy is a necessary characterization requirement for NCPU via TTA. These studies allow the dominant kinetic regime for TTA to be determined, as described in Section 1.3.2. The linearity

claims of the photodetector were tested using the singlet emission of ZnTPP in *N,N*-dimethylformamide (DMF). Since the fluorescence spectra analysed are one photon processes, the integrated fluorescence intensity should increase linearly with excitation power. Similarly, the fluorescence intensity at any wavelength that is far removed from filter effects should vary linearly with excitation power. The results are plotted in Figure 2.3. Similar studies verified the detector manufacturer's claim of linearity up to the saturation limit, 1.6 million counts per second.

Table 2.1: Effect of Neutral Density Filters using the 532 nm Excitation Source

Wheel Setting	**Relative Intensity**	**Wheel Setting**	**Relative Intensity**
11	1.00	53	0.0026
21	0.68	54	0.00081
12	0.55	15	0.00071
31	0.39	25	0.00051
22	0.38	35	0.00027
13	0.32	45	0.00013
41	0.26	61	0.000062
23	0.23	16	0.000055
32	0.23	26	0.000028
42	0.14	36	0.000028
33	0.13	46	0.000028
14	0.099	55	0.000028
43	0.082	56	0.000028
24	0.071	62	0.000028
34	0.040	63	0.000028
44	0.025	64	0.000028
51	0.0084	65	0.000028
52	0.0047	66	0.000028

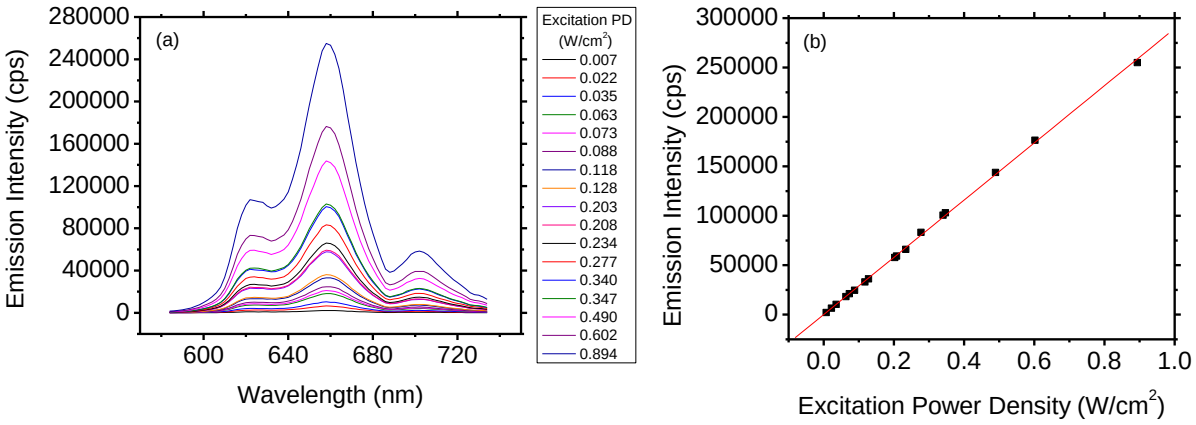

Figure 2.3: *532 nm excitation power-dependent S_1 (a) fluorescence spectrum; and (b) peak fluorescence intensity of 1 mM ZnTPP in DMF. Spectral bandwidth was 1.8 nm, ensuring that the 658 nm emission peak in (a) was well away from any laser or filter effects prior to analysis in (b).*

For meaningful quantitative analysis, the photoluminescence data must be corrected for variations in photodetector sensitivity as a function of wavelength. The manufacturer's sensitivity data is fit to a polynomial as shown in Figure 2.4 and Table 2.2. The detector quickly loses sensitivity beyond 800 nm, but the polynomial fit in the region of 380 - 800 nm is sufficient for modelling in this region.

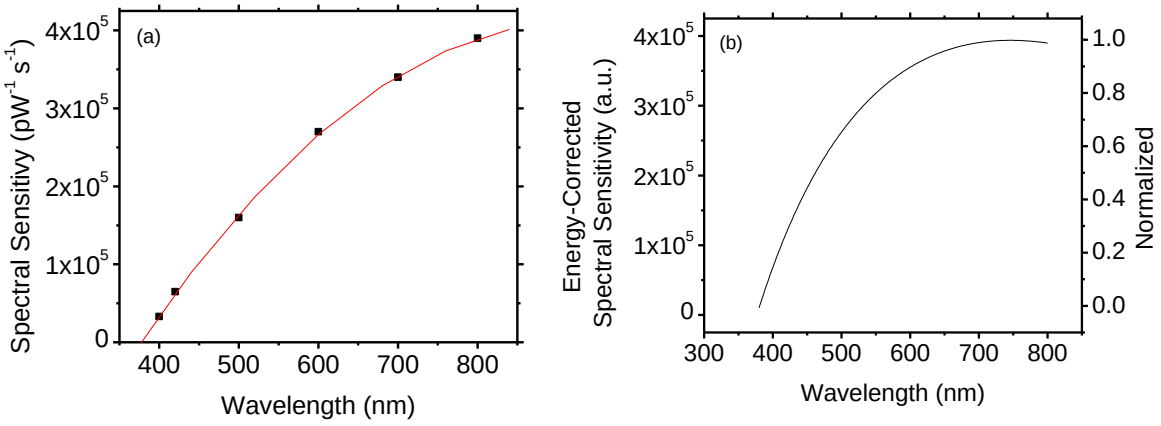

Figure 2.4: *(a) Manufacturer's data with polynomial fit and (b) energy-corrected model for spectral sensitivity (SS) of solid state GaAs photodetector, Hamamatsu H7421-50. The polynomial fit in (a) has equation* $SS = -1.36\lambda^2 + \left(2.52 \cdot 10^3\right)\lambda - \left(7.57 \cdot 10^5\right) pW^{-1}s^{-1}$.

Table 2.2: Spectral Sensitivity of Hamamatsu H7421-50 Photodetector

Wavelength (nm)	**Spectral Sensitivity ($\mathbf{pW^{-1}\ s^{-1}}$)**	**$\mathbf{E}_{photon}$ (J)**	**Quantum Efficiency**
400	33000	5.0×10^{-19}	0.016
420	65000	4.7×10^{-19}	0.031
500	160000	4.0×10^{-19}	0.064
600	270000	3.3×10^{-19}	0.089
700	340000	2.8×10^{-19}	0.096
800	390000	2.5×10^{-19}	0.097
900	2800	2.2×10^{-19}	0.00062

The detector sensitivity is given in units of inverse energy, or counts per unit energy. The quantum efficiency (QE) can be calculated as the product of the detector sensitivity and the energy of a photon at each wavelength. The calculation is outlined in Equation 2.1 and summarized in Table 2.2. At 800 nm,

$$\begin{aligned} SS &= 3.9 \times 10^5 \ \frac{counts}{pWs} = 3.9 \times 10^{17} \ \frac{counts}{Ws} = 3.9 \times 10^{17} \ \frac{counts}{Js^{-1}s} \\ E_{800nm} &= \frac{hc}{\lambda} = \frac{6.626 \times 10^{-34} Js \times 2.998 \times 10^8 m/s}{800 \times 10^{-9} m} = 2.5 \times 10^{-19} \frac{J}{photon} \\ QE_{800nm} &= 3.9 \times 10^{17} \ \frac{counts}{J} \times 2.5 \times 10^{-19} \frac{J}{photon} = 0.097 \end{aligned} \tag{2.1}$$

Table 2.2 states that the photodetector is most efficient at 800 nm, meaning that the apparent photoluminescence intensity at higher energy must be corrected for the relative inefficiency of the photodetector at these wavelengths. This correction will be achieved by normalizing by the energy ratio of the ith wavelength to that which has the highest QE. As per Equation 2.1, the result is a normalization factor equal to the ratio of quantum efficiencies (QE). Equation 2.2 displays this normalization:

$$\begin{aligned} SS_{E-norm} &= (SS_{raw}) \frac{\overline{\nu}_i}{\overline{\nu}_{800nm}} \propto (SS_{raw}) \frac{QE_i}{QE_{800nm}} \\ &= (SS_{raw}) \frac{10^7 \ nm/cm}{\lambda_i} \frac{800nm}{10^7 \ nm/cm} \\ &= (SS_{raw}) \frac{800nm}{\lambda_i} \end{aligned} \tag{2.2}$$

Thus, the spectral sensitivity at each wavelength, i, is energy-corrected through the multiplication of the factor $800/\lambda_i$, where λ_i is in nm. The energy-corrected spectrum is shown in Figure 2.4(b). To account for the variation in quantum efficiencies in a given photoluminescent spectrum, the spectral luminescence is divided by the energy-normalized spectral sensitivity curve shown in Figure 2.4(b).

The spectral bandwidth dependence of Rhodamine 6G fluorescence is shown in Figure 2.5. The red-shift in peak emission in Figure 2.5(a) with increased spectral bandwidth is due to the effects of the 532 nm notch filter situated prior to the emission monochromator, which only affects the spectrum at sufficiently high spectral bandwidths. At wavelengths removed from the notch filter, the effect of increasing bandwidth is a broadening of spectral features. The quadratic bandwidth dependence of integrated fluorescence displayed in Figure 2.5(b) is believed to be due to the Gaussian nature of this peak, and in the region of interest it can be approximated nicely by a second-order polynomial. Thus, an increased spectral width would result in a quadratic increase in the integrated fluorescence.

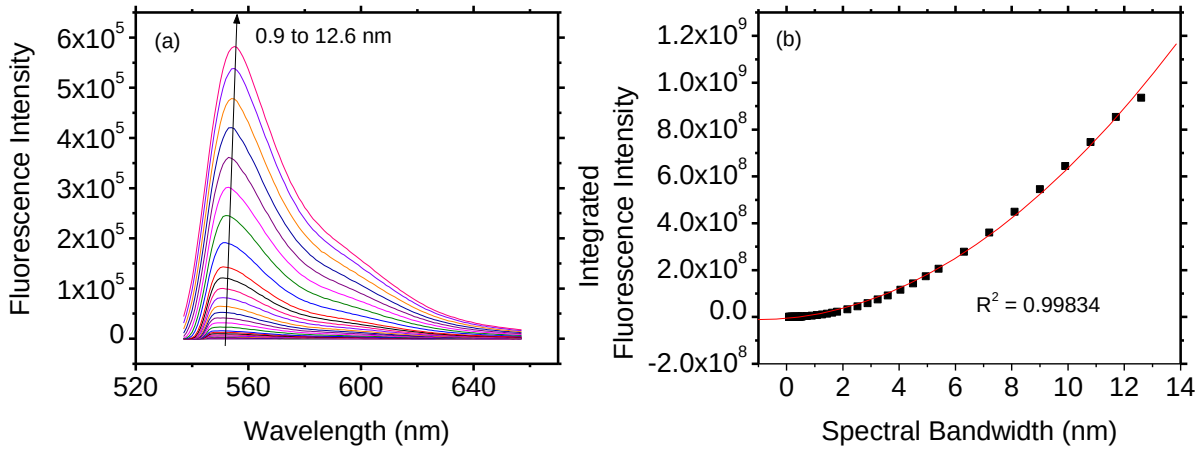

Figure 2.5: *(a) Emission spectrum (truncated on the short wavelength side by the notch filter) and (b) Integrated emission of 1.74 μM Rhodamine 6G in $CHCl_3$ as a function of spectral bandwidth. 532 nm excitation power density was 26.2 $\mu W/cm^2$ in (a), while (b) was obtained by scanning at several excitation powers and normalizing to a common value. The red line in (b) is the second-order polynomial fit.*

Chapter 3

Spectroscopic Studies of ZnTPP in Polymer Matrices

3.1 Introduction to ZnTPP-doped Polymer Systems

Following the design and implementation of the SPEX Fluorolog Spectrofluorometer described in Chapter 2, the apparatus needed to be tested using a well-studied model system. Zinc(II) tetraphenylporphyrin (ZnTPP) was chosen as the model system due to numerous reports in the TTA literature in both homomolecular[53;60;106;115] and heteromolecular[53;142;143] systems. O'Brien *et al.*[60] demonstrated homomolecular TTA by ZnTPP embedded in a PMMA matrix, which was utilized as an experimental starting point in this study.

The current study explores systems of both molecular diffusion-driven and aggregation-driven upconverted fluorescence via homomolecular TTA-UC in ZnTPP. Thin films were obtained by embedding ZnTPP into a variety of polymers with varying glass transition temperatures. Variation of glass transition temperature determines the driving force for TTA as described in Section 1.5. The polymers utilized are shown in Figure 3.1 and their glass transition temperatures are given in Table 3.1. PMMA and PEG data in Table 3.1 were obtained from Sigma-Aldridch.

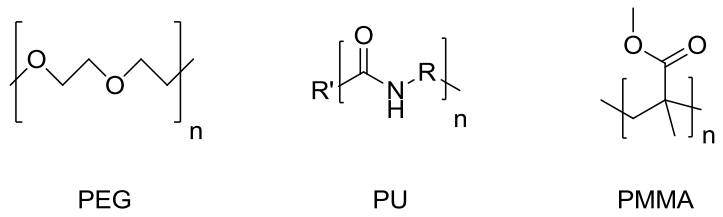

Figure 3.1: *Molecular structures of polymers utilized as matrices for TTA-UC in thin films.*

Table 3.1: Material Properties of Polymers Used

Acronym/Identifier	**Polymer Name**	**Glass Transition Temperature (^{o}C)**
PMMA	Poly(methyl methacrylate)	105
Texin 270	Thermoplastic poly(urethane)	21 [58]
Texin 285	Thermoplastic poly(urethane)	-42 [58]
Tecoflex EG-80A	Thermoplastic poly(urethane)	-70 [58]
PEG	Poly(ethylene glycol)	-66

The requirements of the host polymer are straightforward. First, the polymer must not significantly alter the energetics of the upconversion system, or act as an energy acceptor. Finally, there must not be coordination between dye and polymer. The first condition would introduce an obvious energy sink into the system that would oppose TTA-UC, while the second condition causes dye molecules to be held far apart such that short-range DET cannot occur. [53]

ZnTPP possesses attractive photophysical properties for the study and understanding of hetero- and homomolecular TTA. Noting that fluorescence QYs are solvent-dependent, reported values for S_1 fluorescence, intersystem-crossing, and S_2 fluorescence in ZnTPP are $\sim$0.04,[60;144] $\sim$0.90,[53;145;146] and 0.0011 [53;147–150], respectively. UV-visible excitation of ZnTPP provides the opportunity to monitor both the prompt S_1 and TTA-induced (delayed) upconverted S_2 fluorescence in homomolecular systems. This provides a metric for determining the power dependence of upconverted fluorescence and the dominant annihilation regime, as described in Section 1.3.2. It also provides the ability to observe the simultaneous growth of upconverted fluorescence and quenching of prompt fluorescence in heteromolecular systems.

The efficient ISC in metalloporphyrins is a result of enhanced spin-orbit coupling.[25;50;151] The lifetimes of the S_1, S_2, and T_1 states in ZnTPP are on the order of ns, ps, and ms, respectively.[53;145;146;152–155] Since the T_1 lifetime is orders of magnitude greater than that of the S_1 state, energy pooling occurs in the triplet manifold. This is a result of rapid absorption and ISC into a relatively long-lived triplet state. These long-lived triplet molecules are available for TTA or TTET. A discussion of energy pooling in the triplet manifold of organometallics is given in the literature.[71]

ZnTPP Q-band (S_1) and Soret-band (S_2) excitations are $\pi \rightarrow \pi^*$ transitions.[156;157] The porphyrin is formed through the coordination of the pyrrole rings to the Zn^{2+} ion, by which the Zn^{2+} ion accepts the electron lone pair from the N atom in the pyrrole moieties in the plane of the ring. This porphyrin ring is a highly conjugated system.

ZnTPP is a relatively efficient donor of electrons or electronic energy.[158–160] This potential for electron donation makes ZnTPP derivatives attractive materials for photovoltaic applications. The carboxylated derivative zinc tetra(carboxyphenyl)porphyrin, ZnTCPP, has been studied for use in DSSCs. It has been shown that functionalization of ZnTPP with carboxylate allows for direct binding to a semiconductor[161–165] without greatly affecting the ground-state energetics of the phorphyrin.[166–169] Electron injection from electronically excited ZnTCPP (or similar bridged ZnTPP derivatives) to titanium dioxide has been explored for DSSC applications.[105;161–163;166;170–173]

A detailed review was published on the use of porphyrins in DSSCs[174] but the potential for TTA-UC in systems containing ZnTCPP has not been reported. A recent study reports the use of ZnTPP as sensitizer in BHJ solar cells.[158] The report was not concerned with the study of TTA-UC, but was focused on electron transfer from the S_1 state of ZnTPP to the fullerene-derivative PCBM. This article was followed by a fundamental study of the potential for TTA-UC utilizing ZnTPP as sensitizer and C_{60} fullerene as emitter,[143] a direct exploration of ZnTPP-sensitized TTA-UC with BHJ applications.

The molecular structures for ZnTPP and ZnTCPP are shown in Figure 3.2.

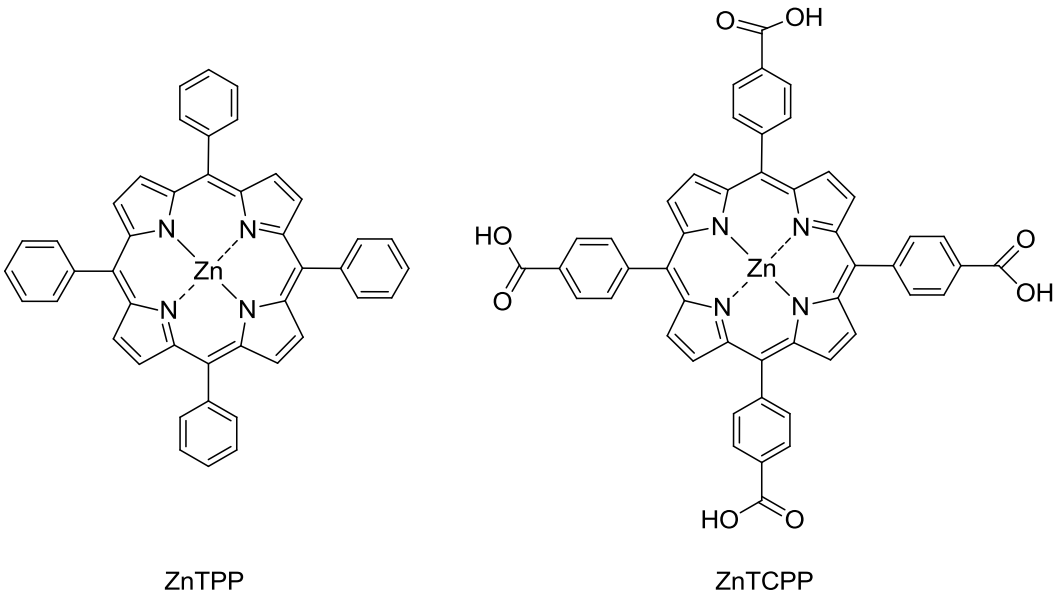

Figure 3.2: *Molecular structures of porphyrins studied.*

Practical applications of TTA-UC in photovoltaics requires the use of thin film systems. When ZnTPP is cast from solution, the solvent is evaporated away leaving aggregated ZnTPP. Upconverted fluorescence in this environment is diminished by a significant degree of self-quenching. The degree of aggregation can be manipulated by casting a film of ZnTPP in polymer matrix - effectively a polymer doped with the upconverting dye. Suitable polymer candidates for homomolecular TTA in ZnTPP were selected based on relevant results from the literature.

3.2 Solution-Phase and Thin Film ZnTPP

Preliminary experiments included solution-phase and thin film steady-state spectroscopic studies of homomolecular TTA-UC in ZnTPP. The purpose of these experiments was to validate the performance of the SPEX Fluorolog Spectrofluorometer. This was achieved by comparing the data from the well-studied ZnTPP system to those previously

reported in the literature.

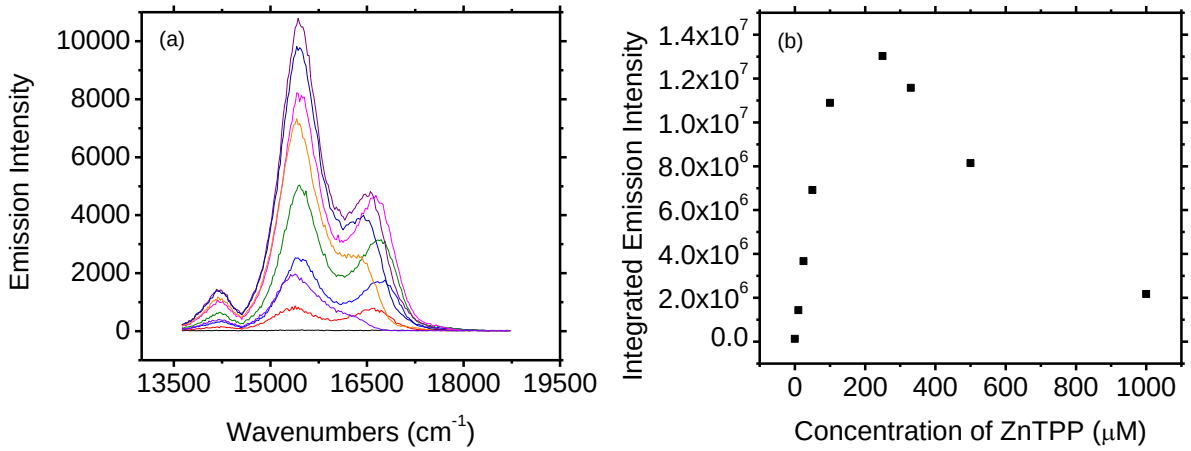

Figure 3.3: *Variations in S_1 (a) fluorescence spectrum; and (b) integrated fluorescence of ZnTPP in toluene as a function of concentration. Excitation was 1 mW 532 nm laser and emission spectral bandwidth was 0.2 nm.*

Figure 3.3(a) shows the S_1 fluorescence spectrum of ZnTPP in toluene. The peaks at about 16 600 and 15 400 cm^{-1} match those in the literature[53;60;141;147–150;152;175–179] in various solvents, while the slight peak at about 14 200 cm^{-1} is an artefact. The origin of the artefact is some undetermined inorganic source within the apparatus. Figure 3.3 provides evidence of ZnTPP self-quenching through the obvious decrease in integrated emission intensity at high ZnTPP concentrations. In the absence of intermolecular effects such as aggregation or self-quenching, the integrated emission intensity in (b) is expected to increase linearly with concentration at low concentrations of ZnTPP. At some threshold concentration, intermolecular interactions become significant. These introduce additional non-radiative relaxation pathways that result in a deviation from linearity. At very high concentrations, fluorescence self-quenching is non-negligible, accounting for the apparent decrease in integrated fluorescence. Porphyrin self-quenching in solution and solid phase has been discussed in the literature.[66]

Intermolecular interaction is a requirement for TTA-UC - excited triplets must be within close proximity for molecular orbital overlap in order for TTA to occur. The active species must be sufficiently concentrated for a significant proportion of excited triplets to exist within a diffusion length of another excited triplet, but dilute enough to

reduce the probability of intermolecular interactions leading to non-radiative decay of the excited state. This optimum concentration is a direct function of molecular environment as physical state of the active species has a dramatic effect on the excited state diffusion length. In solution the molecules can diffuse quite readily, increasing the probability of intermolecular interactions at the concentrations studied in Figure 3.3. Diffusion-driven intermolecular interactions is a possible explanation for the absence of noticeable fluorescence via TTA-UC at the spectral bandwidth utilized in Figure 3.3. A slight peak was found in a similar study of 1 mM ZnTPP in DMF that may be attributed to TTA-UC. This study required a significant spectral bandwidth of 14.4 nm that reflects an inefficient TTA-UC process. The inefficiency is likely due to a combination of self quenching and solvent coordination.

3.3 ZnTPP-doped Thermoplastic Polyurethane Films

Heteromolecular TTA-UC in a PU matrix has been reported in the literature.[55;57;58] For this reason PU was selected for the study of homomolecular TTA in ZnTPP films. The fluorescence spectra are shown in Figure 3.4 for films comprised of ZnTPP-doped PU and ZnTPP in the absence of polymer matrix. ZnTPP films were prepared by spin-casting a single layer from 50 μL of 5 mM ZnTPP in toluene at 1000 rpm onto a clean glass slide. ZnTPP:PU films were drop-cast onto a clean glass slide from solution with 3% (w/w) ZnTPP:PU in DMF. ZnTPP had a concentration of 2 mM in the precursor solution. Significant S_1 fluorescence was measured in these films while S_2 fluorescence via TTA-UC was not observed. Separate experiments varying the dye loading, casting method, and monochromator spectral bandwidth yielded data similar to Figure 3.4 with no observable upconverted fluorescence.

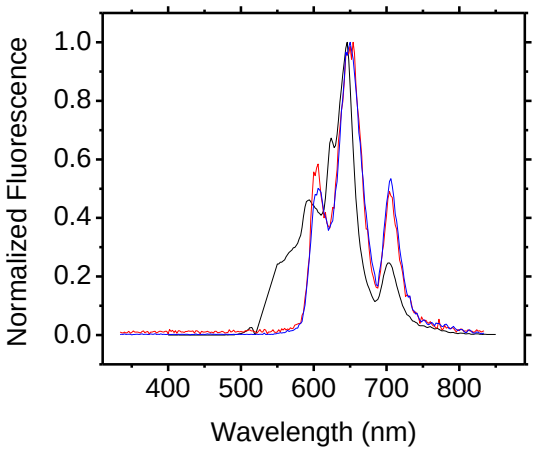

Figure 3.4: *Normalized fluorescence of ZnTPP film (black) and ZnTPP-doped PU film (red, blue) following 532 nm excitation. Spectral bandwidths for the specific data shown were 5.4 nm and 1.8 nm in the absence and presence of PU matrix, respectively. Peak intensities were on the order of 1400, 6400, and 65 000 counts for the red, blue, and black spectra, respectively.*

Sugunan *et al.*[53] investigated the effect of solvent coordination on ZnTPP Soret fluorescence via homomolecular TTA-UC. In this work, the authors demonstrated experimentally how TTA-UC was suppressed in coordinating solvents and supported those results with theoretical calculations based on the required distances for DET. The proposed mechanism is solvent coordination to the axial position of the Zn^{2+} ion. These coordinated solvent molecules provide a steric barrier to TTA-UC as the excited ZnTPP triplets are held apart at a distance greater than that necessary to undergo efficient DET. This proposed mechanism was verified by demonstrating that the quenching of ZnTPP in coordinating solvents sufficiently matched that observed by titrating ZnTPP in degassed benzene with pyridine, a known coordinating material.

An analogous explanation is proposed in the present work, as the N atom in the PU structure (see Figure 3.1) is believed to be coordinating to the Zn^{2+} ion. Thus, PU was deemed an unsuitable host polymer for homomolecular TTA-UC using metalloporphyrins. PU has been reported as a suitable host matrix[55;57;58] for heteromolecular systems. In these studies, an advantageous sensitizer-emitter pair is chosen such that the emitter material has a fluorescence QY approaching unity. In the present study, the S_2 fluorescence QY of ZnTPP is on the order of 10^{-3}. This 1000-fold difference in fluorescence QY is

a possible explanation for why detectable upconverted fluorescence was not observed in the present study despite the previous literature reports.

3.4 ZnTPP-doped Poly(methyl methacrylate) Films

Since PU was an unsuitable host matrix for homomolecular TTA in ZnTPP, it was replaced with a suitable polymer. PMMA has been shown to support homomolecular TTA in ZnTPP.[53] The proof-in-principle experiments from that report were utilized as the experimental starting point in the present work. These slides were fabricated by drop-casting a film of 3.5% (w/w) ZnTPP in PMMA from DMF onto a glass slide and drying under low heat. The S_1 fluorescence spectrum is shown in Figure 3.5(a). The figure also shows a broad peak in the Soret region at high spectral bandwidths, attributed to upconverted fluorescence. This peak was confirmed to be TTA-UC by studying its oxygen dependence. In (c), the sample was pumped down to vacuum at time t_0. The vacuum was released for the first ∼12 minutes, allowing oxygen to diffuse into the film. The sample was then pumped back down to vacuum from t = 12 to 20 mins before the vacuum was released again. Since oxygen is a known triplet quencher,[115;141] this study in consistent with the notion that the observed Soret peak is due to TTA-UC.

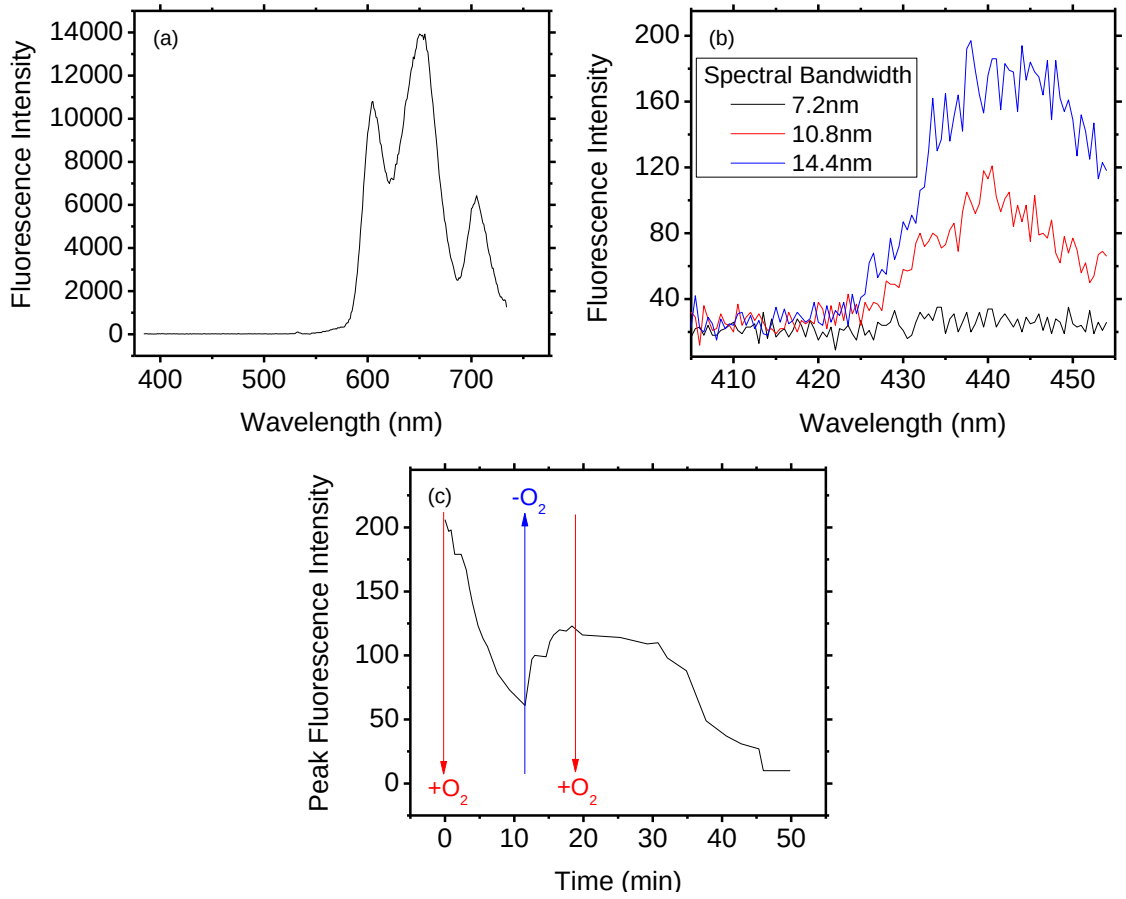

Figure 3.5: *(a) S_1 fluorescence spectrum; (b) spectral bandwidth-dependent upconverted fluorescence; and (c) oxygen dependence of upconverted fluorescence of 3.5% ZnTPP in PMMA drop-cast film. Excitation was at 532 nm and 89 mW/cm^2. Spectral bandwidth in (a) was 3.6 nm. The intensity difference between 0 min and 30 min in (c) is attributed to photodegradation.*

Following the oxygen dependence study, a series of experiments were performed in effort to optimize the upconverted fluorescence in this system. First, the dye-loading ratio was varied significantly in ZnTPP-doped PMMA films. This study effectively explores the upconverted fluorescence as the degree of ZnTPP aggregation is varied. These films were produced by spin-casting ZnTPP:PMMA from DMF at 1000 rpm. Ten consecutive layers were cast onto pre-cleaned slides and films were dried at 100°C. The upconverted fluorescence of these films was scaled by a constant equal to the integrated area of the Soret absorption band. It was believed that this method eliminated the effect of overall variations in dye concentration in the films and isolated the effect of variations in the degree of aggregation. The scaling constants are given in Table 3.2. The reported dye-loading ratios refer to the solution from which the sample is spin-cast. Due to differences

in solubility of the porphyrin and polymer in DMF, they will not be deposited in the film at the same rate during casting. Determining the precise dye loading concentrations in the film would require supplementary techniques such as x-ray fluorescence spectroscopy.[180]

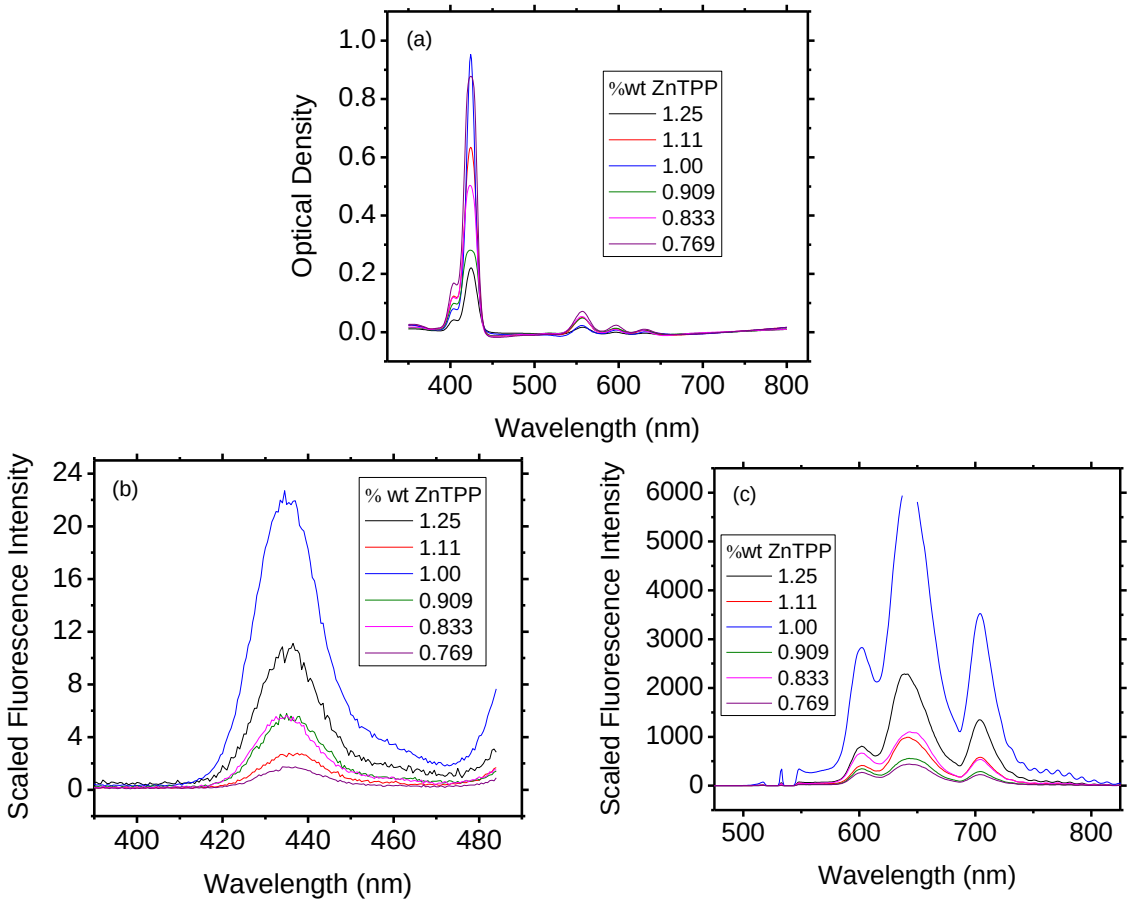

Figure 3.6: *(a) Optical density; (b) scaled upconverted fluorescence; and (c) scaled S_1 fluorescence of films with varying concentrations of ZnTPP in PMMA. Spectral bandwidths were as follows: (a) 2 nm; (b) 14.4 nm; and (c) 1.8 nm. The break in (c) was required to prevent detector saturation. Spectra are not corrected for reabsorption.*

Table 3.2: Correction Factors for ZnTPP:PMMA Films in Figure 3.6

Wt % ZnTPP:PMMA	**Correction Factor**
1.25	73
1.11	201
1.00	270
0.909	142
0.833	188
0.769	299

As seen in Figure 3.6(a), the upconverted fluorescence initially increases with dye

loading concentration up to 1%, after which it decreases. This result is reasonable in an aggregation-driven TTA-UC system. At very low dye-loading, excited molecules are separated by a distance greater than that required for DET within the triplet lifetime. Thus, upconverted fluorescence is not observed. Aggregation increases with dye loading, increasing the probability that two triplet excitons are created in sufficiently close proximity for DET to produce observable TTA-UC. However, significant aggregation also increases the probability of reabsorption effects or self quenching.

The excitation power dependence of prompt and upconverted fluorescence are shown in Figure 3.7 for the film with 1% ZnTPP:PMMA. This sample was chosen because it displayed the greatest upconverted fluorescence in the dye-loading study. In these studies, excitation power was varied over the same range while prompt and upconverted fluorescence were separately monitored. A study of this kind is used to determine the dominant annihilation kinetic regime as detailed in Section 1.3.2.

The slope of 1.30 $\pm$ 0.01 in Figure 3.7 demonstrates that TTA-UC in this sample occurs under conditions that lie between the two kinetic limits, and somewhat nearer the strong annihilation kinetic regime. This notion seems appropriate for the present case, in which a degree of pre-aggregation is required to observe upconverted fluorescence. In this sample the annihilation pathway counts for a considerable fraction of the triplet decays relative to the undesired pseudo first-order quenching pathways. Such conditions are desirable because they lead to the maximum TTA-UC efficiency achievable in the system.

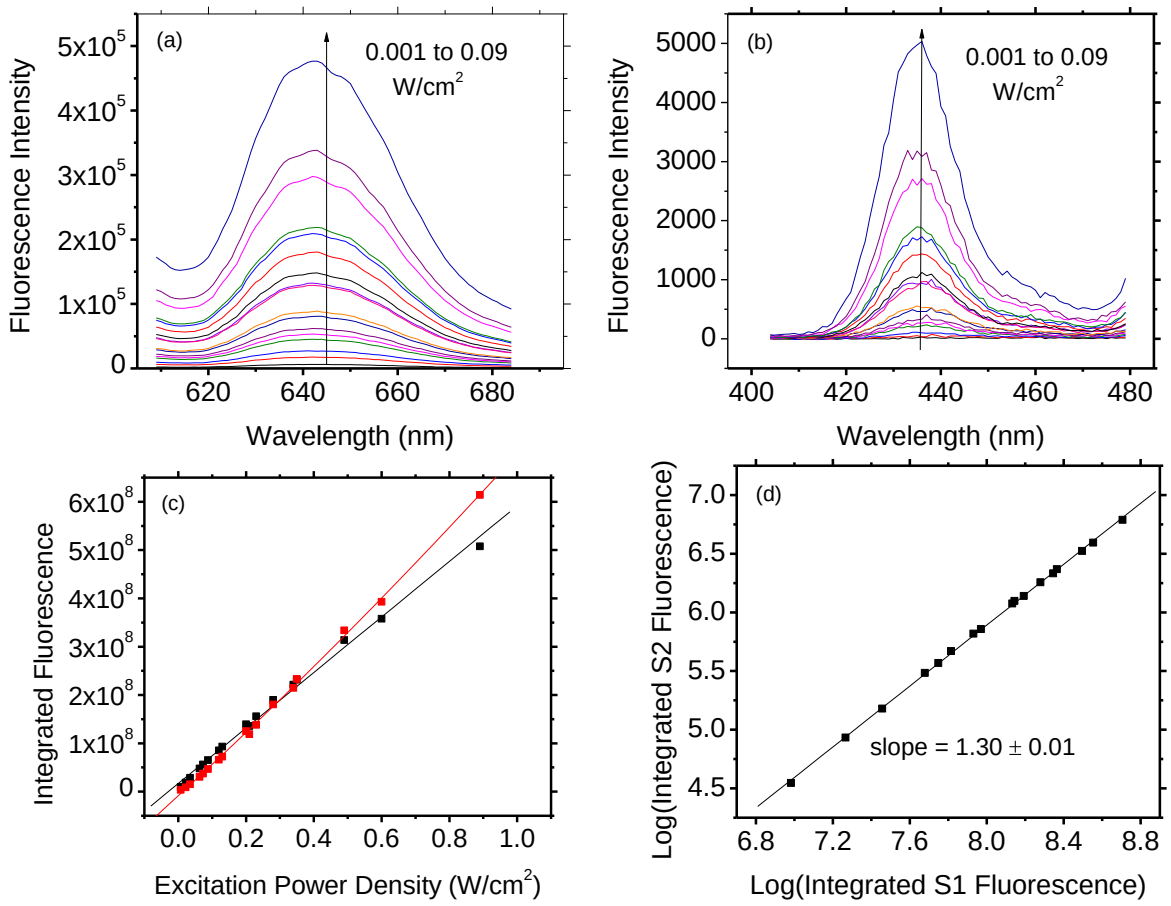

Figure 3.7: *(a) S_1 fluorescence; and (b) S_2 upconverted fluorescence spectra of a 1% wt ZnTPP in PMMA spin-cast film. (c) Excitation power-dependence of ZnTPP integrated direct fluorescence (black) and upconverted fluorescence (red); (d) Variation in upconverted fluorescence with scaling S_1 fluorescence by changing excitation power. In (c), the black line is the linear fit of the S_1 fluorescence data while the red curve is the quadratic fit of the upconverted fluorescence data. The upconverted fluorescence in (c) has been scaled by 100. Spectral bandwidths in (a) and (b) are 0.9 nm and 14.4 nm, respectively.*

Figure 3.8 shows the Soret fluorescence of the 1% wt ZnTPP:PMMA film from two different excitation sources. The violet curve in Figure 3.8 is the prompt Soret fluorescence following Soret (405 nm) excitation, while the green curve shows upconverted fluorescence following 532 nm excitation. Figure 3.8 demonstrates that homomolecular TTA-UC results in delayed fluorescence from the S_2 band of ZnTPP due to its agreement with prompt S_2 fluorescence following Soret excitation. The difference in peak width and the slight red-shift in peak wavelength are attributed to the substantially greater spectral bandwidth utilized in the TTA-UC studies. The effect of bandwidth on fluorescence spectral data is discussed in Section 2.2.

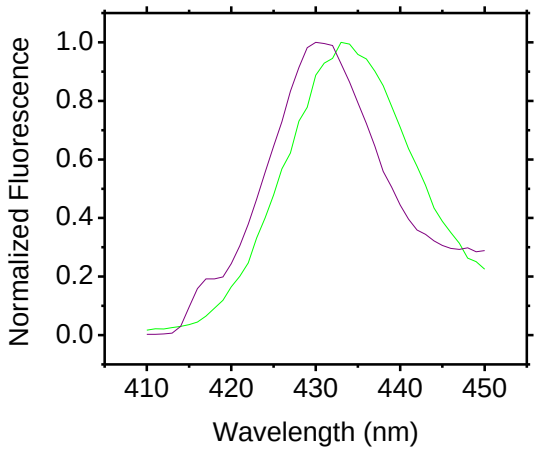

Figure 3.8: *Soret fluorescence of 1%wt ZnTPP:PMMA film via Soret excitation (violet) and upconverted fluorescence via 532 nm excitation (green). Spectral bandwidths are 1.8 nm for direct fluorescence and 14.4 nm for upconverted fluorescence.*

The final study of ZnTPP-doped PMMA films observed the variation in upconverted fluorescence as a function of film thickness. The absorption and fluorescence spectra are shown in Figure 3.9 while Figure 3.10 plots fluorescence as a function of film thickness. Films were prepared by spin-casting ZnTPP:PMMA solution onto clean, dry slides. For these films, 200 μL increments of 1%wt ZnTPP in PMMA were cast from DMF solution at 2000 rpm. The sample films were varied from 1 to 8 layers to facilitate a significant difference in thickness. Drop size was increased substantially in this film preparation to promote film uniformity. Films were cast and dried at ambient temperature.

The films prepared for the dye-loading experiment in Figure 3.6 were white and opaque, indicative of a highly crystalline PMMA domain that can be attributed to drying under moderate heat. The samples prepared here were transparent, indicative of an amorphous PMMA film. This change in PMMA crystallinity suggests an explanation for the blue-shift in ZnTPP absorption and fluorescence spectra in Figure 3.9 relative to the previous figures. Annealing has been reported to enhance aggregation of porphyrin moieties in heterogeneous films,[158;181] a possible explanation for the red-shift in the heat-dried films relative to those presented here.

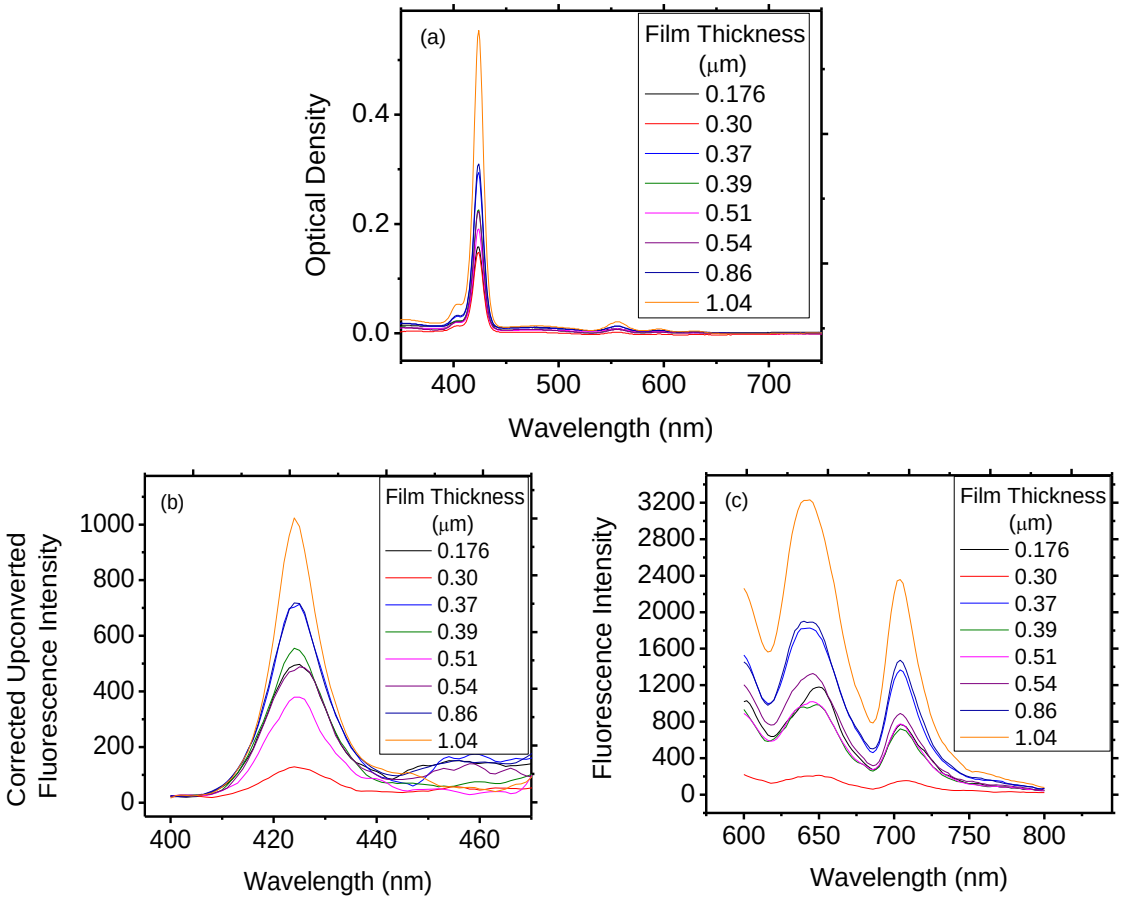

Figure 3.9: *(a) Absorption; (b) reabsorption-corrected upconverted fluorescence; and (c) prompt S_1 fluorescence of ZnTPP:PMMA films as a function of film thickness. Spectral bandwidths were as follows: (a) 2 nm; (b) 14.4 nm; (c) 1.8 nm.*

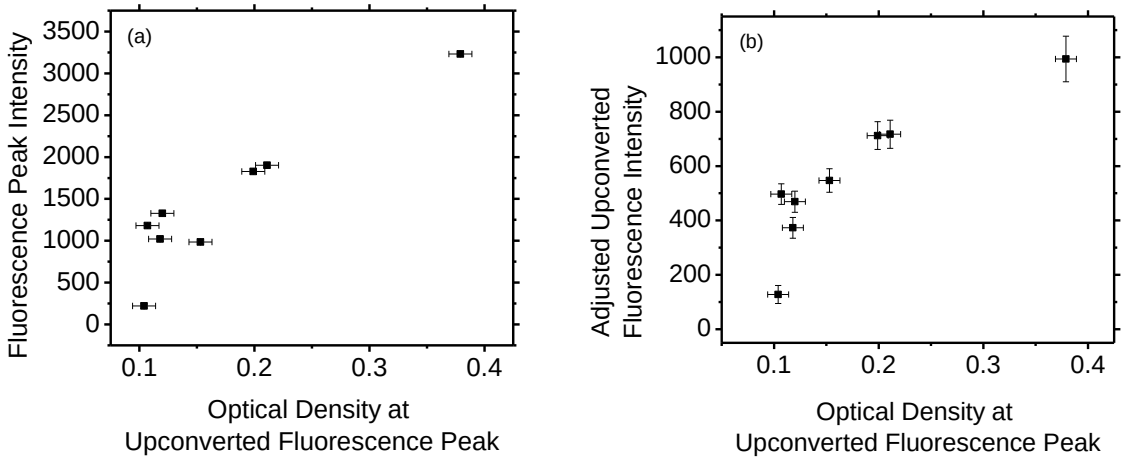

Figure 3.10: *Variations in (a) S_1 peak fluorescence; and (b) reabsorption-corrected upconverted peak fluorescence in a ZnTPP:PMMA film as a function of film thickness. The utilization of film optical density as the independent variable assumes a consistent film composition.*

Assuming a consistent film composition, the total amount of dye present in the film

varies linearly with thickness. Optical density is directly proportional to film thickness via Beer's Law. Hence the use of film optical density as the independent variable is justified in Figure 3.10, reducing the discrepancy in the amount of dye in each film. This discrepancy arises from poor reproducibility of films prepared via spin-casting. Since aggregation-driven TTA-UC in the ZnTPP:PMMA is toward the strong annihilation regime, as demonstrated by Figure 3.7, one would expect upconverted fluorescence intensity to increase linearly with film thickness. Figure 3.10(a) shows the thickness-dependence of S_1 fluorescence while (b) shows the thickness-dependence of upconverted S_2 fluorescence.

The upconverted fluorescence intensity demonstrates a non-linear dependence on film thickness. This relation suggests that the kinetic behaviour of the system at the film surface may differ from that of the bulk film. Specifically, the sub-linear behaviour suggests that upconverted fluorescence by TTA-UC is less efficient in the bulk material than near the surface. Further testing is required to fully understand the dependence of film thickness on upconverted fluorescence. Such experiments would require more precise film preparation methods and experimental techniques. Spin-cast films are not reproducible in terms of thickness or composition. More sophisticated preparation methods could confirm the sub-linear relation observed in Figure 3.10.

3.5 ZnTPP-doped Poly(ethylene glycol) Films

PEG (MW = 10 kDa) was explored as a potential host matrix for TTA-UC on account of its low glass transition temperature, which would facilitate diffusion-driven TTA-UC. Furthermore, its water solubility is desirable for more environmentally-friendly manufacturing of UC-active PEG-based films. Films for the proof of principle studies were fabricated by drop-casting 1%wt ZnTPP:PEG from chloroform solution and drying at 35°C. Phase separation was not observed in these films. Figure 3.11 compares the fluo-

rescence spectra of the drop-cast ZnTPP:PEG and ZnTPP:PMMA films. The absolute peak intensities and peak wavelengths are given in Table 3.3. The S_1 and S_2 fluorescence bands are red-shifted equally in the PEG matrix relative to the PMMA. This consistent shift suggests a change in the electronic environment of the porphyrin. Possible reasons for this shift will be discussed below. The peak at 705 nm matches for the two samples, further pointing to an artefact contained somewhere in the apparatus. The ZnTPP:PEG film had a significantly higher ZnTPP concentration than its PMMA counterpart, justified by a S_1 fluorescence intensity that is an order of magnitude greater in the PEG-based film. However, S_2 upconverted fluorescence intensity was a factor of two smaller than in the PMMA film. Given the significant difference in dye loading, this PEG film exhibits a far less efficient TTA-UC process. Possible reasons for this discrepancy will be discussed.

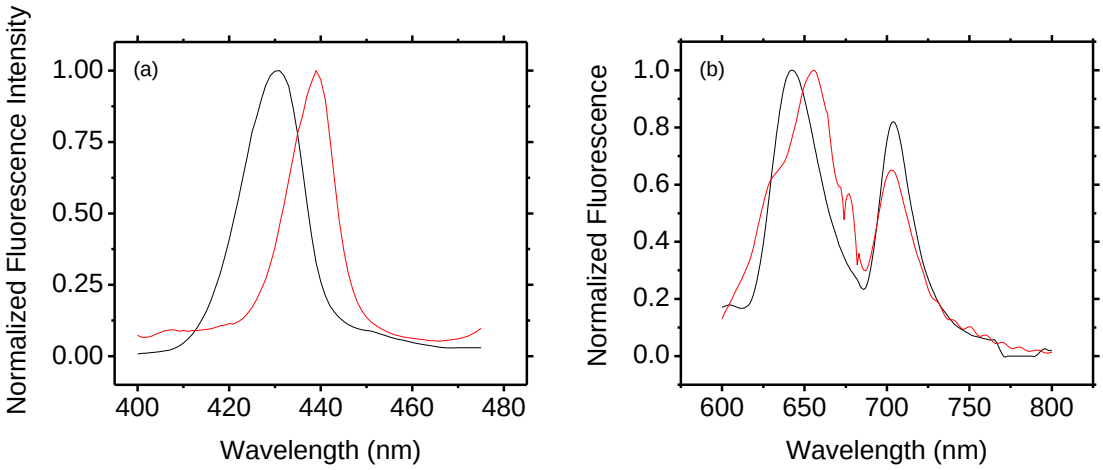

Figure 3.11: *Separately normalized (a) upconverted fluorescence and (b) direct fluorescence spectra of 1%wt ZnTPP:PEG (red) and 3.5% wt ZnTPP:PMMA drop-cast films using a 144 mW/cm^2 532 nm excitation. Spectral bandwidths are: (a) 14.4 nm; (b) 1.8 nm. Spectra are not corrected for reabsorption.*

Table 3.3: Emission Spectral Data for ZnTPP:Polymer Drop-cast Films

		ZnTPP:PMMA	**ZnTPP:PEG**
S_2	Wavelength	431 nm	443 nm
	Intensity	2400 cps	1200 cps
S_1	Wavelength	643 nm	656 nm
	Intensity	36000 cps	285000 cps

The effect of dye-loading on upconverted fluorescence in ZnTPP:PEG films is shown in Figure 3.12. Films were fabricated by spin-casting 5 layers at 2000 rpm onto clean,

dry slides at room temperature. Drop size was sufficiently large as to achieve reasonably uniform films. Reabsorption-corrected spectra in (c) were scaled by the integrated Soret absorption band and replotted in (d) to normalize out the effect of changing dye concentration in the films. The dependence of TTA on excitation intensity was not obtained due to significant photodegradation of the ZnTPP:PEG films. Obvious discolouration of the sample was apparent at the low excitation power utilized in these studies.

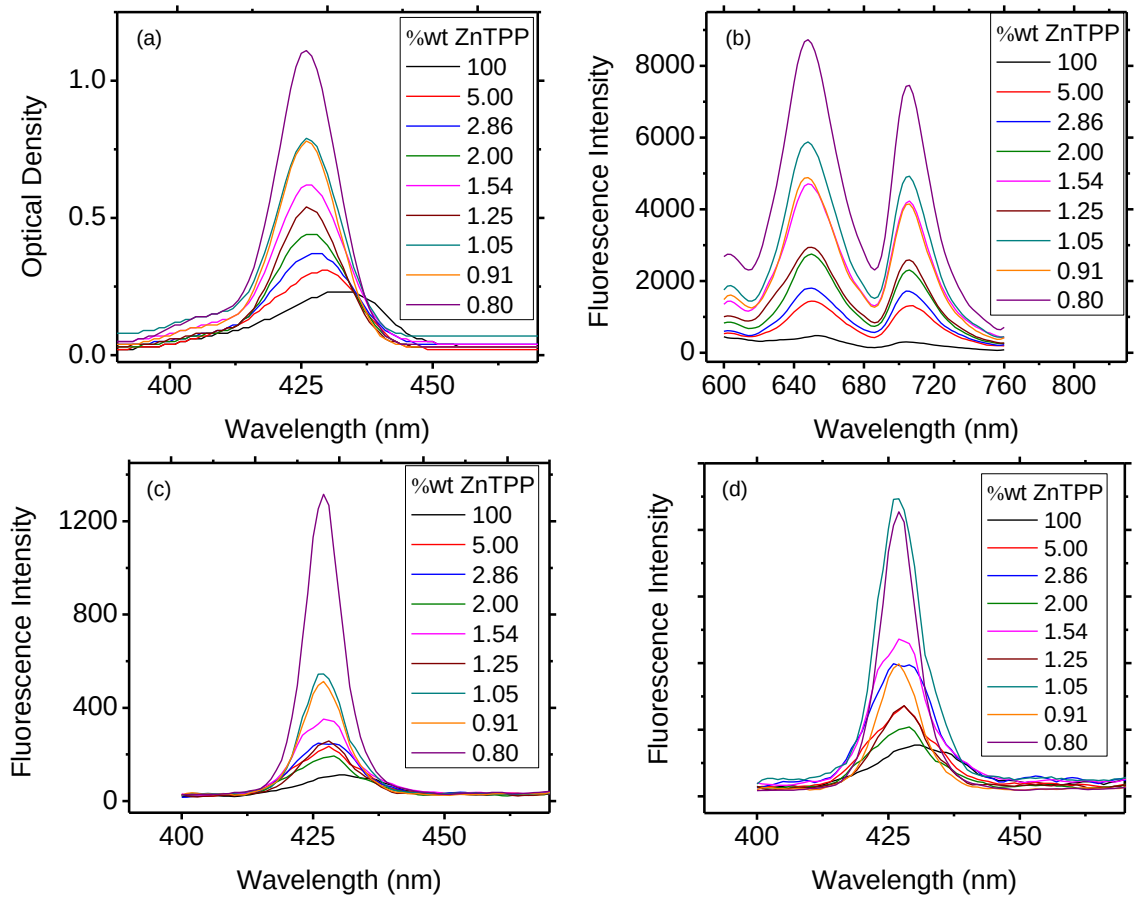

Figure 3.12: *(a) Optical Density; (b) S_1 fluorescence; and (c) reabsorption-corrected upconverted fluorescence; and (d) scaled reabsorption-corrected upconverted fluorescence as a function of ZnTPP:PEG dye loading. Spectral bandwidths are (a) 2 nm; (b) 1.8 nm; (c,d) 14.4 nm. Excitation source in (b-d) was 532 nm at 144 mW/cm^2.*

The spectral data of Figure 3.12 provide evidence of ZnTPP aggregation and self-quenching. As dye loading is increased significantly, the spectral features broaden and shift to lower energies. This threshold dye-loading is lower than that observed in the PMMA films due to the molecule's ability to diffuse in the PEG polymer. The blue-shift in Figure 3.12 relative that of Figure 3.11 is attributed to differences in film morphology.

The dye loading experiment was performed using spin-cast films while the proof of principle data utilized drop-cast films.

The low efficiency of homomolecular TTA-UC in this system may be due to several factors. First, it is conceivable that the threshold dye-loading concentration is low due to the diffusion of ZnTPP through the PEG matrix. Thus, significant self-quenching effects would occur at a much lower concentration in this film. The data of Figure 3.12 demonstrate the greatest fluorescence intensity for the film of lowest dye loading ratio. Further optimization would require a study of lower dye concentrations to obtain the optimum concentration. Additionally, the discolouration of the PEG films suggests photochemical degradation of the film. Increased upconverted fluorescence intensities due to an optimized dye loading ratio would allow for TTA-UC utilizing excitation powers below the degradation threshold. Power dependent study of NCPU would then be possible in this system.

Finally, it is possible that the oxygen atom in the PEG coordinates to the Zn^{2+} ion in the same manner as described for PU in Section 3.3. A study of carbon-only polymers would aid in determining whether coordination of the PEG has any effect of upconverted fluorescence intensity. Candidates for carbon-only polymers are presented in the Future Direction in Section 3.6.

3.6 Summary and Future Direction

NCPU has been explored via homomolecular TTA in ZnTPP in polymer matrices. It has been demonstrated that homomolecular TTA occurs toward the strong annihilation kinetic limit for the champion films spin-cast from 1%wt ZnTPP:PMMA solution. A sub-linear increase in upconverted fluorescence intensity was observed as film thickness is increased. This system represents aggregation-driven homomolecular TTA in ZnTPP

films due to the high glass transition temperature of the PMMA matrix. Further studies are required to verify the thickness-dependence trends to a satisfactory level. With more precise methods, a detailed exploration of film thickness effects would be attainable. These studies would likely include steady-state spectroscopy as well as ultra-fast laser spectroscopy to observe how the triplet lifetime of ZnTPP varies with film thickness. These studies would provide useful insight for the guided future study of homo- or hetero-molecular thin film upconverting systems sensitized by ZnTPP.

Homomolecular TTA in ZnTPP in polymers possessing low glass transition temperatures was also explored. Polyurethane was deemed an unsuitable host matrix in these studies despite its success in the literature for heteromolecular triplet sensitized TTA-UC systems.[55;57;58] It is believed that no upconverted fluorescence was observed in the present study due to polymer coordination to the Zn^{2+} ion. As reported in the literature,[53] such coordination would provide a steric barrier to TTA-UC, as excited triplet molecules would be held apart by a distance greater than that required for DET.

Diffusion-driven homomolecular TTA was then demonstrated for ZnTPP in a PEG matrix. The dominant annihilation kinetic regime was not determined in this system due to significant photochemical changes, but proof in concept of TTA-UC was demonstrated conclusively. A study of the dye-loading ratio in these films verified that the onset of parasitic self-quenching effects was at very low dye concentrations. Upconverted fluorescence yields were very low in these films. It may be that the low yields are due to porphyrin self-quenching that is non-negligible at the concentrations utilized due to diffusion of the porphyrin in this system. Additionally, there may be a possibility polymer coordination to the Zn^{2+} ion. Distinct routes for determining the source of this inefficient TTA through the use of carbon-only polymers are proposed, These polymers are shown in Figure 3.13 and their properties are summarized in Table 3.4.

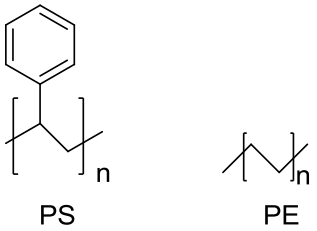

Figure 3.13: *Molecular structures of polymers proposed for future studies of TTA-UC in thin films.*

Table 3.4: Material Properties of Potential Future Polymers

Acronym/Identifier	**Polymer Name**	**Glass Transition Temperature (^{o}C)**
LDPE/HDPE	Poly(ethylene)	-125/-80
PS	Poly(styrene)	95

Polystyrene (PS) and polyethylene (PE), which contain only carbon atoms in the molecular structure, have been deemed attractive materials for future studies of ZnTPP-doped polymer films. Since carbon will not coordinate to the Zn^{2+} ion, these polymers provide the ability to explore aggregation-driven and diffusion-driven homomolecular TTA-UC in the absence of polymer coordination. PE is a particularly interesting choice for polymer matrix due to its availability in high- and low-density forms with a substantial variety in chain length. By studying TTA-UC in a PE matrix as the polymer chain length is varied, upconverted fluorescence can be studied as a function of diffusion rate in a controlled manner. In addition, the source of inefficiency in the PU and PEG matrices can be verified as follows: the carbon-only PE would provide a matrix that does not coordinate to the Zn^{2+} ion. Possible coordination of these polymers to the Zn^{2+} ion can be verified through a Stern-Volmer experiment in which potential quencher is added to a sample of upconverting ZnTPP:PE. If polymer coordination is not occurring in the PU and PEG matrices, then the upconverted fluorescence of the ZnTPP:PE system will resemble that of the ZnTPP:PEG system and the proposed Stern-Volmer experiment will yield no significant difference in upconverted fluorescence. The study of upconverted fluorescence in a PS matrix would provide a carbon-only analogous system to the PMMA study presented in this work.

Chapter 4

Spectroscopic and Photophysical Studies of Ru-DPA Polymers

4.1 Introduction to Ru-DPA Polymer System

TTA-UC has been studied in two photophysically-active polymers in which a $Ru(bpy)_3$ sensitizer and DPA emitter are covalently bonded. The power dependence of TTA-UC and the triplet energy transfer mechanisms were studied by steady state fluorescence spectroscopy. From these experiments, the nature of the energy transfer mechanisms involved in TTA were determined. A version of this work has been published in the Journal of Physical Chemistry Letters.[67] Figure 4.1 gives the molecular structures of the polymers and control samples. pDPA is a polymer chain containing 30 DPA moieties. In Ru2DPA and Ru6DPA, each polymer contains a $Ru(bpy)_3$ core and either two or six DPA-containing pendant arms. These arms are 8 DPA units in length.

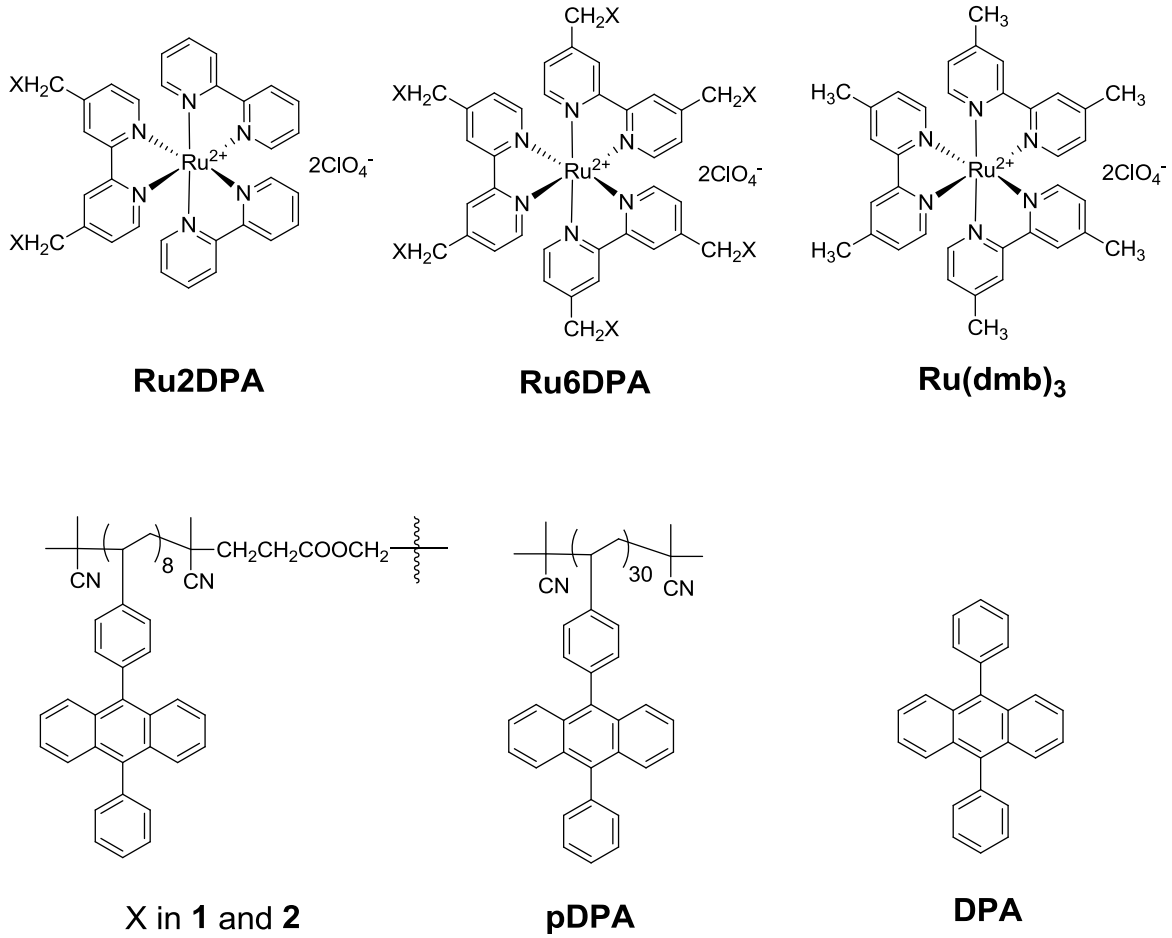

Figure 4.1: *Molecular structures of species studied in this chapter, slightly modified from the literature.*[67;140]

The photochemistry and photophysics of $Ru(bpy)_3$ and its derivatives have been studied for decades, developing widespread application in sensing, displays, electroluminescence, photoelectrochemistry, and artificial photosynthesis.[182] Meyer and associates reported the first detailed study of energy transfer from $([Ru(bpy)_3]^{2+})^*$ in 1974[183] and provided a detailed literature review of energy transfer from derivatives of $([Ru(bpy)_3]^{2+})^*$ in 2013.[182] Of significance to the present work is the summary of Meyer's advancement in energy-transfer systems containing $Ru(dmb)_3$-functionalized polymers. These results were first reported several decades ago with evidence of energy- or electron-transfer polymer structures containing $Ru(dmb)_3$ as a light-harvesting antenna.[184–186] Further studies by Meyer have demonstrated evidence of intramolecular energy transfer[184;185;187] and multiple excitations with adjacent multiple electron transfers during single laser flashes.[188] In 2002,[189] intramolecular energy migration between subsequent Ru(II) moi-

eties en route to an Os(II) trap site was reported with an efficiency >90% at ambient temperature. Examples of $Ru(bpy)_3$-containing polymers reported by Meyer and associates are discussed in the review.[182] These reports have focused on the quenching of $Ru(bpy)_3$ photoluminescence, direct evidence of energy transfer from $Ru(bpy)_3$ to the polymer acceptor moieties.

Energy transfer from functionalized compounds based on $Ru(bpy)_3^*$ in the context of TTA-UC was first reported by the Castellano group.[74] This report demonstrated a delayed and anti-Stokes shifted fluorescence of $Ru(dmb)_2$(bpy-An) in solution. This blue-shifted peak was attributed to TTA-UC in anthracene by comparison to the fluorescence spectrum of singlet-excited anthracene. TTET from $Ru(bpy_3)$ complex to An in this macromolecule proceeds with a QY of unity.[190] This efficient TTET results from the efficient ISC in $Ru(bpy)_3$ complexes and the close proximity of sensitizer and emitter in this material, allowing for efficient DET. Cannizzo *et al.*[191] demonstrated that sensitized $Ru(bpy)_3$ undergoes ISC to a hot triplet state within $\sim$ 10 fs, followed by vibrational relaxation within $\sim$ 10 ps. The efficient ISC in Ru(bpy)-compounds can be attributed to strong spin-orbit coupling,[182] as can the phosphorescence QY, reported to range between 7.3[119] and 9.5[192] percent in acetonitrile. This phosphorescence QY is also solvent-dependent.

This efficient ISC has led to the application of $Ru(bpy)_3$ complexes as sensitizers in heteromolecular TTA-UC systems.[42;57;74–76;117–120;131;138] Castellano's second report[75] of TTA-UC utilizing a $Ru(bpy)_3$ sensitizer was based on a change in emitter from anthracene to DPA. DPA possesses a long-lived triplet state along with a fluorescence QY that is significantly higher than that of anthracene, resulting in a greatly enhanced upconverted fluorescence QY. Since that report, DPA has become a very common emitter material for TTA-UC.

Numerous reports have been published over the past decade on TTA-UC in systems of

polymer glasses,[65;66] dye-doped nanoparticles,[68;70] and sensitizer-doped polymer emitters[61;94] in addition to the polymer films discussed in Section 1.5. In 2013, Ghiggino and associates[140] reported the synthesis and kinetic analysis of the inter-chromophore energy transfer in two novel polymers, each containing a core $Ru(bpy)_3$ unit surrounded by multiple DPA-containing arms. Figure 4.1 gives the molecular structures of the materials studied in that report, which are also studied in the present work. Ru2DPA, Ru6DPA, and pDPA were synthesized via reversible addition fragmentation chain transfer (RAFT) polymerization as described in the literature.[140;193] Significant photophysical highlights from Ghiggino's report with relevance to the present document are shown in Figure 4.2.

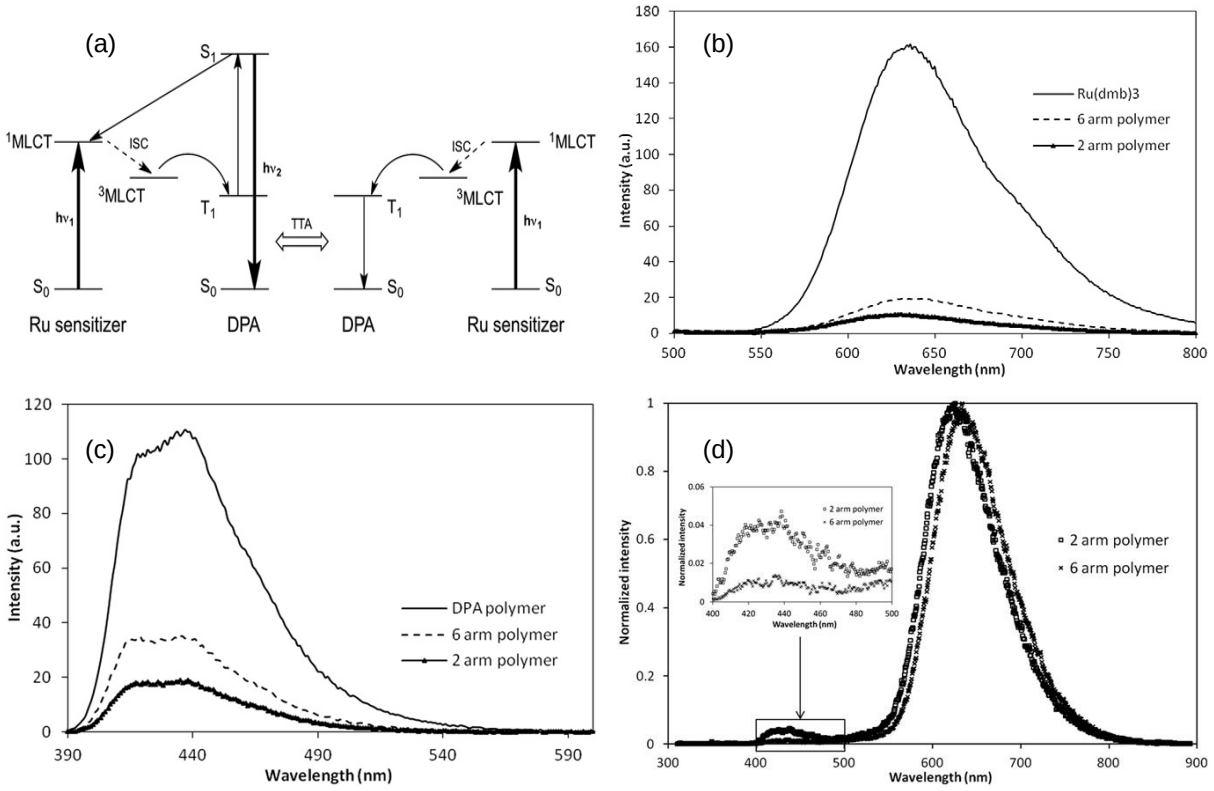

Figure 4.2: *(a) Energy-level diagram for Ru-DPA polymers; (b) Phosphorescence spectra of Ru2DPA, Ru6DPA, and $Ru(dmb)_3$ following 480 nm excitation; (c) Fluorescence spectra of Ru2DPA, Ru6DPA, and pDPA following 370 nm excitation; (d) Normalized photoluminescence spectra of Ru2DPA and Ru6DPA following 485 nm excitation. Studies were performed in degassed $CHCl_3$ using a pulsed excitation source. Compounds in each quenching study had the same optical density at the excitation wavelength. All figures were taken directly from the reference[140] and reproduced with permission by Elsevier.*

Figure 4.2(b and c) provide evidence of energy transfer within the polymer. Figure

4.2(b) demonstrates the quenching of $Ru(bpy)_3$ phosphorescence by the DPA moieties. In Figure 4.2(c), the quenching of DPA fluorescence by the $Ru(bpy)_3$ core (back energy transfer) is demonstrated. These energy mechanisms are shown schematically in (a). Ultra-fast spectroscopy and detailed kinetic analysis supported the steady-state results.[140] As seen in Figure 4.2(d), 485 nm excitation yielded an unexpected peak at $\approx$ 430 nm. This matches the peak shown in (c) for the S_1 excitation and prompt fluorescence of DPA moieties in the polymer. This peak in Figure 4.2(d) was attributed to upconverted fluorescence via TTA but was otherwise not characterized due to experimental constraints. NCPU studies in these polymers are presented here.

4.2 Steady-State Spectroscopy of the $Ru(bpy)_3$-DPA Polymers

Excitation power-dependent photoluminescence spectra of Ru2DPA and Ru6DPA in dilute solution confirmed the notion that TTA-UC occurs in these polymers. Spectroscopic measurements described in this chapter were performed using the SPEX Fluorolog Spectrofluorometer described in Chapter 2. Samples were studied in a 1 cm $\times$ 1 cm quartz cuvette with attached bulb to facilitate degassing of solution.

Figure 4.3 shows the optical density and scaled photoluminescence spectra following 532 nm excitation of these compounds. These spectra are in agreement with those previously reported for these materials.[140] Ru2DPA and Ru6DPA demonstrate the broad metal to ligand charge transfer (MLCT) absorption and phosphorescence bands characteristic of $Ru(bpy)_3$. The multi-peak absorption band of DPA is not observed. At the polymer concentrations utilized, the optical density of these DPA moieties is so great that it saturates the apparatus. In the upconverted fluorescence spectrum, the characteristic DPA multiple-peak structure again loses spectral resolution relative to direct excitation into the DPA absorption band. This loss of resolution is due to a combination

of effects including significant broadening due to the large spectral bandwidths utilized and intermolecular interactions between pendant DPA moieties in the polymer strands. A broadening of the DPA emission bands upon TTA-UC in the polymer compounds is consistent with literature reports for systems containing monomeric DPA.[54;75] The red edge of the upconverted fluorescence peak does not return to baseline in the same manner as the blue edge. The significant increase in the background counts on the red edge is due to laser scatter at the high spectral bandwidths used. The details for data modelling are given in Appendix A.5.

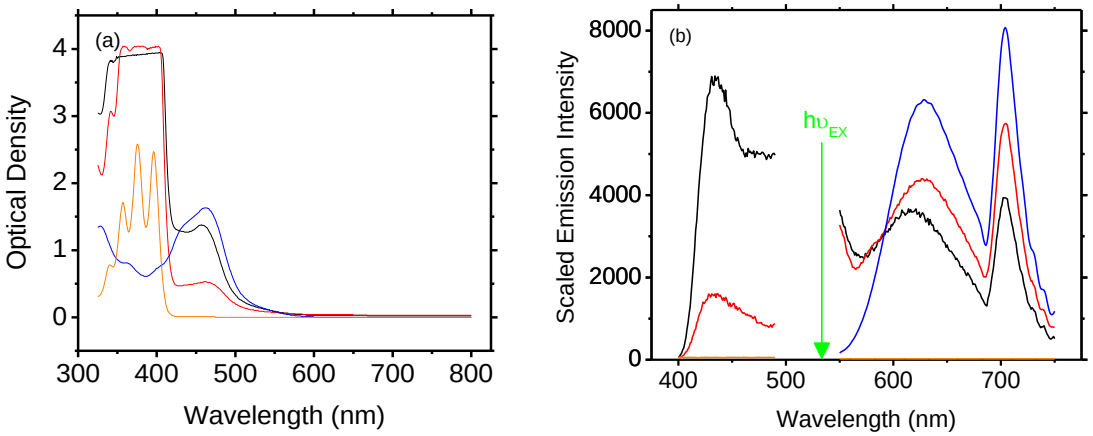

Figure 4.3: *(a) Optical density; and (b) Scaled photoluminescence intensity of Ru2DPA (black), Ru6DPA (red), Ru(dmb)$_3$ (blue) and pDPA (orange) with 14 mW/cm^2 532 nm excitation. Spectral bandwidths were 2 nm for optical density, 12.6 nm for upconverted fluorescence and 2 to 4 nm for phosphorescence spectra. Phosphorescence spectra were scaled via division by the following constants: 2.5× for Ru2DPA; 8.5× for RU6DPA; 75× for Ru(dmb)$_3$. The peaks in (b) were oxygen-sensitive.*

Figure 4.4 shows the upconverted fluorescence and phosphorescence spectra of Ru2DPA and Ru6DPA as a function of excitation power. These data allow for the determination of the dominant kinetic regime for the decay of emitter triplets. These compounds were thoroughly degassed in the following manner: samples were sparged with high-purity N_2 gas for thirty seconds in a glove bag and then degassed via five freeze-pump-thaw cycles prior to spectroscopic study. The absorbance spectrum was recorded before and after each photoluminescence experiment in order to verify the photostability of these polymers. Polymer samples were diluted such that the optical density at the excitation

wavelength was below 0.15 to minimize reabsorption effects.[140] The optical density at the excitation wavelength was kept nearly constant for all samples studied for meaningful comparison of the data through QY calculations.

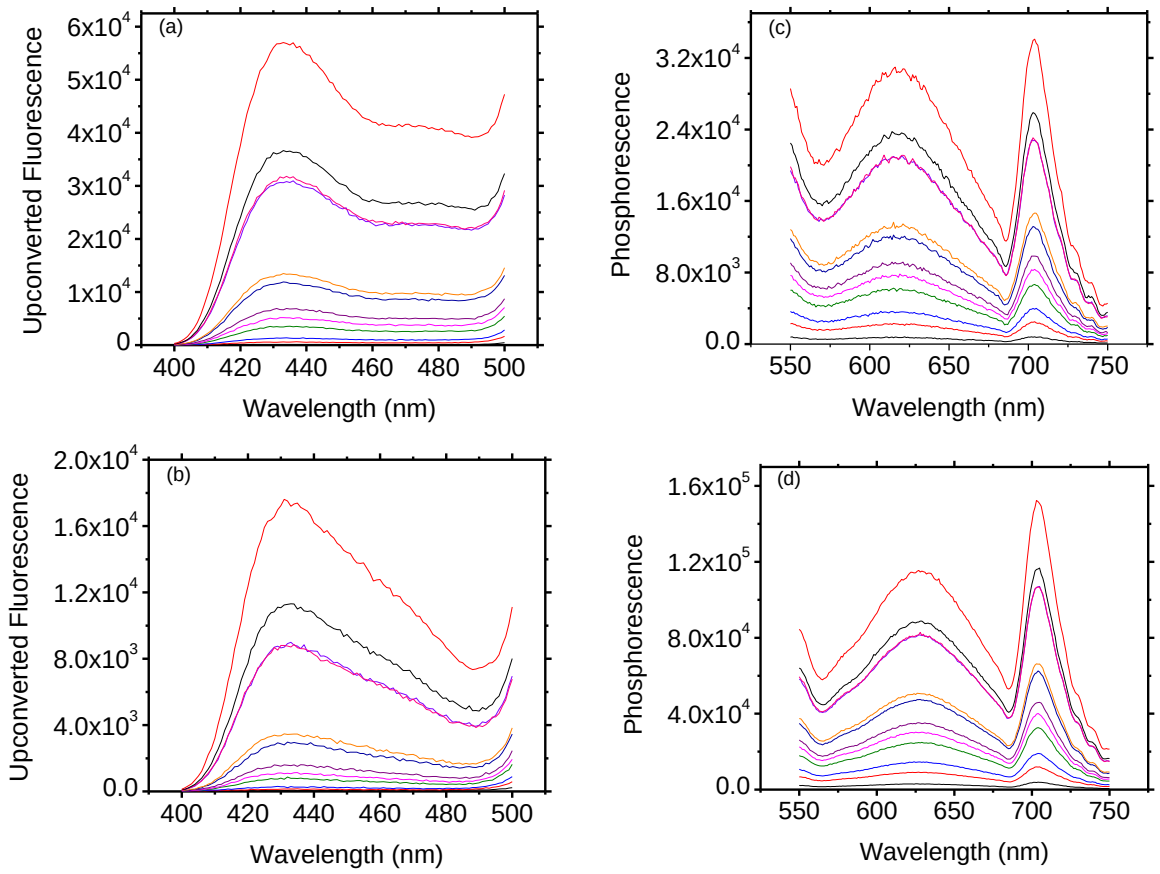

Figure 4.4: *Photoluminescence spectra of ≈75 μM (a, b,) Ru2DPA; and (c, d) Ru6DPA in degassed chloroform as 532 nm excitation power density is varied from 1 to 50 mW/cm^2. Spectral bandwidths are: (a) 12.6 nm; (b) 1.8 nm; (c) 12.6 nm; (d) 3.6 nm.*

The data are replotted in double-logarithmic plots in Figure 4.5. The phosphorescence intensity in these compounds varied linearly with excitation power. Ru6DPA has a slope nearing 2, demonstrating TTA-UC in the weak annihilation kinetic limit, while the slope for Ru2DPA approaches 2 but begins to drop off at higher power densities. This latter tendency is evidence of the beginning of a shift from the weak to strong annihilation kinetic limit, consistent with the higher upconverted fluorescence intensity observed in Ru2DPA relative to Ru6DPA. The decrease in slope for Ru2DPA was realized by taking

the best fit line of the three terminal data points at the high- and low-excitation power regions of those utilized in the present study.

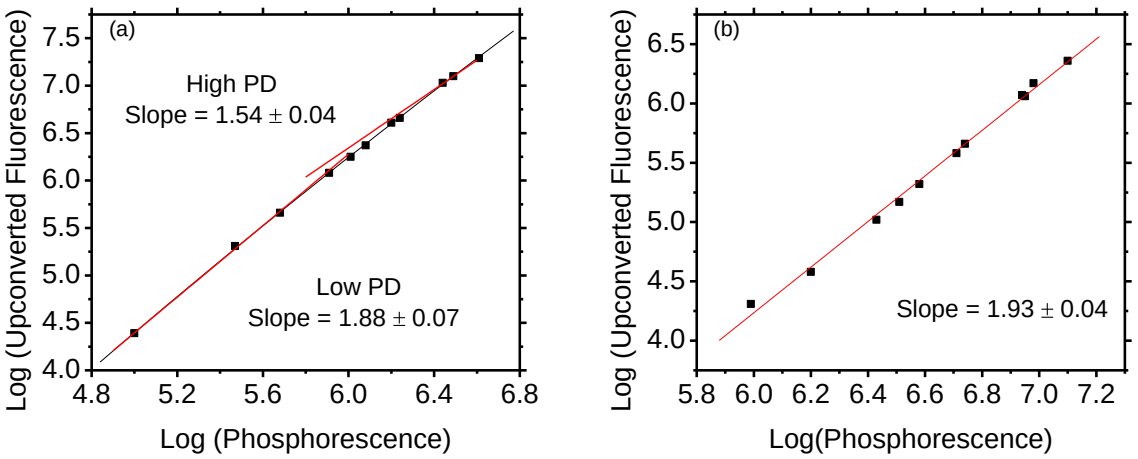

Figure 4.5: *Double logarithmic plot of upconverted fluorescence peak intensity vs. phosphorescence peak intensity of ≈75 μM solutions of (a) Ru2DPA; and (b) Ru6DPA in degassed chloroform at room temperature. The corresponding incident power density range is 1 to 50* mW/cm^2.

Discussion of the difference in upconverted fluorescence intensities of Ru2DPA and Ru6DPA is deferred to the comparison of QYs in Section 4.5. Presently, the double-logarithmic results verify that the 430 nm fluorescence peak observed by Ghiggino[140] is of TTA-UC origin in the weak annihilation kinetic limit.

4.3 Quenching of $Ru(dmb)_3$ Phosphorescence by DPA

Quenching studies of $Ru(dmb)_3$ by pDPA and DPA were performed to simulate the energy-transfer processes occurring in the Ru-DPA polymers. Variations in optical density, phosphorescence, and upconverted fluorescence as pDPA and DPA are added to $Ru(dmb)_3$ are shown in Figures 4.6 and 4.7. These experiments were performed as a titration of the sensitizer with DPA. Solutions of sensitizer and emitter were separately sparged with high-purity nitrogen gas for thirty seconds prior to experiments. Titrations were performed in a nitrogen-flushed glove bag and the mixture was degassed via five freeze-pump-thaw cycles prior to photoluminescence spectroscopy. The absorbance spec-

trum of the mixture was recorded before and after each photoluminescence experiment. This verified that the samples were not subject to photodegradation at the low power density utilized. It also allowed for concentration corrections due to variations in optical density of the Ru-core as a consequence of diluting with the added DPA solution.

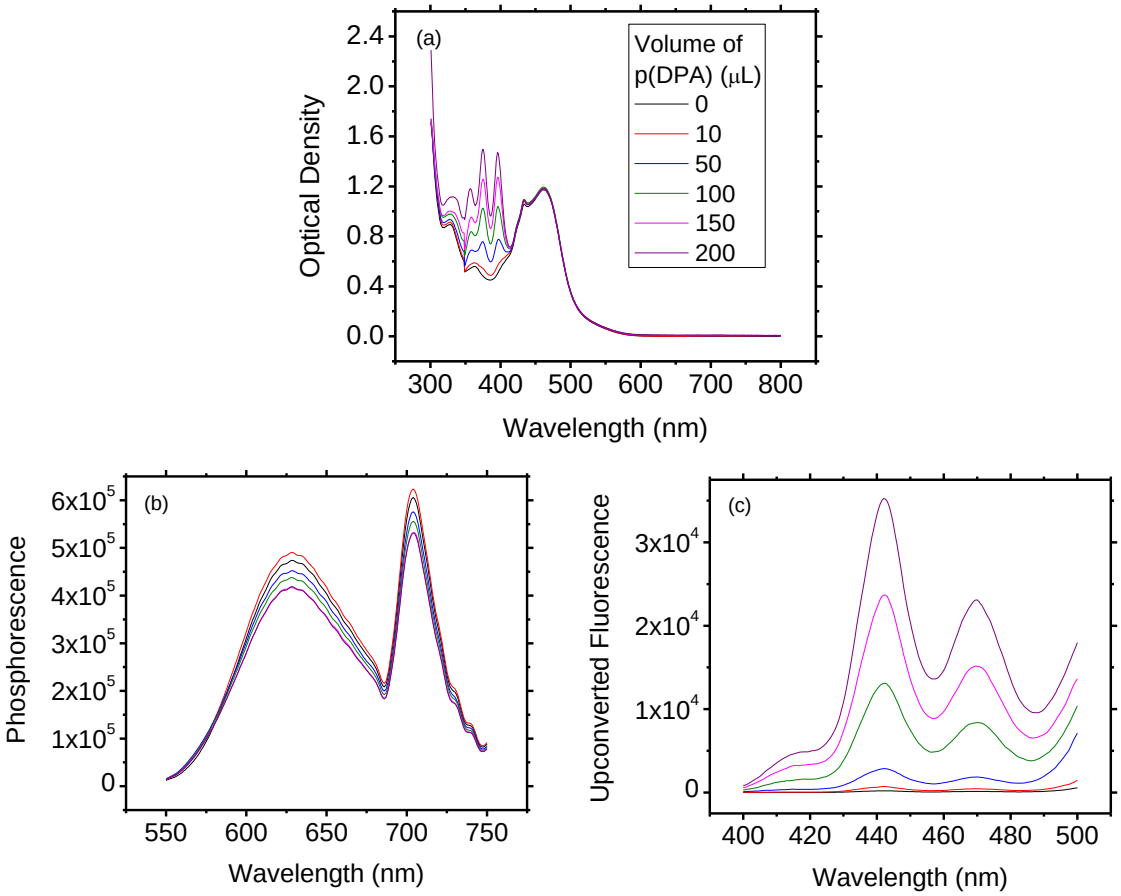

Figure 4.6: *Variation in (a) optical density; (b) phosphorescence; and (c) upconverted fluorescence as volumes of 2 mM of pDPA are added to 75 μM Ru(dmb)$_3$ in degassed chloroform. Spectral bandwidths are: (a) 2 nm; (b) 1.8 nm; (c) 14.4 nm. Excitation power was 14 mW/cm^2 at 532 nm.*

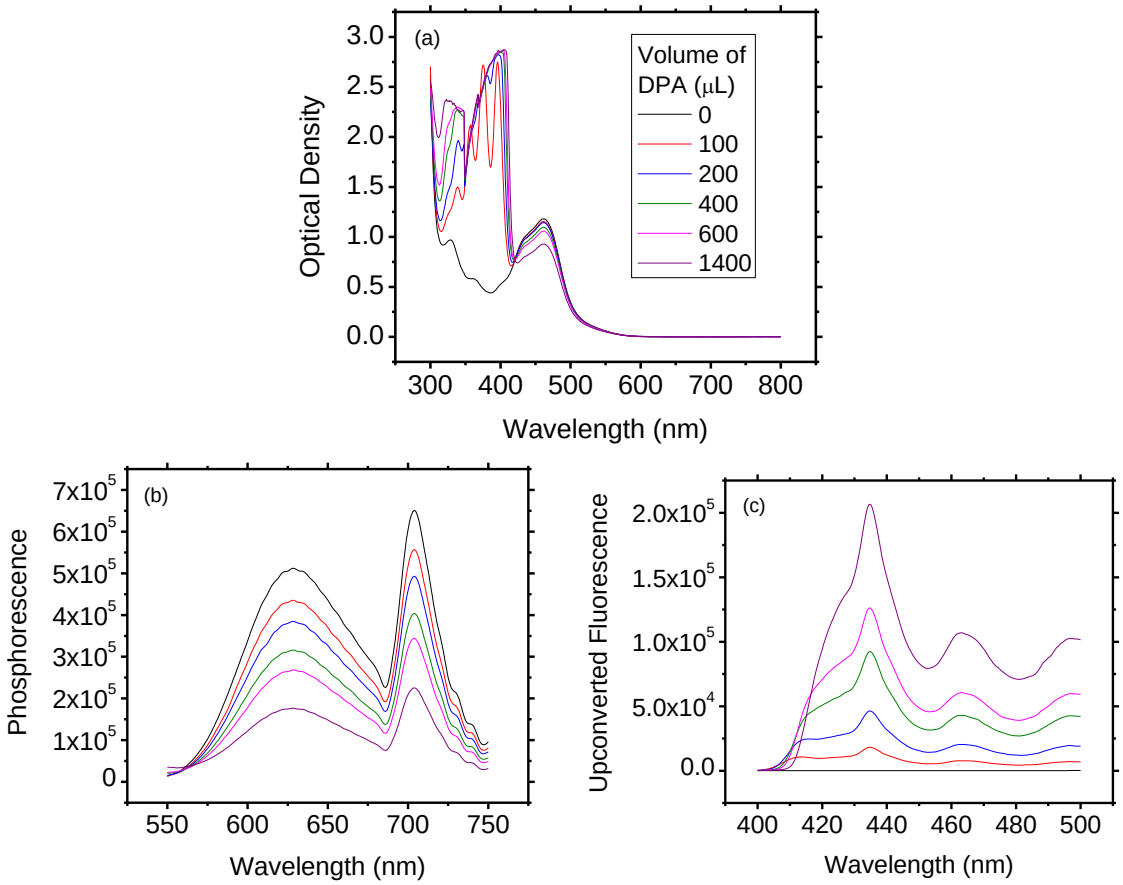

Figure 4.7: *Variation in (a) optical density; (b) phosphorescence; and (c) upconverted fluorescence as volumes of 10 mM DPA are added to 75 μM Ru(dmb)$_3$ in degassed chloroform. Spectral bandwidths are: (a) 2 nm; (b,) 1.8 nm. Excitation power was 14 mW/cm^2 at 532 nm.*

As pDPA is added to Ru(dmb)$_3$, the onset of upconverted fluorescence and incorporation of the DPA absorption band into the absorption spectrum are observed (Figure 4.6). These effects coincide with decreased phosphorescence from Ru(dmb)$_3$. The effects are gradual due to the limited amount of pDPA available for these experiments, necessitating the use of very small volumes at relatively low concentrations of pDPA. For this reason, spectral changes observed in Figure 4.6 are less pronounced than those observed in Figure 4.7. Phosphorescence quenching is shown in the Stern-Volmer plots in Figure 4.8. From these Stern-Volmer plots, the kinetic rate constant of TTET from Ru(dmb)$_3$ to DPA and pDPA can be determined. The ability to carry out the experiment to quenching ratios of $I_0/I \rightarrow 2$ or 3 would have likely decreased the noise in Figure 4.8(b).

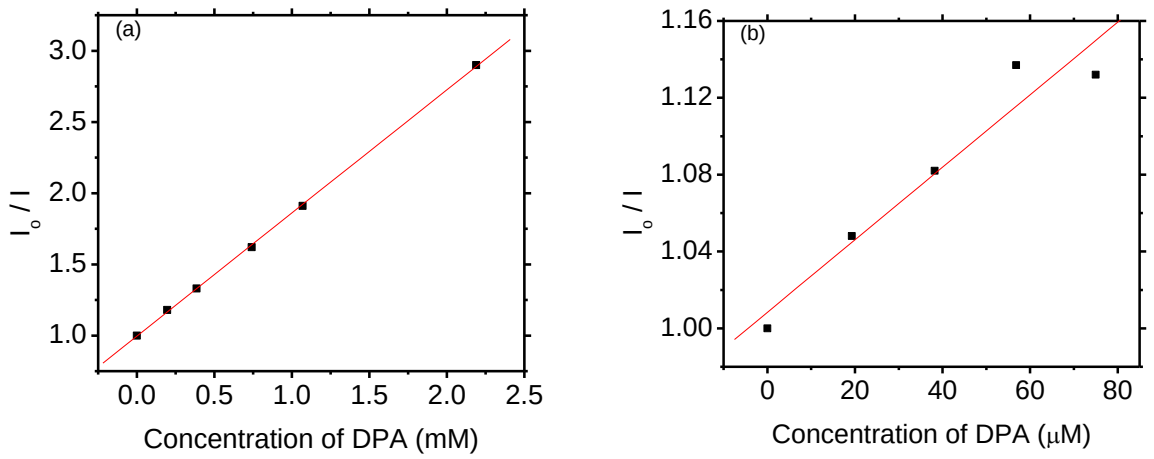

Figure 4.8: *Stern-Volmer plots for the phosphorescence quenching of 75 μM Ru(dmb)$_3$ by (a) DPA; and (b) pDPA. Excitation power was 14 mW/cm^2 at 532 nm. Slopes are given in Table 4.1.*

Since quenching of Ru(dmb)$_3$ is via TTET to a DPA moiety, the rate constant for TTET from sensitizer to emitter is calculated from the slope of the Stern-Volmer plots in Figure 4.8. The values are summarized in Table 4.1 below.

$$\frac{I_0^{Ph}}{I_{[DPA]}^{Ph}} = 1 + k_{TTET} \times \tau_0 \, [DPA] \tag{4.1}$$

where τ_0 is the lifetime of Ru(dmb)$_3$ at the concentration utilized in the experiment. This value is 871.2 ± 0.1 ns, as determined by LFP and outlined in the Appendix A.4.

Table 4.1: TTET Rate Constants from Ru(dmb)$_3$ to DPA Moieties

Quencher	**Slope**	**Rate Constant**
pDPA	0.0019 ± 0.0003 μM^{-1}	2.2 ± 0.3 × $10^9 M^{-1}s^{-1}$
DPA	0.865 ± 0.008 mM^{-1}	1.00 ± 0.01 × $10^9 M^{-1}s^{-1}$

The rate constant for energy transfer between Ru(dmb)$_3$ and DPA monomers can be compared to the diffusion-limited value of $k_{TET} = 1.0 \times 10^{10} M^{-1}s^{-1}$ in $CHCl_3$ using the Stokes-Einstein model,[194] which does not take spin statistics into account. The results are not intuitive, since the quenching rate constant of the slower-diffusing pDPA is a factor of 2.2 greater than the DPA monomer. From the DOSY experiment discussed in Appendix A.4, the diffusion rate of the DPA monomer is a factor of 3.3 greater than that

of pDPA. These data suggest that the rate constant for the DPA polymer should be a factor of 3.3 *less* than that of the monomer, based solely on diffusion limitations. Thus the quenching rate constant of pDPA is a factor of $2.2 \times 3.3 = 7.3$ greater than expected. This significantly enhanced quenching may be due to a greatly increased interaction cross section as a consequence of tethering many DPA moieties together. Since pDPA is a chain containing thirty DPA units, the availability of DPA moieties in pDPA for short-range DET is $7.3/30 \approx 1/4$ that of a single DPA unit. This calculation is consistent with the notion that the DPA polymer can bend or fold in solution, shielding some of the interior DPA units such that they are not available for DET.

4.4 Nature of Energy Transfer Processes

Consideration was given as to whether the energy transfer processes required for TTA-UC are occurring between adjacent macromolecules (interchain) or within a single macromolecule (intrachain) based on the present[67] and previous[140] results. Laser flash photolysis (LFP) determined the weighted averages of the four component lifetimes of the Ru-core phosphorescence to be 99 and 33 ns in Ru2DPA and Ru6DPA, respectively. Given the slow diffusion rate of the polymers and the low concentrations utilized in the steady-state experiments, it is not probable that Ru-DPA TTET occurs between adjacent chains.[67] Thus TTET from Ru-core to DPA moieties is considered to be an intrachain process.

Similar analysis demonstrates that TTA is an interchain process.[67] DPA triplets in Ru2DPA and Ru6DPA decay by first order processes with a lifetime >100 μs in degassed chloroform.[140] Figure 4.5 shows that the triplet DPA moieties produced in the steady-state experiment are also decaying by first order or pseudo-first order processes,[57] as evidenced by the weak annihilation kinetic limit observed at the low excitation powers utilized. Typical second-order rate constants for homomolecular TTA in aromatic

monomers such as DPA are generally 1 to 5 $\times$ 10^9 $M^{-1}s^{-1}$.[25;45] Calculating interaction cross-sections and relative diffusion coefficients justifies intermolecular TTA in the polymers at the low power densities utilized in these studies.

The above result can be supported by determining the probability of sequential two-photon absorption by a macromolecule resulting in intrachain TTA-UC. A conservative calculation utilizing the parameters listed in Table 4.2 yields an absorption rate of 12 photons per second,[67] or a photon absorption event occurring every $\frac{1}{12}$ s. The excited triplet state of DPA has a lifetime on the order of 100 μs in the polymer species. Since $\frac{1}{12}$ s $\approx 10^5 \mu s \gg 100$ μs, it is not probable that the sensitizing core will absorb a second photon before relaxation of the DPA triplet in the same chain. Thus TTA must be an intermolecular process.

Table 4.2: Parameters for Calculation of Sequential Two-Photon Absorption

Excitation Wavelength	**Excitation Power**	**Excitation Diameter**	**Optical Density at 532 nm**	**Concentration of Ru(bpy)$_3$**
532 nm	1 W/cm^2	2 mm	0.15	100 μM

A cartoon summary of the energy processes involved in Ru2DPA and Ru6DPA in this study is shown in Figure 4.9 below. At the low power densities utilized, sensitized Ru-cores exhibit intrachain TTET to DPA moieties, which undergo interchain TTA leading to upconverted fluorescence.

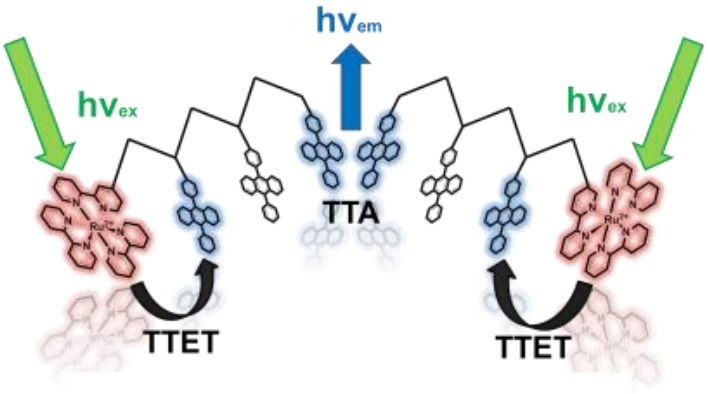

Figure 4.9: *Cartoon depiction of the energy transfer processes occurring in Ru2DPA and Ru6DPA.*

4.5 Photoluminescence Quantum Yields

Photoluminescence QYs were calculated via the comparative method[195] using rhodamine 6G in $CHCl_3$ as the standard, which has a QY of 0.75.[196] Details of QY calculations, explanation of data modelling, and tabulated excitation power-dependent QYs of Ru2DPA, Ru6DPA, and control samples comprised of $Ru(dmb)_3$ and DPA are given in Appendix A.5. The mean phosphorescence QYs for Ru2DPA, Ru6DPA, and $Ru(dmb)_3$ are given in Table 4.3, along with the upconverted fluorescence QYs as a function of excitation power density for Ru2DPA and Ru6DPA. Upconverted fluorescence QYs are reported as a function of the power-dependent slope Ψ, where Ψ is the excitation power density in $mW/cm^2 \times 10^{-5}$. This is because TTA-UC is occurring in the weak annihilation limit at the low power densities used in this study, as described in Section 1.3.2. At high power densities, ϕ_{UC} would reach a maximum value independent of excitation power. The tabulated data from Appendix A.5 is plotted in Figures 4.10 and 4.11 for the polymers and controls, respectively.

Table 4.3: Summary of QY Results

Species	ϕ_{Ph}	ϕ_{UC}
$Ru(dmb)_3$	0.022 ± 0.003	
Ru2DPA	$1.8 \pm 0.1 \times 10^{-3}$	$3.1 \pm 0.1\ \Psi$
Ru6DPA	$1.9 \pm 0.1 \times 10^{-3}$	$0.39 \pm 0.01\ \Psi$

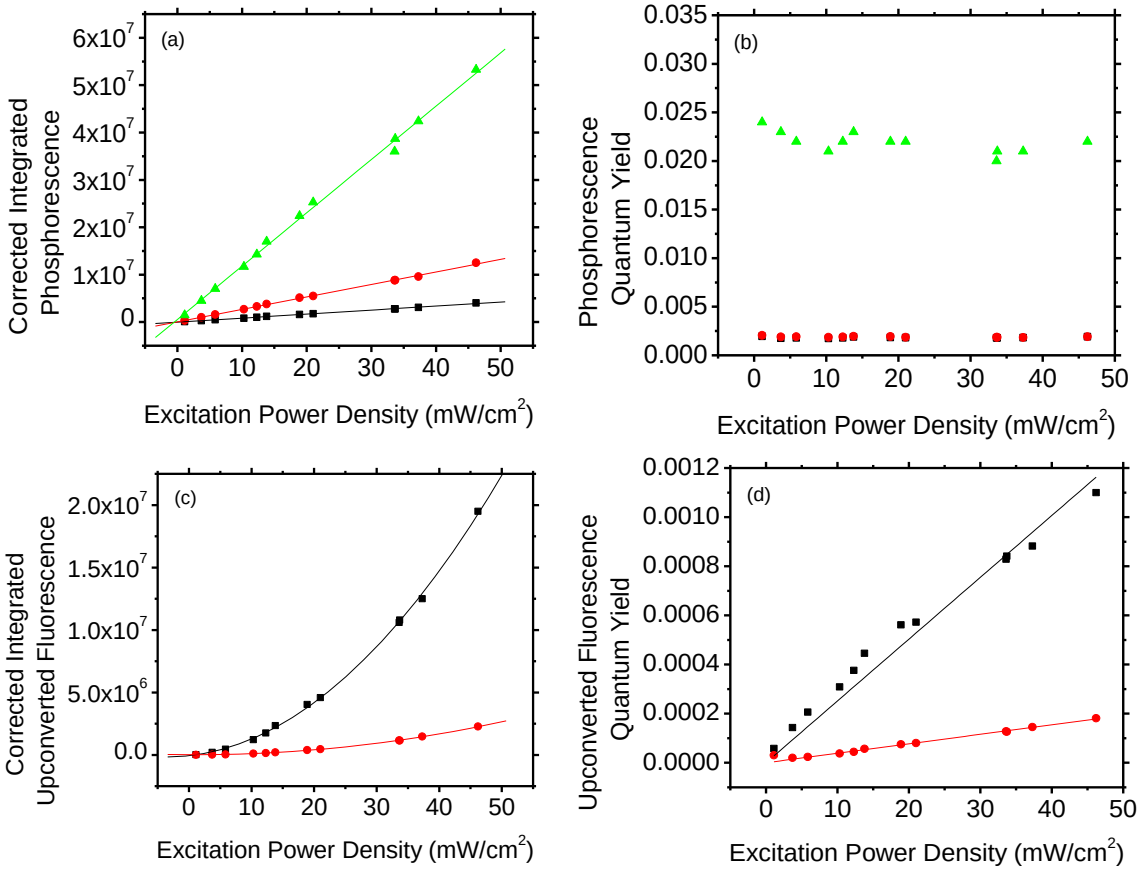

Figure 4.10: *532 nm excitation power dependence of (a) integrated phosphorescence; (b) phosphorescence QY; (c) integrated upconverted fluorescence; and (d) upconverted fluorescence QY of Ru2DPA (black), Ru6DPA (red), and Ru(dmb)$_3$ (green). Linear correlations are forced fit through the origin. Details of data correcting are given in Appendix A.5.*

The excitation power-dependence of QYs shown in Figure 4.10 matches the trends reported in the literature.[43] Briefly: in the weak annihilation kinetic regime, upconverted fluorescence intensity has a quadratic dependence on triplet concentration as shown in Appendix A.1. Since the fluorescence intensity of the reference standard varies linearly with power density, the net result is an increase in QY with excitation power in this kinetic regime. From Equation A.6,

$$\phi_{UC,weak} \propto \frac{I_{UC}}{I_{ref}} \propto \frac{(PD)^2}{(PD)} \propto PD$$

in the weak annihilation kinetic regime. In the strong annihilation kinetic regime, upconverted fluorescence varies linearly with excitation power. Thus the QY is independent

of excitation power in this kinetic regime. The calculation of power dependence of phosphorescence is identical to the strong annihilation kinetic regime.

$$\phi_{UC,strong} \propto \frac{I_{UC}}{I_{ref}} \propto \frac{(PD)}{(PD)} \propto (PD)^0$$

The QY trends reported in Figure 4.10 are consistent with the trends of the integrated photoluminescence intensity. A control experiment was performed using solutions of $Ru(dmb)_3$ and DPA in $CHCl_3$ in a ratio equal to that of Ru2DPA and Ru6DPA - 1:16 and 1:48, respectively. Each control sample had 74 μM $Ru(dmb)_3$, while DPA concentrations were 1.18 mM and 3.52 mM, respectively. This experiment was designed to monitor the power dependence of the upconverted fluroescence QY as the system shifts from the weak to strong annihilation kinetic limit. This range will demonstrate a change in the power dependence of the upconverted fluorescence (Figure 4.11). The 74 μM $Ru(dmb)_3$ + 3.52 mM DPA solution yielded poor results, likely resulting from significant DPA aggregation and self-quenching at the high concentrations utilized. The 74 μM $Ru(dmb)_3$ + 1.18 mM DPA solution yielded better results, demonstrating asymptotic behaviour in QY as excitation power increased. This strong annihilation kinetic limit represents the maximum upconverted fluorescence QY, or highest efficiency, attainable in the system. The sample of 74 μM $Ru(dmb)_3$ + 1.18 mM DPA in degassed chloroform reached a maximum QY of over 30%, consistent with literature reports.[55]

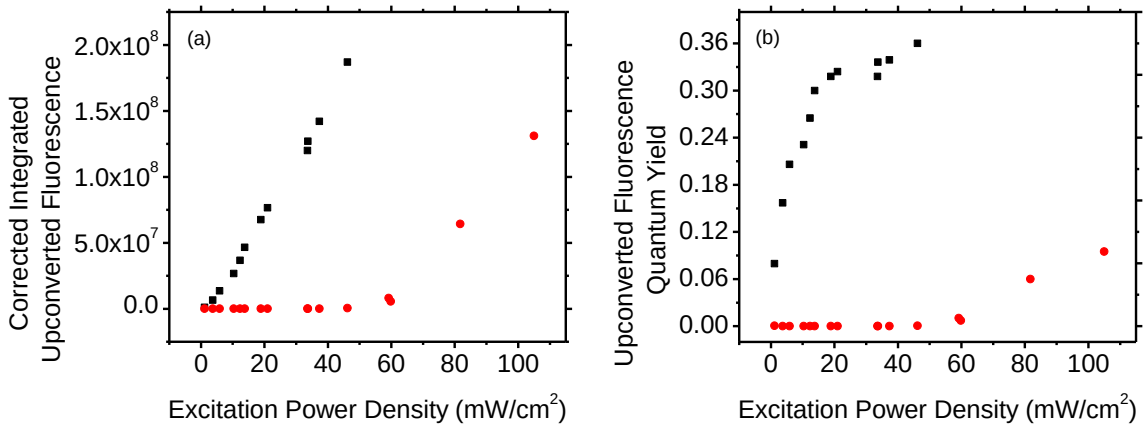

Figure 4.11: *532 nm excitation power dependence of (a) integrated upconverted fluorescence; and (b) upconverted fluorescence QY of control samples made of 74 μM Ru(dmb)$_3$ + 1.18 mM DPA (black) and 74 μM Ru(dmb)$_3$ + 3.52 mM DPA (red). Details of data correcting are given in Appendix A.5.*

Consider the slopes of the power-dependent upconverted fluorescence QYs in Figure 4.10(d). The slope of Ru2DPA is a factor of 8 greater than that of Ru6DPA. This result is consistent with the interpretation of the relative accessibility of DPA moieties within the polymer to interchain TTA. A greater degree of polymer folding is expected in Ru6DPA due to the greater number of pendant arms. The relative accessibility will then be decreased in Ru6DPA relative to Ru2DPA, leading to lower upconverted fluorescence QYs. This is because polymer folding can hold excited triplets at distances too great for DET to occur. This notion is consistent with the significant decrease in the fluorescence QY of pDPA (0.61) relative to monomeric DPA (1).[140]

Ghiggino's previous report[140] demonstrated that the intensities of DPA fluorescence in Ru2DPA and Ru6DPA are 83% and 69% lower than that of pDPA - attributed to intrachain FRET from the DPA excited singlet state to the MLCT band of the Ru(bpy)$_3$ core. This quenching result, shown in Figure 4.2, was obtained by exciting directly into the DPA band of each polymer. This significant quenching of DPA fluorescence helps justify the very low upconverted fluorescence QYs reported in Figure 4.10 - the corrected QYs in the absence of back-energy transfer would be a factor of about 7 or 8 greater than those observed. In the absence of these quenching losses, the upconverted fluorescence

QY of Ru2DPA would approach 1%. The maximum QY is likely greater than 1%, as it would only be reached in the strong annihilation kinetic limit.

Phosphorescence QY data show agreement between the Ru2DPA and Ru6DPA at 0.0018 to 0.0019 percent, a quenching efficiency of ≈ 91 % for each polymer. These values are in reasonable agreement with Ghiggino's previous report in which phosphorescence intensity was quenched by 93% and 88% for Ru2DPA and Ru6DPA, respectively.[140] The experimental value reported here for $Ru(dmb)_3$ phosphorescence in $CHCl_3$ is 0.022, which can be compared to literature values of 0.095[192] and 0.073[119] in CH_3CN. The low value measured in the present study may be due to weak intermolecular spin-orbit coupling attributed to the Cl atoms in the solvent utilized. This would open an additional non-radiative $T_1 \rightarrow S_0$ pathway in competition with phosphorescence. This discrepancy in QYs cannot be attributed to the difference in counter ion between the present study and the literature values.[192]

4.6 Upconverted Fluorescence in Thin Films

Thin films of Ru2DPA and Ru6DPA were fabricated by drop-casting polymers from cholroform solution onto masked glass slides and evaporating the solvent in air. Weak but measurable anti-Stokes' shifted photoluminescence was detected upon 532 nm excitation and attributed to TTA-UC. Figure 4.12 gives the scaled upconverted fluorescence as a function of excitation power. Due to significantly lower upconverted fluorescence intensities in the solid state, these spectra are greatly obscured by scatter. The baseline scatter (in the regions away from the upconverted fluorescence peaks) was fit to a polynomial function. The raw data were then divided by this polynomial, leaving the spectra in Figure 4.12(a and c). The adjusted spectra obtained using 105 mW/cm^2 excitation are fit to a two-Gaussian model.

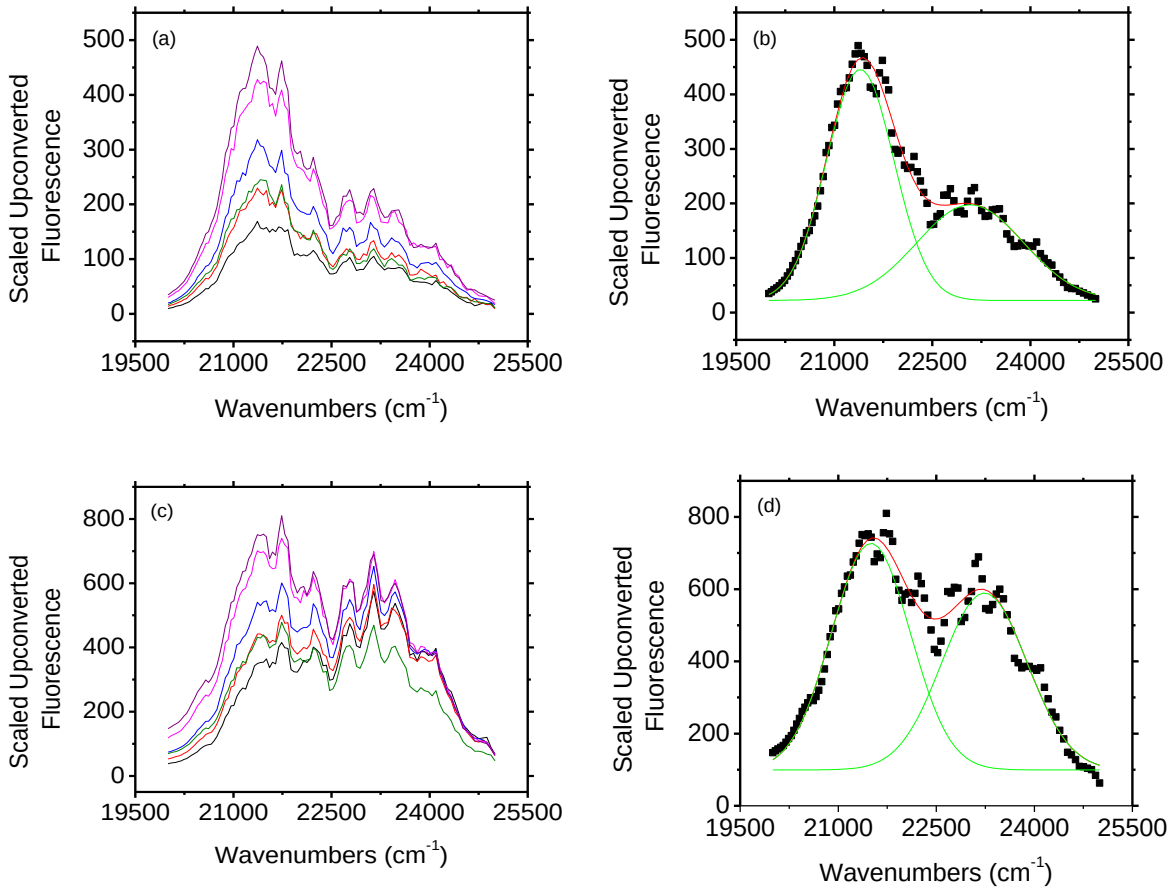

Figure 4.12: *(a) Scaled upconverted fluorescence with changing excitation power density; and (b) double-Gaussian fit of upconverted fluorescence for Ru2DPA. (c) Scaled upconverted fluorescence with changing excitation power density; and (d) double-Gaussian fit of upconverted fluorescence for Ru6DPA. 532 nm excitation power density was varied from 37 to 105 mW/cm^2 and Gaussian fits were done using the spectrum obtained via 105 mW/cm^2 excitation.*

The double-peak structure of the upconverted fluorescence resembles the results in solution, save for a slight variation of the relative peak intensity of the two Gaussian components. The agreement between the solid state and solution-phase results suggests that the peak in Figure 4.12 should be attributed to upconverted fluorescence. Correcting to a common excitation power and spectral bandwidth, the upconverted fluorescence intensity in these films is a factor of 1000 lower than that measured in solution. This substantial decrease is expected due to the intermolecular nature of TTA in this system and the restricted diffusion of these macromolecules in thin films. Furthermore, parasitic inter-chain effects will be enhanced in the film. The aggregation of polymer chains in the drop-cast film increases the concentration of static trap states that rival TTA-UC.

An apparatus allowing for spectroscopic study while wetting the film would provide the opportunity to study these latter two concepts. It is expected that wetting the film with solvent would significantly enhance upconverted fluorescence due to the greater diffusion rate and decrease in static traps in small amounts of solvent.

4.7 Summary and Future Direction

A detailed study of upconverted fluorescence has been presented in dilute solutions of two photophysically active polymers, each containing a single $Ru(bpy)_3$ core and multiple DPA-containing pendant arms. At the low power densities utilized, TTA is occurring in the weak annihilation kinetic limit and the majority of triplet molecules are decaying by first order or pseudo-first order processes. Upconverted fluorescence QYs vary linearly with excitation power in this kinetic regime, reaching a value of 0.1% for Ru2DPA. This value does not represent the maximum QY achievable in this system, as the maximum value would only be realized in the strong annihilation regime. Also the initial upconverted fluorescence would be a factor of 7 or 8 greater than that observed due to quenching of DPA singlets by back energy transfer from the initially excited singlet DPA moieties to the $Ru(bpy)_3$ core.

Ru6DPA had an upconverted fluorescence QY whose slope was about 0.125 that of Ru2DPA. This diminished QY is likely due to a greater degree of polymer folding, stemming from the greater number of DPA pendant arms in polymer Ru6DPA. QY calculations also demonstrate that phosphorescence from the $Ru(bpy)_3$ core is quenched by 91% in each of the polymers, consistent with previous studies.[140] The control experiment yielded a phosphorescence QY of 0.022 for $Ru(dmb)_3$ in chloroform, comparable to literature values of 0.073[119] and 0.095[192] in acetonitrile.

As a proof-in-principle study, upconverted fluorescence was observed in drop-cast films

comprised of either Ru2DPA or Ru6DPA. Upconverted fluorescence intensities were a factor of 1000 less than those observed in solution. This substantial decrease is attributed to the prevention of diffusion in the solid state and a significant concentration of static trap states stemming from enhanced polymer folding in the solid state. This result is consistent with the diminished upconverted fluorescence of Ru6DPA relative to Ru2DPA.

The previous discussion of the detrimental effects of polymer folding is consistent with the quenching data. Based on the Stern-Volmer experiment, quenching of $Ru(dmb)_3$ phosphorescence via TTET occurred with a rate constant of 2.2×10^9 and 1.00×10^9 $M^{-1}s^{-1}$ for pDPA and DPA, respectively. The 2.2-fold enhancement of phosphorescence quenching of pDPA relative to its monomer component was unexpected given the experimentally-determined 1 to 3.3 ratio in diffusion rates. This quenching rate enhancement is attributed to the increase in interaction cross section as a result of tethering thirty monomer units together. The factor of quenching enhancement in pDPA and the number of monomer units tethered together demonstrate a short-range interaction availability of 1/4 of a monomer DPA unit. This result is consistent with the notion of polymer folding in the pendant arms since some DPA moieties would be shielded from DET in the folded polymer. Kinetic analysis of the quenching data demonstrate intramolecular TTET from Ru-core to DPA moiety in the pendant arms followed by intermolecular TTA between DPA moieties.

Low upconverted fluorescence intensities were observed in these photophysically active polymers. With respect to meaningful application as low-wavelength augmenting layers in photovoltaics, two points of concern exist in the current system that can guide the design of future systems. First, polymers should be designed to undergo fast intramolecular TTA. Realization of this energy mechanism would remove the dependence of TTA-UC on slow diffusion processes and offer potential for solid-state application without the intensity losses associated with diminished diffusion rates. To realize intramolecular TTA, polymers must be comprised of many sensitizing moieties and many annihilator moieties - a

sensitizer-emitter copolymer system. Theoretical structures for upconverting copolymers have been proposed by Simon and Weder.[33] This copolymer system would experience enhanced light-harvesting characteristics and an increased probability for multiple one-photon absorption events within a polymer - a requirement for intramolecular TTA-UC. Based on the study at hand, it is estimated that a polymer with thirty chromophores possessing an oscillator strength approaching 1 would result in a shift in the dominant TTA process from intermolecular to intramolecular under the experimental conditions employed in this study.

The second limitation is with regards to the energetic pathways available in the system. The sensitizer and emitter must have energy levels such that TTET and TTA are rapid while back-energy transfer is non-competitive. In order to utilize the upconverted energy in this system, electron or electronic energy transfer from the upconverted singlet to some acceptor must be more rapid than intramolecular EET via any spin-allowed channels. Two significant obstacles for the guiding of new photophisically active upconverting polymers are presented here. A copolymer system which meets these challenges would become a very strong candidate for potential photovoltaic augmentation via TTA-UC.

Chapter 5

Overall Summary and Future Work

5.1 Overall Scope

The present study investigated photon upconversion by TTA in polymers. Chapter 2 introduced an experimental apparatus designed for steady-state spectroscopic study of TTA-UC in films. In Chapter 3, this apparatus was utilized to study homomolecular TTA in ZnTPP:polymer films. This chapter sought out to study the effect of polymer glass transition temperature on TTA-UC mechanisms. Chapter 4 extended the study of polymer-based TTA to a system in which the sensitizer and emitter are covalently bound together within a polymer. Power-dependent studies of TTA-UC and kinetic studies of sensitier-emitter polymers in solution are presented to better understand the limiting factors of TTA-UC in this polymer system.

5.2 ZnTPP-doped Polymer Films

Aggregation-driven TTA was demonstrated in ZnTPP in PMMA films, which have a glass transition temperature well above ambient temperature. In this system, ZnTPP molecules must be pre-aggregated in order for TTA to occur due to the low molecular diffusion coefficient in the glassy polymer. Homomolecular TTA occurs toward the strong annihilation kinetic limit in films cast from 1% wt ZnTPP:PMMA solution. Upconverted

fluorescence was observed to have a sub-linear dependence on film thickness. Further studies are required to determine the source of the trend.

Homomolecular TTA was also explored in ZnTPP in polymers possessing low glass transition temperatures. Molecular diffusion-driven TTA was demonstrated in ZnTPP in a PEG matrix. Here, upconverted fluorescence is achievable through the diffusion of two excited triplets and subsequent TTA. Determination of the dominant kinetic regime was not attainable due to significant photochemical changes in the films. A study of dye-loading ratio in these films revealed significant porphyrin self-quenching effects beginning at very low dye concentrations, a possible explanation for the low upconverted fluorescence intensities observed.

Homomolecular TTA was not observed in ZnTPP in a polyurethane matrix. It is proposed that the N atom of PU coordinates to the axial position of the Zn^{2+} ion. Such coordination would provide a steric barrier to TTA, as excited triplets would be held sufficiently far apart that short-range DET cannot occur.

Photobleaching and porphyrin self-quenching are considered the likely reasons for the low upconverted fluorescence intensities observed in the ZnTPP:PEG system, though PEG coordination to the Zn^{2+} ion is also considered. Whether polymer coordination plays a significant role in preventing NCPU would require a study of polymers comprised only of carbon atoms. Specifically, polystyrene (PS) and polyethylene (PE) have been identified as suitable polymers possessing high and low glass transition temperatures, respectively. Carbon would not coordinate to the Zn^{2+} ion, so a comparison of upconverted fluorescence in a ZnTPP:PE system to that of ZnTPP:PEG and ZnTPP:PU could be used to verify the coordination effect of PEG and PU. If high upconverted fluorescence intensities are observed in ZnTPP:PE, Stern-Volmer experiments can be performed to determine the degree of quenching by PEG and PU. If polymer binding is insignificant in the ZnTPP:PEG or ZnTPP:PU systems, the upconverted fluorescence intensities ob-

served in the ZnTPP:PE system would match those of the previous systems. Finally, PE would provide opportunity for unique additional experiments that vary the degree of diffusion allowed in the polymer matrix. By varying the PE chain length in a series of ZnTPP:PE systems, upconverted fluorescence can be monitored in a controlled manner as the porphyrin diffusion properties in the matrix are varied. PS is a proposed as a carbon-only analogous to the PMMA-based system.

5.3 Ru- DPA-containing Polymers

A detailed solution-phase characterization of TTA is presented for two photophysically-active polymers, each containing a single $Ru(bpy)_3$ sensitizing core and multiple DPA-containing pendant arms, where DPA is the emitter species. At the low power densities utilized, TTA is occurring in the weak annihilation kinetic limit and the dominant decay channel for DPA triplets is by first or pseudo-first order processes. Ru2DPA exhibited an upconverted fluorescence QY approaching 0.1% at the low excitation powers utilized. The QY maximum would be realized in the strong annihilation kinetic limit and the incident upconverted fluorescence QY would be a factor of 7 or 8 greater than that calculated due to singlet energy transfer from the DPA moieties back to the $Ru(bpy)_3$ core.

The low upconverted fluorescence QY of Ru6DPA relative to Ru2DPA is attributed to a greater degree of polymer folding in the former, which is due to the greater number of DPA-containing pendant arms. Such an increase in polymer folding introduces a greater concentration of energy traps parasitic to TTA-UC. It also enhances the probability of DPA moieties being shielded from DET. This result is consistent with the 1000 - fold decrease in upconverted fluorescence in drop-cast films of Ru2DPA and Ru6DPA and with the results of the quenching experiment.

Stern-Volmer analysis of the quenching of $Ru(bpy)_3$ revealed that the rate constant

for TTET to pDPA is 2.2× greater than that of monomeric DPA, a result attributed to an enhanced interaction cross section in pDPA. When diffusion rates of each quencher are considered, the tethered DPA moieties in pDPA demonstrate a short-range interaction availability of 1/4 that of the monomer per DPA unit in the polymer. This is consistent with the notion of polymer folding. Kinetic analysis revealed the dominant processes are intramolecular TTET from $Ru(bpy)_3$ core to DPA moiety followed by intermolecular TTA between DPA moieties. This result is consistent with the substantial decrease in upconverted fluorescence in the solid state, where molecular diffusion is severely limited.

5.4 Future Outlook

Chapter 3 gave insight into the effects of glass transition temperature on TTA-UC in ZnTPP:polymer films. Inefficient aggregation- and diffusion-driven TTA-UC was demonstrated, while self-quenching was likely a significant factor in the low upconverted fluorescence observed. The Ru-DPA polymers in Chapter 4 also realized intermolecular TTA-UC. These materials were subject to diminished TTA-UC yields in thin films in a similar manner to the system studied in Chapter 3. Both of these thin film upconverting systems lack efficiency for implementation into photovoltaics.

From the data presented in this work, a strategy for achieving upconverted fluorescence relevant to the augmentation of photovoltaics is proposed. Thin film upconverters with high fluorescence yields would require that TTA occur by intramolecular processes. A copolymer comprised of many sensitizers and many emitters would be capable of multiple one-photon absorptions and subsequent intramolecular TTA. Based on the parameters utilized in the current study, a polymer containing thirty sensitizers with oscillator strength approaching 1 should shift the dominant TTA process from intermolecular to intramolecular. Furthermore, back energy transfer must be non-competitive. To utilize the upconverted energy in this polymer, electron or electronic energy transfer from the

upconverted singlet to some acceptor must be more rapid than intramolecular EET. A copolymer which meets these challenges would become a candidate for photovoltaic augmentation via TTA-UC.

Appendices

A.1 Justification of Excitation Power Dependence of Upconverted Fluorescence

Kinetics of TTA-UC:

The general kinetic scheme for NCPU via TTA is described in Section 1.3 and outlined in the following mechanism for a sensitizer-emitter system:[92]

$$h\nu_{ex} + {}^1S \rightarrow {}^1S^* \tag{A.1a}$$

$${}^1S^* \rightarrow {}^3S^* \tag{A.1b}$$

$${}^3S^* + {}^1E \rightarrow {}^1S + {}^3E^* \tag{A.1c}$$

$${}^3E^* + {}^3E^* \rightarrow {}^1E^* + {}^1E \tag{A.1d}$$

$${}^1E^* \rightarrow {}^1E + h\nu_{em} \tag{A.1e}$$

where ISC and TTET (b and c, respectively) are fast relative to TTA (d). This notion is justified by the long-lived emitter triplet state relative to its singlet state and both the singlet and triplet states of the sensitizer. In addition to the desired TTA pathway, emitter triplets can also decay through other channels including bimolecular quenching, self-quenching, and non-radiative relaxation. These relaxation schemes are generalized as first order or pseudo-first order. Following light absorption and ISC the emitter triplet concentration decays as follows:

$$\frac{d}{dt}[{}^3E^*]_t = -k_d[{}^3E^*]_0 - k_{TTA}\left([{}^3E^*]_0\right)^2 \tag{A.2}$$

where k_d is the sum of the rate constants of the unimolecular first order or pseudo-first order decay pathways for emitter triplets. Generally, k_d represents all pathways that rival the decay of emitter triplets via bimolecular TTA. Equation A.2 has the exact solution

$$\begin{aligned} \left[{}^3E^*\right]_t &= \left[{}^3E^*\right]_0 \frac{1-\beta}{e^{k_d t} - \beta} \\ \beta &= \frac{k_{TTA}\left[{}^3E^*\right]_0}{k_d + k_{TTA}\left[{}^3E^*\right]_0} \end{aligned} \tag{A.3}$$

The upconverted fluorescence from the emitter species is integrated with respect to time, yielding

$$\begin{aligned} N_{UC} &= \int_0^\infty I_{UC} dt \\ I_{UC} &= \Phi_F k_{TTA} \left([^3E^*]_t \right)^2 \end{aligned} \tag{A.4}$$

where I_{UC} and N_{UC} are the time-dependent and time-independent upconverted fluorescence intensity, respectively.[43] As shown, I_{UC} depends on the probability of producing a fluorescent state via bimolecular TTA, $k_{TTA} \left([^3E^*]_t \right)^2$, and the probability of fluorescence from that state, Φ_F. N_{UC} is dependent on excitation power through the dependence on emitter triplet concentration, $[^3E^*]_t$. This power dependence can be quantified by considering the strong and weak annihilation kinetic limits. These are the extreme cases in which TTA accounts for a majority and negligible proportion of triplet decay occurrences, respectively.

Weak Annihilation Kinetic Limit ($k_d >> k_{TTA} [^3E^*]_0$)

In this limit, β can be determined by dividing the numerator and denominator of Equation A.3 by k_d.

$$\beta = \frac{k_d \left(k_{TTA} [^3E^*]_0 / k_d \right)}{k_d \left(1 + k_{TTA} [^3E^*]_0 / k_d \right)} = 0$$

since

$$\left(k_{TTA} \left[^3E^* \right]_0 / k_d \right) \rightarrow 0$$

$$\therefore \left[^3E^* \right]_t = \left[^3E^* \right]_0 e^{-k_d t}$$

Substituting this result into Equation A.4 yields

$$N_{UC} = \int_0^\infty \Phi_F k_{TTA} \left(\left[^3E^* \right]_0 e^{-k_d t} \right)^2 dt = \Phi_F k_{TTA} \left(\left[^3E^* \right]_0 \right)^2 \int_0^\infty e^{-2k_d t} dt$$

$$N_{UC} = \frac{\Phi_F k_{TTA}}{2k_d} \left(\left[^3E^* \right]_0 \right)^2 = \Phi_F k_{eff} \left(\left[^3E^* \right]_0 \right)^2$$

where $k_{eff} = k_{TTA}/2k_d$.

Thus in the weak annihilation kinetic regime, N_{UC} has a quadratic dependence on the

initial triplet concentration.

Strong Annihilation Kinetic Limit ($k_d << k_{TTA}\left[{}^3E^*\right]_0$)

Since k_d is assumed to be small, the exponential term in β can be expanded in a Taylor Series to obtain $e^{k_d t} = 1 + k_d t +$ negligible terms. Then

$$\left[{}^3E^*\right]_t = \left[{}^3E^*\right]_0 \left[\frac{1-\beta}{1+k_d t-\beta}\right] = \left[{}^3E^*\right]_0 \left[\frac{1-\left[\dfrac{k_{TTA}\left[{}^3E^*\right]_0}{k_d+k_{TTA}\left[{}^3E^*\right]_0}\right]}{1+k_d t-\dfrac{k_{TTA}\left[{}^3E^*\right]_0}{k_d+k_{TTA}\left[{}^3E^*\right]_0}}\right]$$

Multiplying numerator and denominator by the sum of the decay rate constant terms ($k_d + k_{TTA}\left[{}^3E^*\right]_0$) yields

$$\left[{}^3E^*\right]_t = \left[{}^3E^*\right]_0 \left[\frac{k_d+k_{TTA}\left[{}^3E^*\right]_0-k_{TTA}\left[{}^3E^*\right]_0}{k_d+k_{TTA}\left[{}^3E^*\right]_0+\left(k_d\right)^2 t+k_d k_{TTA} t\left[{}^3E^*\right]_0-k_{TTA}\left[{}^3E^*\right]_0}\right]$$

Terms two and three in the numerator cancel out, as do terms two and five in the denominator.

$$\left[{}^3E^*\right]_t = \left[{}^3E^*\right]_0 \left[\frac{k_d}{k_d+\left(k_d\right)^2 t+k_d k_{TTA} t\left[{}^3E^*\right]_0}\right] = \left[{}^3E^*\right]_0 \left[\frac{1}{1+k_d t+k_{TTA} t\left[{}^3E^*\right]_0}\right]$$

Term two in the denominator can be neglected by recalling the initial condition for the strong annihilation limit. If $k_d << k_{TTA}\left[{}^3E^*\right]_0$ then $k_d t << k_{TTA} t\left[{}^3E^*\right]_0$.

$$\therefore \left[{}^3E^*\right]_t = \left[{}^3E^*\right]_0 \left[\frac{1}{1+k_{TTA} t\left[{}^3E^*\right]_0}\right]$$

The above expression can be inserted into Equation A.4, yielding

$$\begin{aligned} N_{UC} &= \int_0^\infty \phi_F k_{TTA}\left(\left[{}^3E^*\right]_0\left[\frac{1}{1+k_{TTA} t\left[{}^3E^*\right]_0}\right]\right)^2 dt \\ &= \phi_F k_{TTA}\left(\left[{}^3E^*\right]_0\right)^2 \int_0^\infty \left(\frac{dt}{1+k_{TTA} t\left[{}^3E^*\right]_0}\right)^2 \\ &= \phi_F k_{TTA}\left(\left[{}^3E^*\right]_0\right)^2 \left(\frac{1}{k_{TTA}\left[{}^3E^*\right]_0}\right) \\ &\therefore N_{UC} = \phi_F\left[{}^3E^*\right]_0 \end{aligned}$$

Thus in the strong annihilation limit, N_{UC} varies linearly with initial concentration of emitter triplets.

A.2 Reabsorption Model for SPEX Experimental Setup

For sufficiently concentrated samples with a small Stokes' shift, overlap between the absorption and emission spectra results in significant reabsorption losses, which skew the emission spectrum. This skewed portion of the emission spectrum can be corrected quantitatively through geometric considerations provided that the absorption spectrum of the sample has been obtained. Figure A.1 provides an example of such a system.

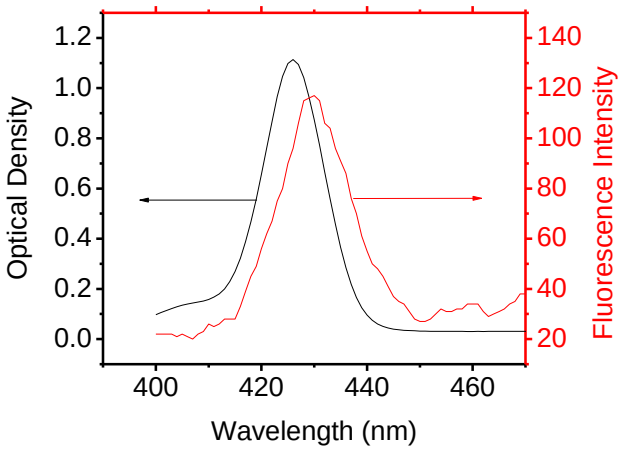

Figure A.1: *Optical density (black) and upconverted fluorescence (red) of a ZnTPP:PEG thin film. Spectral bandwidths are 2 nm for the optical density spectrum and 14.4 nm for the fluorescence spectrum.*

Of interest in Figure A.1 is the significant overlap between the absorption and fluorescence spectra. Because of this overlap, it is conceivable that the photon emitted from an excited ZnTPP molecule can be reabsorbed by adjacent ground-state molecules. This potential for reabsorption is very likely in this case by noting how the emission spectrum appears to rise to a peak located exactly at the intersection point of the two spectra. It is possible the emission spectrum peaks at higher energies than shown in Figure A.1 but is overcome by the enhanced optical density of the ground-state molecules at energies above the intersection point of the two spectra. Thus a model capable of correcting for

reabsorption effects is needed.

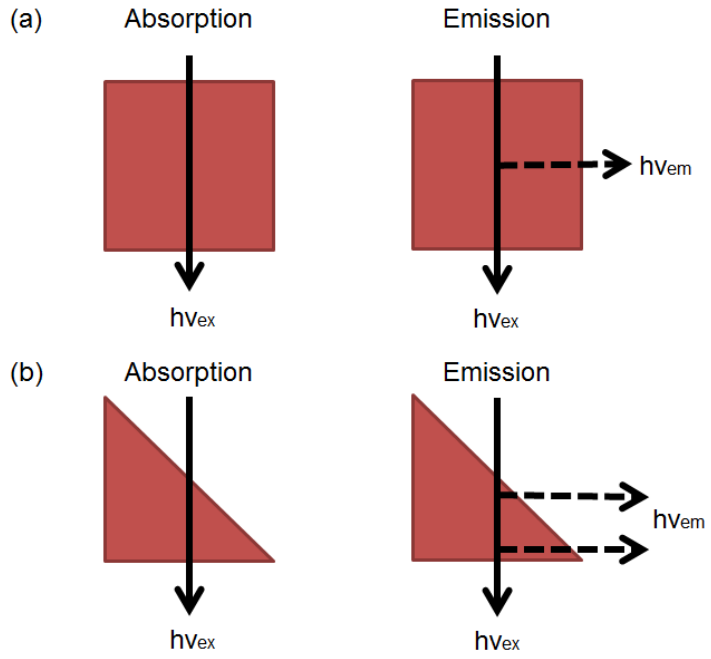

Figure A.2: *Schematic diagram of absorption and emission spectroscopy for solution-phase samples in a (a) 1 cm × 1 cm cuvette; and (b) 1 cm triangular cuvette.*

Figure A.2 provides a schematic of solution-phase absorption and emission spectroscopy for reabsorption considerations. In an absorption experiment, a known intensity of light is passed through the sample and the optical density of the sample is determined by the relationship between the incident and detected light, $A = -log\left(\frac{I}{I_0}\right)$, where I_0 is the incident light intensity and I is the intensity of detected light. The present reabsorption model considers the sample fluorescence in the same manner, where the emission signal that passes through the sample slice to reach the detector is I and the initial fluorescence of the sample is I_0. This model is appropriate under the condition that the sample is sufficiently dilute such that the majority of the light transmits through the sample. This condition is necessary to ensure that the excitation intensity does not vary through the depth profile of the sample.

In Figure A.2(a), it is clear that a photon emitted from an excited sample molecule along the excitation axis must pass through 0.5 cm of solution before it can reach the

SPEX optics and be focused on the detector. Thus the wavelength-dependent optical density of this 0.5 cm path length is obtained by taking $A^* = A/2$, assuming the raw optical density, A, was obtained in a 1 cm × 1 cm cuvette. Once A^* is known, the incident emission intensity at the excitation axis can be determined by solving the general optical density equation for I_0:

$$\begin{aligned} A^* &= -log\left(\frac{I}{I_0}\right) \\ \therefore I_0 &= I \cdot 10^{A^*} \\ \delta I_0 &= 10^{A^*}\delta I + I \cdot 10^{A^*}\delta A^* = I_0\left[\frac{\delta I}{I} + \delta A^*\right] \end{aligned} \tag{A.5}$$

where the error in A^* is determined via the method of partial derivatives. Equation A.5 is sufficient for samples in solid or solution phase, noting that A^* will be scaled as appropriate with changes to the experimental geometry. For a sufficiently dilute solution sample in a triangular cuvette, emission can occur with equal probability from any point along the excitation axis. A photon emitted at the front face and back face of the cuvette must transmit through a solution path length of 0 cm and 0.5 cm, respectively. Since the probability of absorption (and emission) is equal along the excitation axis, the average photon must transmit through a solution path length of 0.25 cm prior to detection. Thus $A^* = A/4$ in a triangular solution sample.

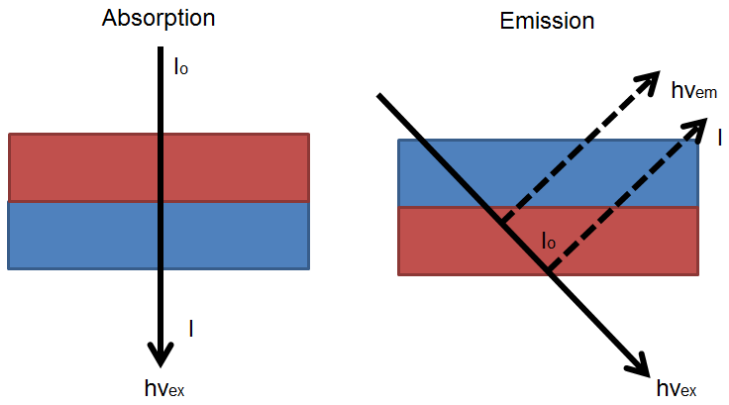

Figure A.3: *Schematic diagram of absorption and emission spectroscopy for thin film samples. Sample film and glass slide are shown as red and blue, respectively.*

Figure A.3 shows the spectroscopic geometry for a thin film sample, with the excitation occuring at 0.25π radians from the normal direction of the film. Due to this geometry, the effective excitation path length of the film is $l_{ex} = \sqrt{2}t$, where t is the film thickness. Again assuming the probability of absorption to be equal along the excitation axis, the probability of photon emission at any point along the excitation axis is equal so the average effective path length a photon must pass through to reach the detector is $l_{em} = t/\sqrt{2}$. The effective optical density of the film slice a photon must transmit through in the emission experiment can be calculated by the ratio of the path lengths:

$$\frac{A^*}{A} = \frac{\varepsilon c l_{em}}{\varepsilon c l_{ex}} = \frac{\left(t/\sqrt{2}\right)}{t} = 1/\sqrt{2}$$
$$\therefore A^* = A/\sqrt{2}$$

The wavelength-dependent correction can then be obtained using Equation A.5.

A.3 Steady-State Spectroscopy of Solution-phase ZnTCPP

The spectroscopic behaviour of ZnTCPP in DMF is shown in Figure A.4. The normalized spectra shown in (a) agree with those previously reported in various solvents with respect to the S_1 peak locations.[105;161–163;166] A low-intensity peak was observed at 460 nm and believed to be due to TTA-UC. Upconverted fluorescence was not studied in this compound beyond proof in concept. DMF is a coordinating solvent which is detrimental to TTA-UC, a possible explanation for the low raw intensity of the upconverted fluorescence peak. Furthermore, it is conceivable that ZnTCPP deprotonates in solution, leaving an anionic molecule whose charge varies with the series of deprotonation. Thus a Coulombic barrier to TTA-UC in this system exist in addition to the steric barrier introduced by the coordinating solvent. A proposed strategy for overcoming this barrier is discussed later in the section.

Concentration-dependent absorption and fluorescence were measured for ZnTCPP in DMF solution. Figure A.4 shows no evidence of significant porphyrin aggregation at the low concentrations utilized in the study. Peak positions of ZnTCPP in DMF reasonably match those of ZnTPP in DMF. This observation is consistent with the notion that incorporation of the carboxylate moieties does not greatly affect the ground-state energetics of ZnTPP.[166–169]

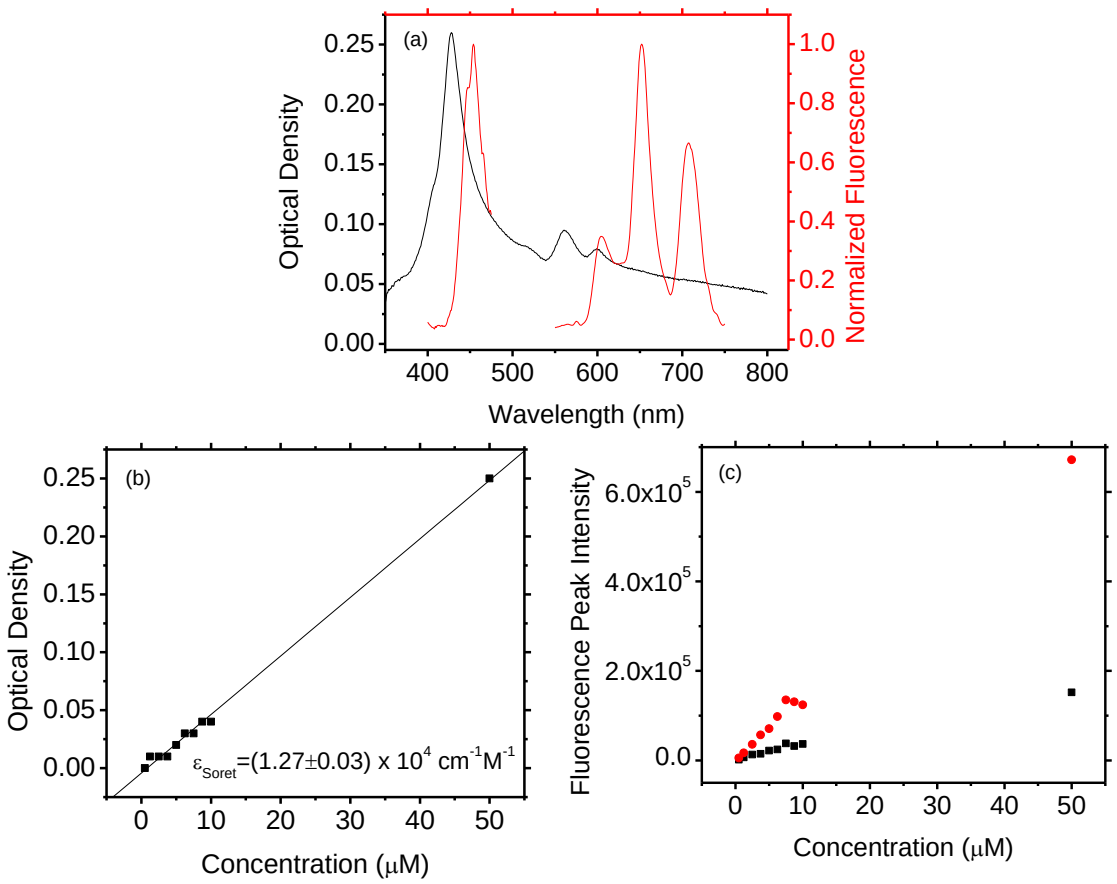

Figure A.4: *(a) Optical density and separately normalized S_1 and upconverted S_2 fluorescence of 50 μM ZnTCPP in DMF; (b) Optical Density; and (c) S_1 fluorescence at the 650 nm (red) and 600 nm (black) peaks as a function of ZnTCPP concentration in DMF. Spectral bandwidths are: 2 nm for optical density measurements in (a) and (b); 14.4 nm for upconverted fluorescence measurement in (a); 1.8 nm for prompt fluorescence in (a) and 3.6 nm in (c). Raw intensities in (a) are 500 and 170 000 cps for upconverted fluorescence and prompt fluorescence, respectively.*

A potential strategy for overcoming the steric and coulombic barriers opposing TTA-UC in ZnTCPP is functionalization with an amine-containing molecule. The prospect of functionalizing ZnTCPP with amine end-capped PEG was considered an interesting

direction for further research. The amine undergoes a rapid nucleophilic attack on the carbonyl group in a reaction that has been studied extensively under a variety of experimental conditions.[197] It was believed this PEG-functionalized ZnTCPP would have good compatibility with bulk PEG, resulting in a PEG film with good morphology that facilitated molecular diffusion-driven TTA-UC.

A.4 Supplementary Experiments for Ruthenium-DPA Polymer System

Laser Flash Photolysis

LFP was utilized to determine the concentration-dependent triplet lifetime of $Ru(dmb)_3$ used in the triplet quenching experiment. The Stern-Volmer Plot for the self-quenching of $Ru(dmb)_3$ triplets is shown in Figure A.5.

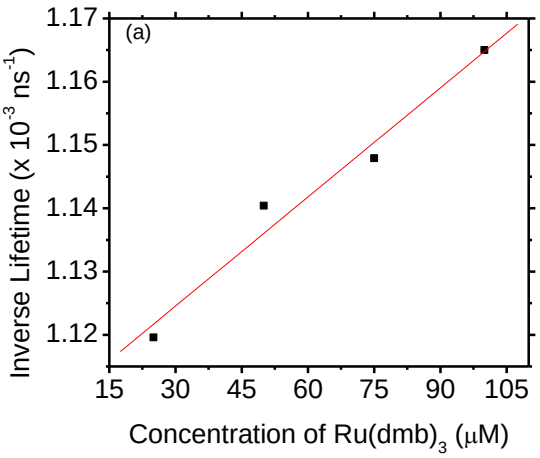

Figure A.5: *Stern-Volmer Plot for the self-quenching of $Ru(dmb)_3$ triplet states. The triplet lifetimes were determined by LFP The LFP experiment was performed by Chelsea S. M. Greenwald.*

The LFP experiment was performed by pulsing with a 532 nm excitation source and monitoring the decay rate of the phosphorescence at 630 nm. The phosphorescence decay was fit reasonably well to a single exponential function. Phosphorescence decay, exponential fits and residuals are shown in Figure A.6.

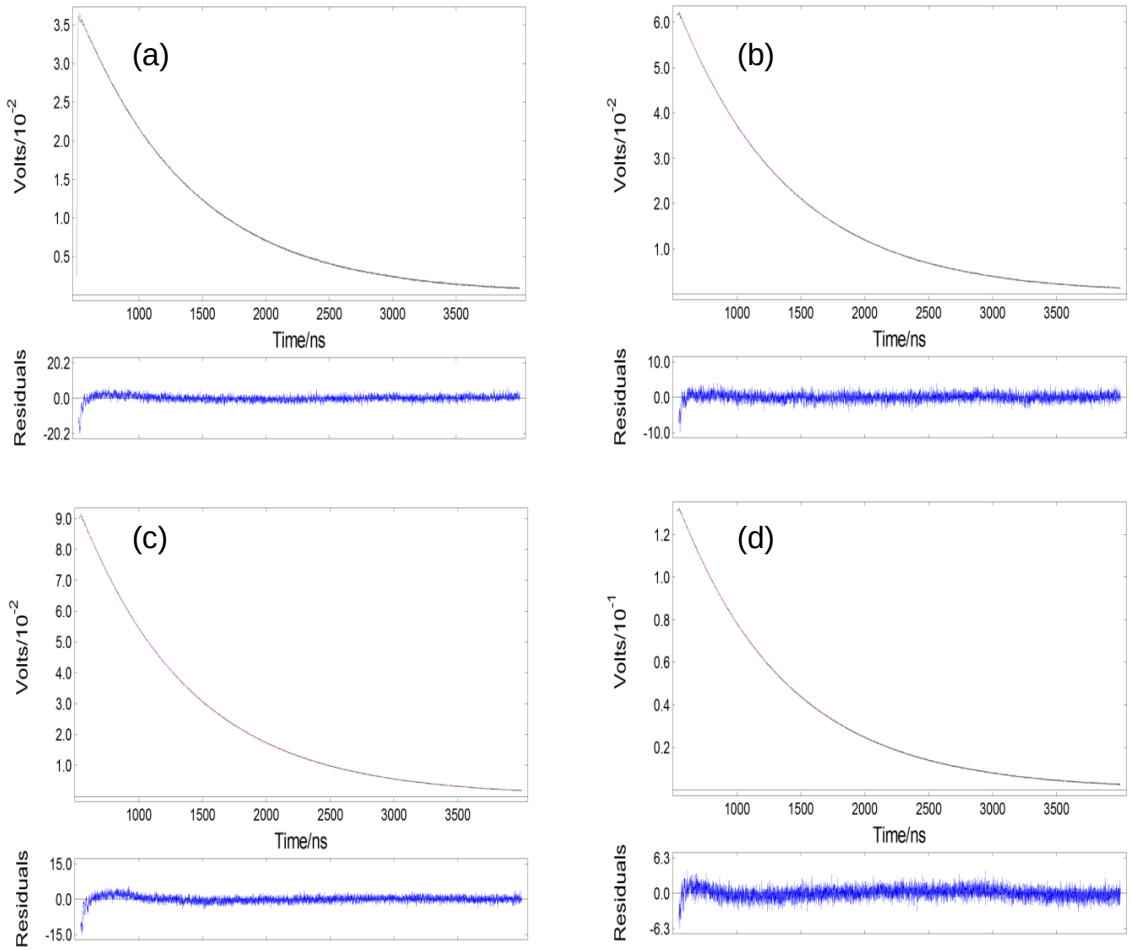

Figure A.6: *Phosphorescence decays, exponential fits and residual plots for Ru(dmb)$_3$ in CHCl$_3$ at concentrations of: (a) 25 μM; (b) 50 μM; (c) 75 μM; (d) 100 μM. The LFP experiment was performed by Chelsea S. M. Greenwald.*

The results show only slight variance in concentration-dependent triplet lifetime in Ru(dmb)$_3$, evidence of very little self-quenching. From the slope of Figure A.5, the lifetime of Ru(dmb)$_3$ at the 74 μM concentration utilized in the quenching experiments is 870 ns, which can be compared to reported literature values of 704 ns[140], 840 ns[75], and 920 ns[42] in various solvents.

Diffusion Ordered Spectroscopy

Diffusion coefficients of the ruthenium- and DPA-containing compounds studied in Chapter 4 were measured by two-dimensional diffusion ordered spectroscopy (DOSY) at

room temperature in $CDCl_3$. Calibration was performed using caffeine in $CDCl_3$.[198] The results are summarized in Table A.1. The data in column 3 is based on the DOSY experiment with analytical methods outlined in the literature,[198] while column 4 was obtained by modelling the molecules as spherical and assuming that diffusion coefficients scale as the square root of molar mass. The diffusion coefficients are normalized to that of DPA for direct comparison of the two quenching experiments discussed in Section 4.3. The DOSY experiment was performed by Dr. Keith C. Brown.

Table A.1: Diffusion Coefficients of Ru and DPA Containing Species

Species	**D x 10^{10}m^2/s**	**Experimental D_{DPA}/D_x**	**Stokes-Einstein D_{DPA}/D_x**
DPA	10	1	1
$Ru(dmb)_3$	6.5	1.54	
Ru2DPA	2.3	4.35	4.50
Ru6DPA	1.9	5.26	7.58
pDPA	3.0	3.33	5.74

A.5 Mathematical Processing of Ru-DPA Polymer Spectral Data for Quantum Yield Calculations

General Method for the Determination of Quantum Yields

Phosphorescence and upconverted fluorescence QYs for the Ru- and DPA-functionalized polymers described in Chapter 4 have been determined using the comparative method. By this method, the QY of a luminescence process can be calculated through comparison with a known reference material - Rhodamine 6G in $CHCl_3$ in this experiment, which has a fluorescence QY of 0.75.[196] If the luminescence experiments are performed under identical conditions, the QY of the sample material (x) can be calculated relative to that of the reference, R, by Equation A.6.[24;55;72;77;195;199;200]

$$\phi_x = N\xi\phi_R \frac{1-10^{-OD_R}}{1-10^{-OD_x}} \frac{I_x}{I_R} \frac{n_x^2}{n_R^2} \tag{A.6}$$

where ϕ, OD, I and n are the QY, optical density at the excitation wavelength, integrated emission intensity and solvent refractive index, respectively. ξ accounts for the variation in photodetector sensitivity from the emission region of the reference to that of the sample material. This factor varies with each sample material studied and is quantified in Table A.6. N is the number of photons required for the process under study: 2 for upconverted fluorescence and 1 for phosphorescence.[24;25;55;72;119] The origin of the factor of two for upconverted fluorescence is the fact that NCPU via TTA requires two incident photons. Without this factor, a theoretical material that has completely efficient upconverted fluorescence in the absence of losses would have a QY of only 0.5. This factor of two offers a scale such that the theoretical completely efficient system will have a QY of unity.[119] The power-dependent upconverted fluorescence QYs are calculated for Ru2DPA, Ru6DPA, and reference materials containing varied concentrations of $Ru(dmb)_3$ and DPA. Phosphorescence QYs are calculated for Ru2DPA, Ru6DPA and $Ru(dmb)_3$. These values are summarized in Tables A.7, A.8, A.9, and A.10. In the present study,

$$\phi_{Ph} = \xi\phi_{Rh6G}\frac{1-10^{-OD_{Rh6G}}}{1-10^{-OD_{Ph}}}\frac{I_{Ph}}{I_{Rh6G}} \tag{A.7}$$

and

$$\phi_{UC} = 2\xi\phi_{Rh6G}\frac{1-10^{-OD_{Rh6G}}}{1-10^{-OD_{UC}}}\frac{I_{UC}}{I_{Rh6G}} \tag{A.8}$$

The refractive index term is unity since all samples are prepared in degassed chloroform. Once the upconverted fluorescence QY is known, the QY for TTA can be calculated by considering upconverted fluorescence as the product of three processes following light harvesting,[23;33;34]

$$\phi_{UC} = \frac{1}{2}f\phi_{TTET}\phi_{TTA}\phi_F \tag{A.9}$$

taking the QY for intersystem-crossing in $Ru(dmb)_3$ to be unity.[182;201] f is the probability that TTA results in an excited singlet and the factor of 1/2 accounts for the fact that two incident photons yield one emitted photon.[33] Schmidt and co-workers[45;46] have demonstrated that f is well beyond the 11.1% suggested by spin statistics. The spin-

statistical limit of TTA is discussed in Section 1.3.3. Ghiggino and coworkers[140] reported a fluorescence QY of 0.61 for pDPA, which is estimated to be equal to the fluorescence QYs of the DPA-moieties in the polymer pendent arms. Thus, a determination of the factor f would result in the ability to calculate ϕ_{TTA} for the DPA moieties in the arms of the polymer materials.

Determination of TTET Efficiency

The efficiency of triplet energy transfer from sensitizing $Ru(bpy)_3$ core to DPA pendant arms is calculated from the results of the Stern-Volmer experiments (Section 4.3) since the DPA quenching of phosphorescence of $Ru(dmb)_3$ is a triplet energy process. Thus the quenching rate constant is equal to the rate constant of TTET. Using a triplet lifetime of τ=870 ns for $Ru(dmb)_3$ (as determined by LFP) the rate constant for TTET from $Ru(dmb)_3$ to DPA is $(2.2 \pm 0.2) \times 10^9$ $M^{-1}s^{-1}$.

The QY for TTET is the fraction of DPA triplets produced from the photoexcited sensitizer triplets. Quantitatively, it is the product of intersystem-crossing in $Ru(dmb)_3$ and the QE, η, of TTET from sensitizer to emitter. Since intersystem-crossing is unity in $Ru(dmb)_3$, then $\phi_{TTET} = \eta_{TTET}$. Since TTET is a competitive pathway to the radiative and non-radiative relaxation pathways for triplet-sensitized $Ru(dmb)_3$, the efficiency of TTET is determined by the ratio[34]

$$\eta_{TTET} = \frac{k_Q\,[DPA]}{\dfrac{1}{\tau_0} + k_Q\,[DPA]} \tag{A.10}$$

TTET efficiency as a function of DPA concentration is shown in Figure A.7 using the quenching rate constant and triplet lifetime reported in this section.

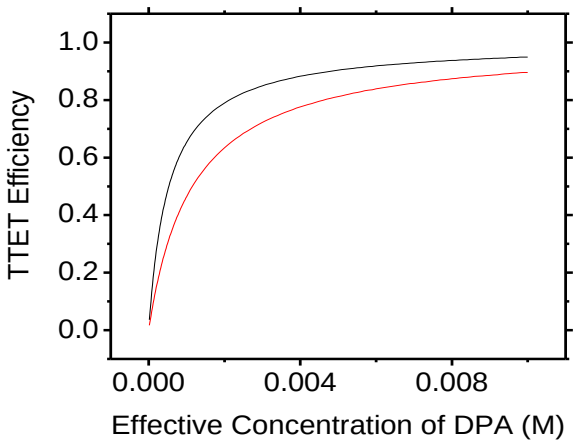

Figure A.7: *Theoretical variation in TTET Efficiency from Ru(dmb)$_3$ to pDPA (black) and DPA (red) with varying DPA concentration. Triplet lifetime of 74 μM Ru(dmb)$_3$ is 870 ns.*

The sample of Ru(dmb)$_3$ utilized in the quenching experiments had an initial concentration of 74 μM and optical density of 0.15 at the 532 nm excitation source utilized. In the upconverted fluorescence experiments, the optical densities at 532 nm of Ru2DPA and Ru6DPA were 0.13 and 0.09, respectively. From the measured optical densities and the known concentration of the control sample, the effective concentration of Ru(dmb)$_3$ cores in each upconverting polymer can be calculated. Since the ratio of cores to DPA moieties in each upconverting polymer is known, the concentration of DPA moieties in each polymer can be calculated. TTET QY is then calculated via Equation A.10. The results are summarized in Table A.2.

Table A.2: Summary of Results for TTET Efficiency Calculations in Polymers

Polymer	**[Ru(dmb)$_3$] (μM)**	**Effective [DPA] (mM)**	τ_0 **(ns)**	$\mathbf{k}_{TTET}$ $\mathbf{M^{-1}s^{-1}}$	ϕ_{TTET}
Ru2DPA	67	1.1	873	2.2x10^9	0.67
Ru6DPA	47	2.3	881	2.2x10^9	0.81

Spectroscopy of Rhodamine 6G Standard

The reference standard was Rhodamine 6G in $CHCl_3$, which has a fluorescence QY of 0.75.[196] The reference was diluted such that the optical density at 532 nm was comparable to that of the polymers under study. The fluorescence spectrum of Rhodamine 6G was measured as a function of excitation power density. A reference compound was

included for each spectral bandwidth utilized in the polymer experiments. To prevent saturation of the photodetector, the reference material was studied at very low power densities. The integrated fluorescence intensity was then plotted as a function of excitation power density and from the slope, the integrated fluorescence intensity was extrapolated up to the power densities utilized in the upconverted fluorescence and phosphorescence experiments. It is reasonable to assume that the singlet fluorescence of Rhodamine 6G varies linearly with excitation power at the very low concentrations (1.6 μM) and power densities (< 100 mW/cm^2) utilized in these experiments. The raw data at each spectral bandwidth utilized in the polymer spectroscopy experiments is given in Figure A.8, and the results are summarized in Table A.3.

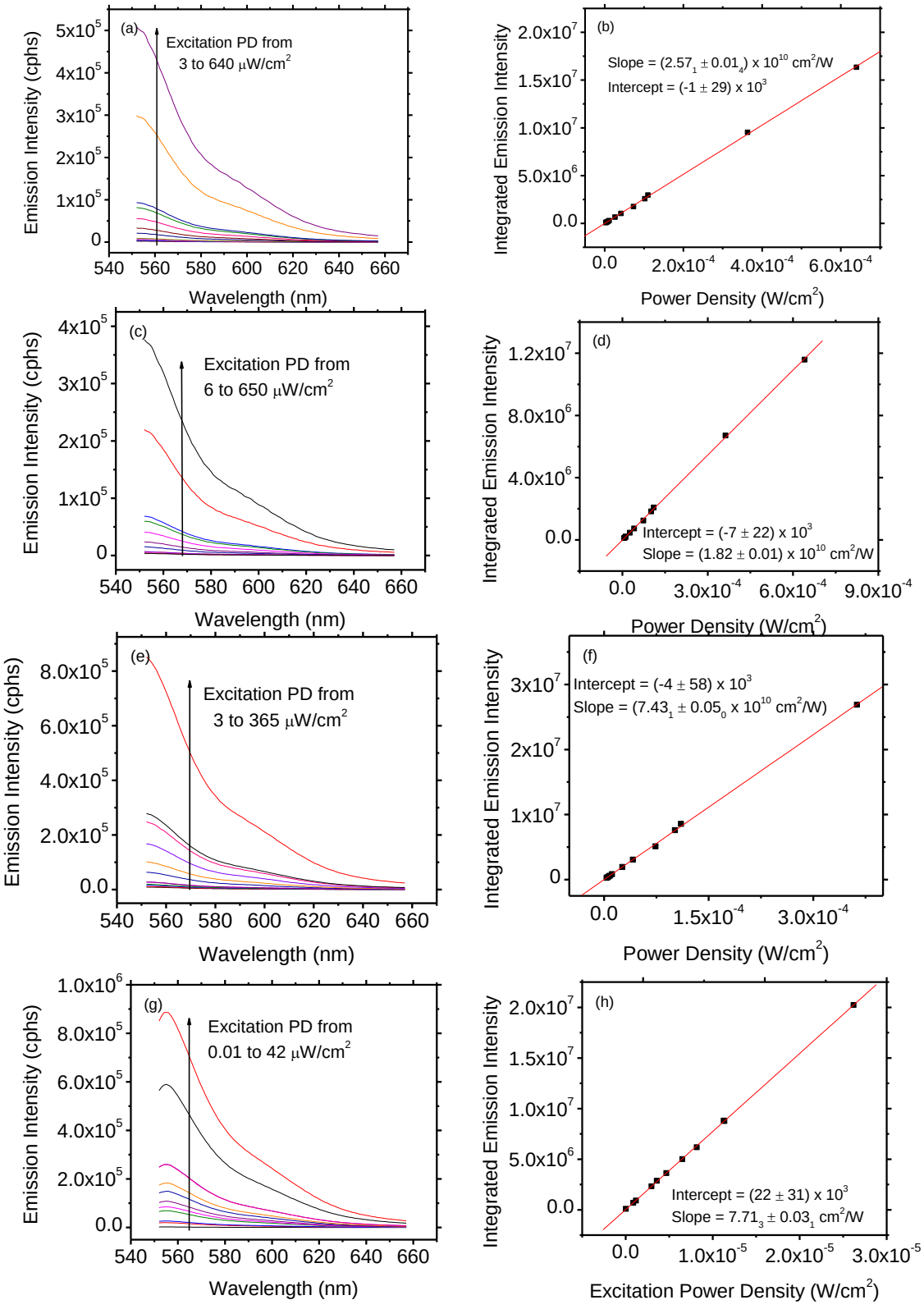

Figure A.8: *Emission spectra and the variation in integrated emission intensity with excitation power density for Rhodamine 6G in $CHCl_3$, taken at the spectral bandwidths utilized in the polymer luminescence experiments. Concentrations and spectral bandwiths are as follows: (a, b) 2.66 μM, 1.8 nm; (c, d) 1.58 μM, 1.8 nm; (e, f) 1.58 μM, 3.6 nm; (g, h) 1.58μM, 12.6 nm.*

Table A.3: Extrapolated Singlet Emission Intensities of Rhodamine 6G Standard

Power Density (mW/cm^2)	**Rhodamine 6G Integrated Emission**			
	Sample A	**Sample B**	**Sample C**	**Sample D**
1.12	2.88×10^7	2.04×10^7	8.32×10^7	8.64×10^8
3.71	9.54×10^7	6.75×10^7	2.76×10^8	2.86×10^9
5.85	1.50×10^8	1.06×10^8	4.35×10^8	4.51×10^9
10.3	2.65×10^8	1.87×10^8	7.65×10^8	7.94×10^9
12.3	3.16×10^8	2.24×10^8	9.14×10^8	9.49×10^9
13.8	3.55×10^8	2.51×10^8	1.03×10^9	1.06×10^{10}
18.9	4.86×10^8	3.44×10^8	1.40×10^9	1.46×10^{10}
21.0	5.40×10^8	3.82×10^8	1.56×10^9	1.62×10^{10}
33.6	8.64×10^8	6.11×10^8	2.50×10^9	2.59×10^{10}
33.7	8.66×10^8	6.13×10^8	2.50×10^9	2.60×10^{10}
37.3	9.59×10^8	6.79×10^8	2.77×10^9	2.88×10^{10}
46.2	1.19×10^9	8.41×10^8	3.43×10^9	3.56×10^{10}
59.2	1.52×10^9	1.08×10^9	4.40×10^9	4.57×10^{10}
59.8	1.54×10^9	1.09×10^9	4.44×10^9	4.61×10^{10}
81.7	2.10×10^9	1.49×10^9	6.07×10^9	6.30×10^{10}
105	2.70×10^9	1.91×10^9	7.80×10^9	8.10×10^{10}
Slope (cm^2/W)	$(2.57 \pm 0.01) \times 10^{10}$	$(1.82 \pm 0.01) \times 10^{10}$	$(7.43 \pm 0.05) \times 10^{10}$	$(7.71 \pm 0.03) \times 10^{11}$
Intercept	$(-13 \pm 29) \times 10^3$	$(-7 \pm 22) \times 10^3$	$(-4 \pm 58) \times 10^3$	$(22 \pm 31) \times 10^3$
Concentration (μM)	2.66	1.58	1.58	1.58
Spectral Bandwidth	0.9 nm	1.8 nm	3.6 nm	12.6 nm
Samples for Which That Standard was Utilized	Ph in $Ru(dmb)_3$, UC in control mixtures	Ph in Ru2DPA	Ph in Ru6DPA	UC in Ru2DPA and Ru6DPA

The linear relations in Figure A.8(b, d, f, h) were used to extrapolate integrated emission intensity up to the power densities utilized in the polymer spectroscopic experiments, reported in Table A.3. The spectra in Figure A.8(a, c, e, g) are truncated to the region in which the SPEX data is independent of filter effects and laser scatter. The 532 nm excitation source is aligned well to the peak of the absorption band of Rhodamine 6G.[202] Since Rhodamine 6G has a small Stokes' shift, it is conceivable that a significant portion of the fluorescence spectrum is lost due to the 532 nm notch filter. The region of the fluorescence spectrum independent of filter effects was determined by comparing the fluorescence spectrum obtained via 532 nm laser excitation in the SPEX fluorolog spec-

trophotometer to that obtained via 342 nm excitation in the PTI spectrophotometer. Thus, the extrapolated fluorescence intensities reported in Table A.3 will be multiplied by a factor describing the area of the spectrum lost to filter and laser scatter effects. Figure A.9 compares the spectral sensitivity-corrected fluorescence obtained via 532 nm excitation in the SPEX apparatus to that obtained via 342 nm excitation in the PTI apparatus.

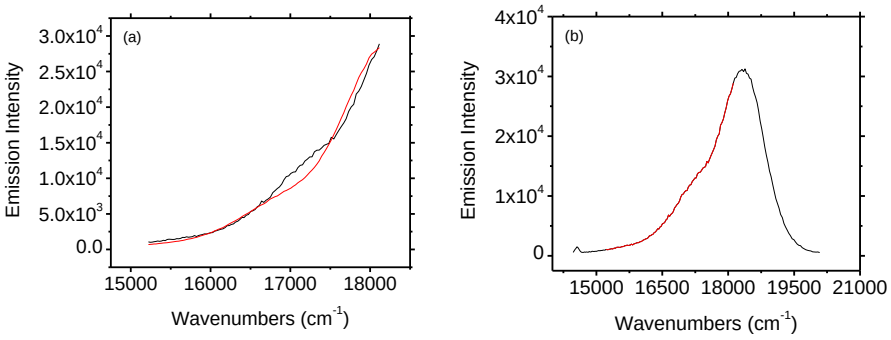

Figure A.9: *(a) Comparison of scaled SPEX data (red) to PTI data (black) in the range of 552 to 657 nm; (b) Comparison of full spectral data obtained via 342 nm excitation in PTI apparatus (black) to that obtained via 532 nm excitation in SPEX apparatus (red) for 1.58 μM Rhodamine 6G in $CHCl_3$.*

The area underneath the curves in Figure A.9(a) matched sufficiently well for the comparison of SPEX data to full PTI fluorescence spectrum to be meaningful. By integrating the two curves in Figure A.9(b), the portion of the spectrum lost to filter effects in the SPEX apparatus was determined. The determination of the area correction factor is given in Equation A.11 below and summarized in Table A.5.

Data Modelling for Integrated Area Corrections

The Rhodamine 6G control required a correction factor for the region of the spectrum affected by filter and laser scatter effects as previously described. Polymer luminescence spectra required a more rigorous modelling method. Phosphorescence spectra contained an anomaly at 705 nm and laser filter and scatter effects on the blue edge of the phosphorescence spectrum. Since the phosphorescence peak is expected to be Gaussian on an energy axis, the scatter and anomaly can be modelled out by fitting the center region of the data to a Gaussian and modelling the tails. For a single intensity measurement

for each sample, the "middle" region - region of the spectrum with good Gaussian fit - was plotted along with the Gaussian model. Each curve was integrated to determine the necessary correction factor that would account for the region of the spectrum lost to undesired effects. Modelled data for phosphorescence spectra are given in Figure A.10.

$$CF = 1 + \frac{A_{tails}}{A_{mid}} \tag{A.11}$$

since

$$A_{Tot} = A_{mid} + A_{tails}$$
$$A_{Tot} = \left(1 + \frac{A_{tails}}{A_{mid}}\right) \cdot A_{mid} = CF \cdot A_{mid}$$

The correction factor makes it possible to determine the total integrated phosphorescence intensity for each sample at each excitation power by simply knowing the area underneath the spectrum's region of good Gaussian fit.

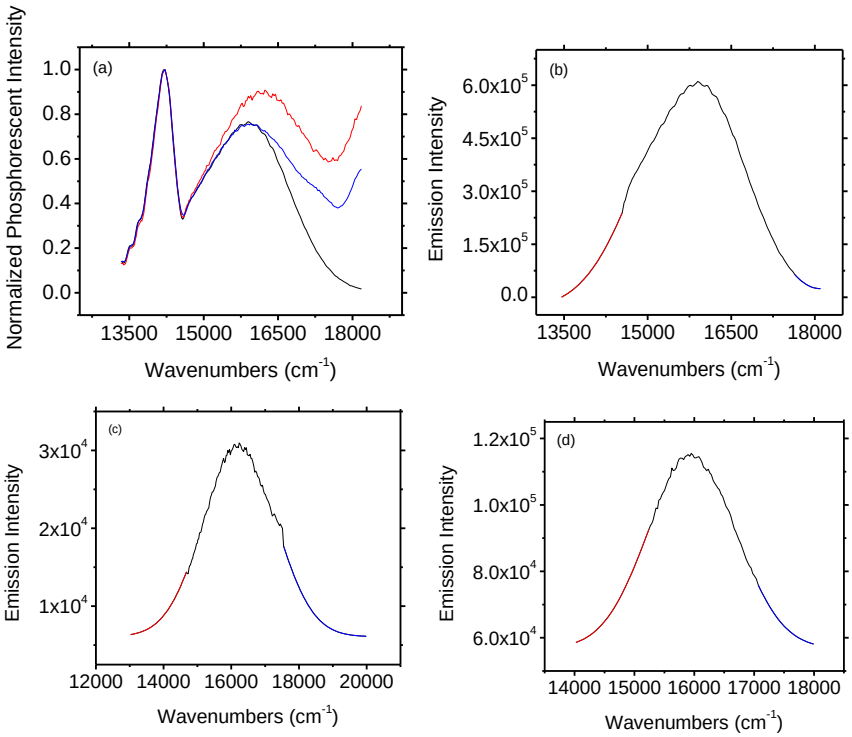

Figure A.10: *(a) Normalized raw phosphorescence spectra for Ru2DPA (red), Ru6DPA (blue), and Ru(dmb)$_3$ (black); Gaussian fits to raw data and extrapolated tails for (b) Ru(dmb)$_3$; (c) Ru2DPA; (d) Ru6DPA. (b-d) show the Gaussian fit to the data (black) with the low energy (red) and high energy (blue) tails. Spectral bandwidths for the phosphorescence spectra (b), (c), and (d) are 0.9 nm, 1.8 nm, and 3.6 nm, respectively.*

Upconverted fluorescence spectra had to be modelled due to intense reabsorption effects in the high-energy portion of the spectrum and laser scatter effects in the low-energy portion that stem from the large spectral bandwidths necessary to obtain meaningful upconverted fluorescence intensities in these polymer samples. The absorption of Ru2DPA, Ru6DPA, pDPA, and mixtures of $Ru(dmb)_3$ and DPA are given in Figure A.11. The broad band centred about 21500 cm^{-1} in Figure A.11(b) corresponds to the $Ru(dmb)_3$ core. Of particular interest is the multi-peak structure in Figure A.11(a), characteristic of DPA.[50] Control experiments verified that the absorption of pDPA exactly matched the multi-peak structure of monomer DPA - sufficiently dilute pDPA does not provide evidence of any intramolecular effect on the absorption tendencies of the DPA moieties in the polymer. The intensity ratio of the middle (26600 cm^{-1}) to high-energy (28000 cm^{-1}) peak is 1.5 and the peaks are spaced by about 1400 cm^{-1}.

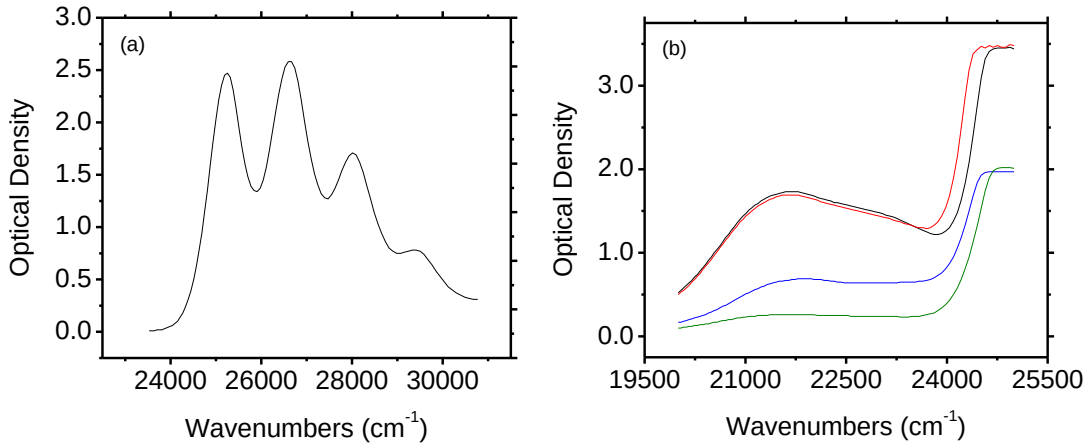

Figure A.11: *Optical Density of: (a) $10^{-4}M$ pDPA; (b) $Ru(dmb)_3$ + 16× DPA (black), $Ru(dmb)_3$ + 48× DPA (red), Ru2DPA (blue) and Ru6DPA (green). Spectral bandwidths are equal in (a) and (b). $CHCl_3$ was used as the solvent for all materials.*

Photoluminescence spectra of the upconverting samples were corrected as outlined in Equation A.5 and corresponding text. Reabsorption-corrected photoluminescence spectra for these materials are given in Figure A.12(a). Due the large optical density in the DPA region in Figure A.11(b), the reabsorption model utilized exaggerates the upconverted fluorescence spectrum in this region by an unrealistic amount. It is expected that the fluorescence spectrum should be the mirror image of the absorption spectrum, so it is unrealistic that the high-energy fluorescence peak should be significantly greater in intensity

than the other peaks in the triplet. Each peak in the fluorescence spectrum is expected to be Gaussian in nature. Since the DPA multi-peak has significant reabsorption in the region of the high-energy peak, the upconverted fluorescence spectrum of each species under study has been truncated to the two low-energy peaks and modelled as a double Gaussian function in Figure A.12(b-e). A summary of the experimental parameters utilized for each modelled sample in Figure A.12 is given in Table A.4.

Table A.4: Experimental Parameters for the Upconverted Fluorescence Spectra Modelled in Figure A.12

Species	**OD**$_{532nm}$	**Excitation Power Density (mW/cm^2)**	**Spectral Bandwidth (nm)**
Ru(dmb)$_3$ + 16× DPA	0.17	46.2	0.9
Ru(dmb)$_3$ + 48× DPA	0.15	105	0.9
Ru2DPA	0.13	46.2	12.6
Ru6DPA	0.09	46.2	12.6

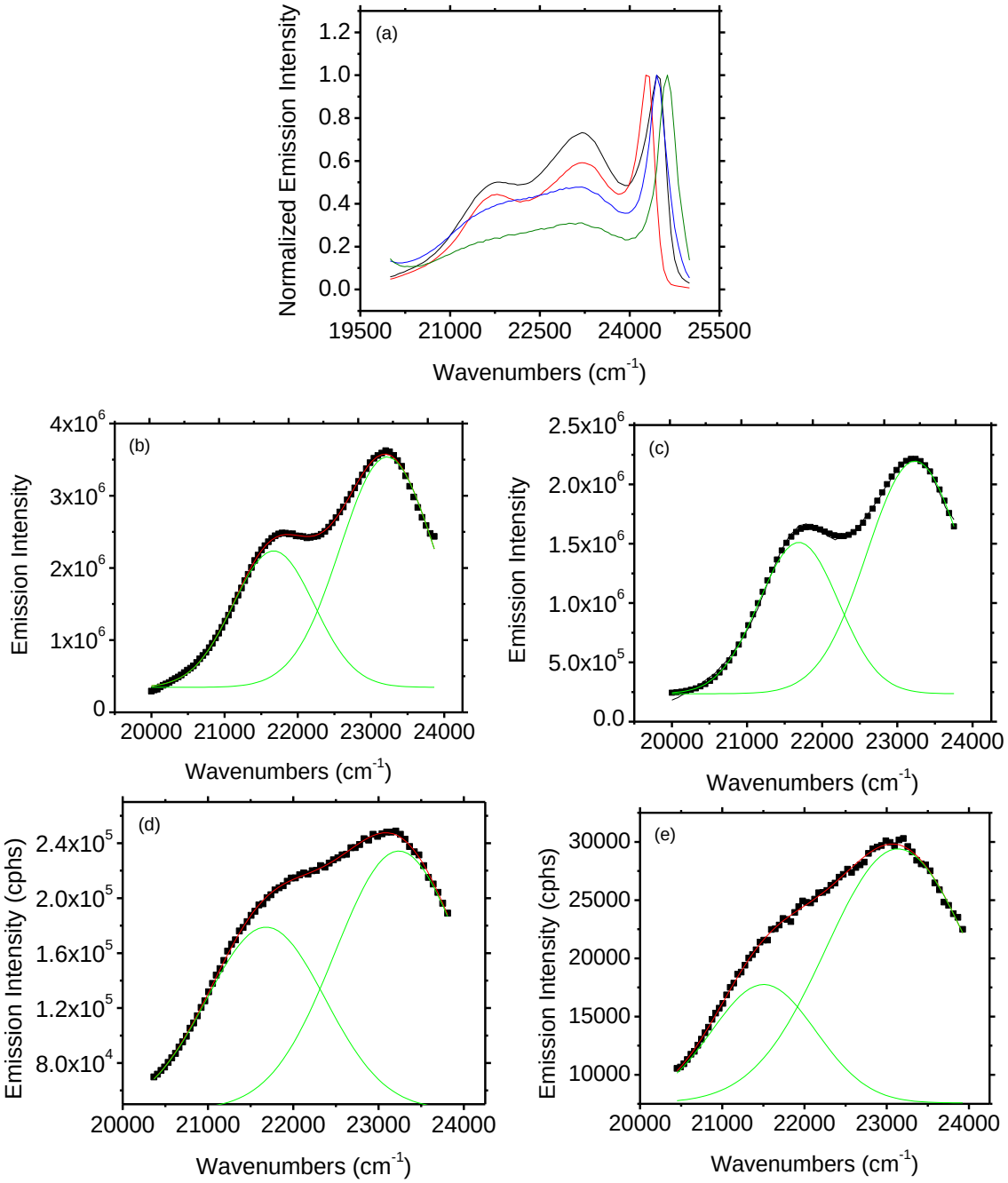

Figure A.12: *(a) Reabsorption-corrected normalized upconverted fluorescence spectra for $Ru(dmb)_3$ + 16× DPA (black), $Ru(dmb)_3$ + 48× DPA (red), Ru2DPA (blue) and Ru6DPA (green); (b-e) Double-Gaussian fits of the raw data for: (b) $Ru(dmb)_3$ + 16× DPA; (c) $Ru(dmb)_3$ + 48× DPA; (d) Ru2DPA; and (e) Ru6DPA, excluding that which is subject to intense laser scatter or reabsorption effects.*

Despite the accuracy of the two-Gaussian fit, the data must be modelled further to account for the three-peak structure of monomeric or polymeric DPA. Again, it is postulated here that the fluorescence spectrum should mirror the absorption spectrum in

each sample. Thus the upconverted fluorescence spectra should have a third peak (or shoulder) 1400 cm^{-1} to the violet of the modelled two-Gaussian spectrum with a peak ratio of 1.5 as described previously. The peak emerging from the reabsorption model that was truncated prior to two-Gaussian fitting occurred in the expected region, 1400 cm^{-1} to the violet of the two-Gaussian model. The least arbitrary way of incorporating this missing peak into the existing model and data was deemed the scaling of this high-energy peak introduced by the reabsorption model such that it has the correct intensity relative to the two-Gaussian peaks. It is conceivable that this peak does exist in the right region of the spectrum but is artificially intensified by the significant optical density of the polymer samples in that region of the spectrum. The modelled data including the scaled third peak is shown in Figure A.13. The added peak is more narrow than each of the peaks in the two-Gaussian fit. Manually widening this peak to match the existing peak widths was not considered, as it would be an inappropriate fabrication of data. The high-energy peak was plotted with the existing two-Gaussian model to find the region of overlap between the two data sets. The high-energy peak was then merely spliced into the high-energy tail of the two-Gaussian model. The high- and low-energy tails in Figure A.13 are important in determining the area-correction factor for each sample, as explained in Equation A.11. A summary of correction factors for all samples utilized is given in Table A.5.

Table A.5: Area Correction Factors for Quantum Yield Calculation

Species	$\mathbf{A}_{mid}$	$\mathbf{A}_{total}$	$\mathbf{A}_{tails}$	$\mathbf{A}_{tails}/\mathbf{A}_{mid}$	**C. F.**
Ru2DPA UC	6.58x10^8	9.65x10^8	3.07x10^8	0.467	1.467
Ru6DPA UC	8.08x10^7	1.13x10^8	3.24x10^7	0.401	1.401
$Ru(dmb)_3$ + 16× DPA UC	8.10x10^9	9.90x10^9	1.80x10^9	0.222	1.222
$Ru(dmb)_3$ + 48× DPA UC	4.82x10^9	6.13x10^9	1.31x10^9	0.271	1.271
Rhodamine 6G	2.65x10^7	5.34x10^7	2.69x10^7	1.014	2.014
Ru2DPA Ph	7.13x10^7	1.08x10^8	3.62x10^7	0.507	1.507
Ru6DPA Ph	1.86x10^8	3.32x10^8	1.46x10^8	0.785	1.785
$Ru(dmb)_3$ Ph	1.25x10^9	1.36x10^9	1.18x10^8	0.087	1.087

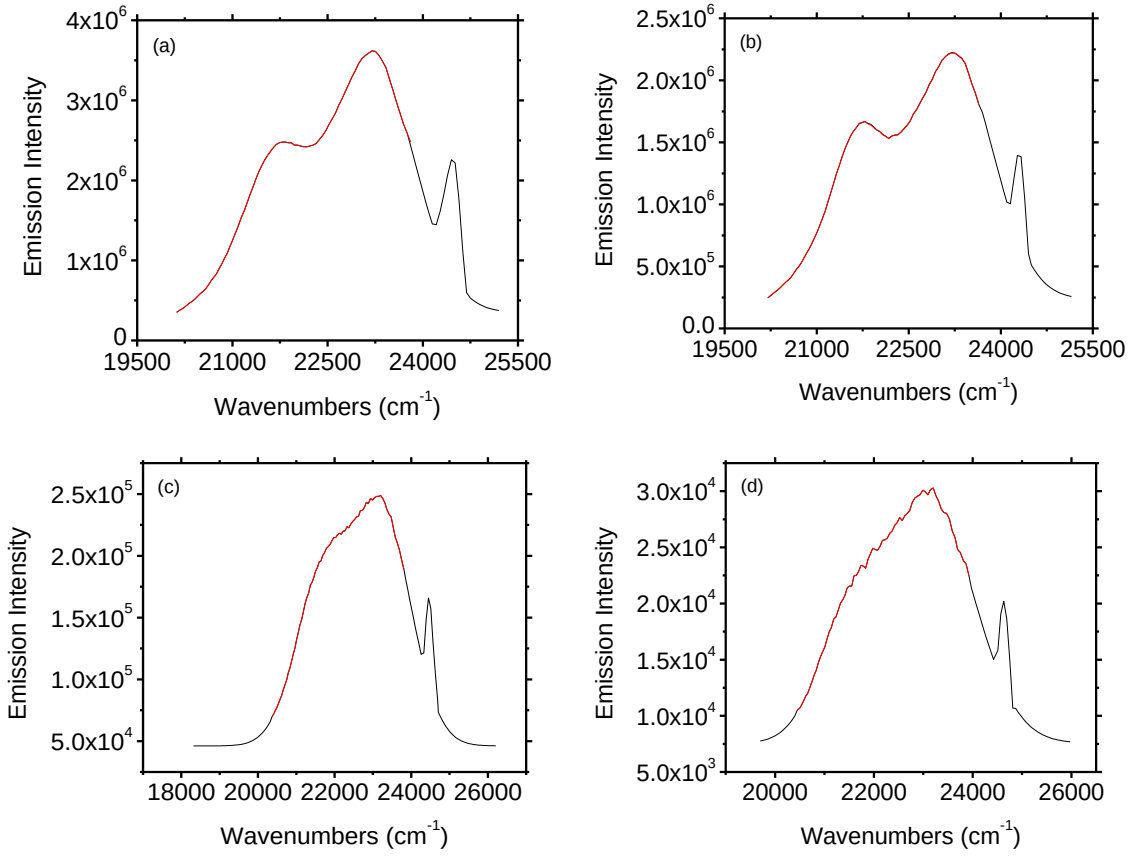

Figure A.13: *Upconverted fluorescence intensity models, including two-Gaussian model regions with high-energy peak and tails for (a) Ru(dmb)$_3$ + 16× DPA; (b) Ru(dmb)$_3$ + 48× DPA; (c) Ru2DPA; (d) Ru6DPA. (a-d) show the Gaussian fit data (red) and the tails (black).*

Corrections for Photodetector Spectral Sensitivity

Spectral variations in photodetector sensitivity are accounted for in the factor ξ in Equation A.6 through its relation to the spectral sensitivity effects on the photoluminescence intensity of the reference compound and the sample, as shown in Equation A.12. Here, c is a constant for each luminescence process of each sample as it is independent of excitation power. Thus, c need only be calculated at one excitation power for each photoluminescence process under study. For convenience, the constant was determined using the spectra modelled in Figures A.10 and A.13. The results are shown in Figure A.14 and summarized in Table A.6.

$$\xi = c_x/c_{ref}; \;\; c_x = \frac{I_{SS-corrected}}{I_{SS-uncorrected}} \tag{A.12}$$

where x is the photoluminescence process under study, ref is the reference material and I is the integrated photoluminescence intensity. In effect, c_x is the factor of increased integrated photoluminescence due to spectral sensitivity corrections and ξ is the effect of c for the photoluminescence process under study relative to that of the reference material.

Table A.6: Spectral Sensitivity Correction Factors

Process	**Uncorrected Area**	**Corrected Area**	**c**	ξ
Rhodamine 6G Fluorescence	1.63×10^7	1.90×10^7	1.161	1
UC Fluorescence of $Ru(dmb)_3$ + 16× DPA	1.92×10^8	5.01×10^8	2.605	2.244
UC Fluorescence of $Ru(dmb)_3$ + 48× DPA	1.20×10^8	3.07×10^8	2.567	2.211
Phosphorescence of 74 μM $Ru(dmb)_3$	5.51×10^7	5.85×10^7	1.062	0.915
UC Fluorescence of Ru2DPA	1.93×10^7	5.39×10^7	2.785	2.399
Phosphorescence of Ru2DPA	4.13×10^6	4.54×10^6	1.098	0.946
UC Fluorescence of Ru6DPA	2.20×10^6	6.38×10^6	2.893	2.492
Phosphorescence of Ru6DPA	1.31×10^7	1.41×10^7	1.073	0.924

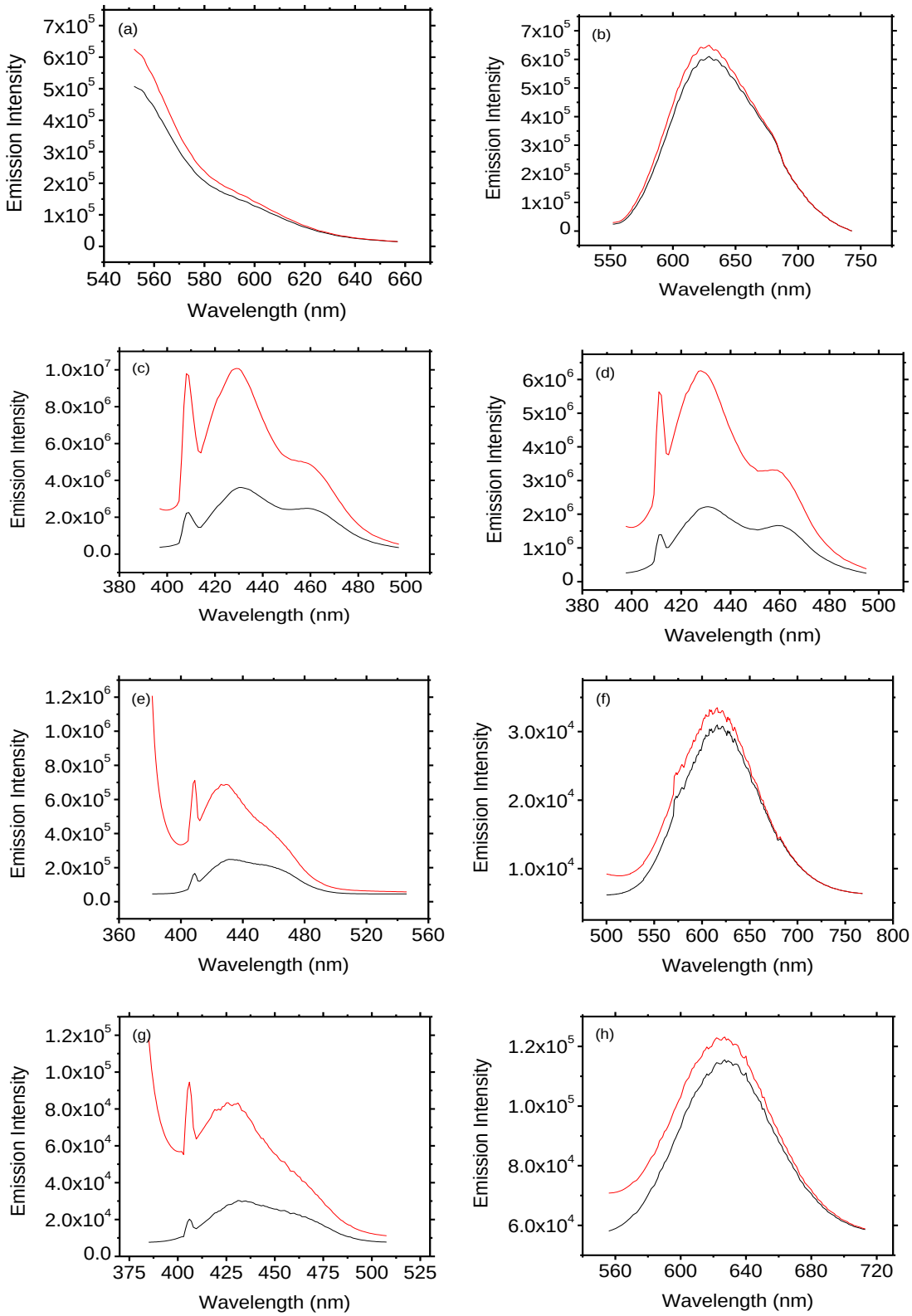

Figure A.14: *Uncorrected (black) and photodetector sensitivity-corrected (red) data for: (a) Rhodamine 6G; (b) Ru(dmb)$_3$ phosphorescence; (c) Ru(dmb)$_3$ + 16× DPA upconverted fluorescence; (d) Ru(dmb)$_3$ + 48× DPA upconverted fluorescence; (e) Ru2DPA upconverted fluorescence; (f) Ru2DPA phosphorescence; (g) Ru6DPA upconverted fluorescence; (h) Ru6DPA phosphorescence.*

Calculation of Quantum Yields

Once the correction factors for spectral sensitivity variations and lost spectral regions due to scatter effects are known and accounted for, photoluminescence QYs can be calculated via Equations A.7 and A.8. For consistency, experimental data were truncated exactly as the modelled data prior to application of the correction factors. A summary of QYs data is presented here, while the data is plotted in Figures 4.10 and 4.11.

Table A.7: Upconverted Fluorescence Quantum Yields of Control Monomer Mixtures

Power Density (mW/cm^2)	**Upconverted Fluorescence Data**					
	$Ru(dmb)_3$ + 16× DPA			**$Ru(dmb)_3$ + 48× DPA**		
	I	**Corr I**	**QY**	**I**	**Corr I**	**QY**
1.12	8.21×10^{5}	1.00×10^{6}	0.0796	7.90×10^{3}	1.00×10^{4}	6.84×10^{-4}
3.71	5.38×10^{6}	6.57×10^{6}	0.157	8.24×10^{3}	1.05×10^{4}	2.15×10^{-4}
5.85	1.11×10^{7}	1.36×10^{7}	0.206	7.91×10^{3}	1.01×10^{4}	1.31×10^{-4}
10.3	2.19×10^{7}	2.67×10^{7}	0.231	8.74×10^{3}	1.11×10^{4}	8.22×10^{-5}
12.3	3.01×10^{7}	3.67×10^{7}	0.265	9.05×10^{3}	1.15×10^{4}	7.13×10^{-5}
13.8	3.81×10^{7}	4.66×10^{7}	0.300	9.77×10^{3}	1.24×10^{4}	6.86×10^{-5}
18.9	5.53×10^{7}	6.76×10^{7}	0.318	1.31×10^{4}	1.67×10^{4}	6.72×10^{-5}
21.0	6.26×10^{7}	7.65×10^{7}	0.324	1.47×10^{4}	1.87×10^{4}	6.79×10^{-5}
33.6	9.85×10^{7}	1.20×10^{8}	0.318	2.92×10^{4}	3.71×10^{4}	8.42×10^{-5}
33.7	1.04×10^{8}	1.27×10^{8}	0.336	3.36×10^{4}	4.27×10^{4}	$9.67\text{x}10^{-5}$
37.3	1.17×10^{8}	1.42×10^{8}	0.339	4.42×10^{4}	5.62×10^{4}	$1.15\text{x}10^{-4}$
46.2	1.53×10^{8}	1.87×10^{8}	0.360	3.33×10^{5}	4.23×10^{5}	$6.98\text{x}10^{-4}$
59.2				6.33×10^{6}	8.04×10^{6}	0.0104
59.8				4.38×10^{6}	5.57×10^{6}	7.10×10^{-3}
81.7				5.06×10^{7}	6.43×10^{7}	0.0600
105				1.03×10^{8}	1.31×10^{8}	0.0949

Table A.8: Upconverted Fluorescence Quantum Yields of Polymers

Power Density (mW/cm^2)	**Upconverted Fluorescence Data**					
	Ru2DPA			**Ru6DPA**		
	I	**Corr I**	**QY**	**I**	**Corr I**	**QY**
1.12	1.69×10^{4}	2.47×10^{4}	5.79×10^{-5}	6.55×10^{3}	9.17×10^{3}	3.02×10^{-5}
3.71	1.38×10^{5}	2.03×10^{5}	1.43×10^{-4}	1.44×10^{4}	2.02×10^{4}	2.01×10^{-5}
5.85	3.14×10^{5}	4.60×10^{5}	2.06×10^{-4}	2.69×10^{4}	3.77×10^{4}	2.38×10^{-5}
10.3	8.29×10^{5}	1.22×10^{6}	3.09×10^{-4}	7.47×10^{4}	1.05×10^{5}	3.75×10^{-5}
12.3	1.20×10^{6}	1.76×10^{6}	3.76×10^{-4}	1.05×10^{5}	1.47×10^{5}	4.41×10^{-5}
13.8	1.60×10^{6}	2.35×10^{6}	4.46×10^{-4}	1.50×10^{5}	2.11×10^{5}	5.64×10^{-5}
18.9	2.76×10^{6}	4.04×10^{6}	5.61×10^{-4}	2.74×10^{5}	3.84×10^{5}	7.51×10^{-5}
21.0	3.12×10^{6}	4.58×10^{6}	5.72×10^{-4}	3.25×10^{5}	4.55×10^{5}	8.00×10^{-5}
33.6	7.24×10^{6}	1.06×10^{7}	8.29×10^{-4}	8.29×10^{5}	1.16×10^{6}	1.28×10^{-4}
33.7	$7.37\text{x}10^{6}$	$1.08\text{x}10^{7}$	$8.41\text{x}10^{-4}$	$8.19\text{x}10^{5}$	1.15×10^{6}	1.26×10^{-4}
37.3	$8.55\text{x}10^{6}$	$1.25\text{x}10^{7}$	$8.82\text{x}10^{-4}$	$1.05\text{x}10^{6}$	1.47×10^{6}	1.45×10^{-4}
46.2	$1.33\text{x}10^{7}$	$1.95\text{x}10^{7}$	$1.10\text{x}10^{-3}$	$1.62\text{x}10^{6}$	2.27×10^{6}	1.81×10^{-4}

Table A.9: Phosphorescence Quantum Yields of Polymers

Power Density (mW/cm^2)	**Phosphorescence Data**					
	Ru2DPA			**Ru6DPA**		
	I	**Corr I**	**QY**	**I**	**Corr I**	**QY**
1.12	6.65×10^{4}	1.00×10^{5}	0.00196	1.82×10^{5}	3.24×10^{5}	0.00206
3.71	1.98×10^{5}	2.98×10^{5}	0.00176	5.51×10^{5}	9.84×10^{5}	0.00189
5.85	3.17×10^{5}	4.78×10^{5}	0.00179	8.80×10^{5}	1.57×10^{6}	0.00191
10.3	5.40×10^{5}	8.13×10^{5}	0.00173	1.50×10^{6}	2.68×10^{6}	0.00185
12.3	6.72×10^{5}	1.01×10^{6}	0.00180	1.83×10^{6}	3.27×10^{6}	0.00189
13.8	7.93×10^{5}	1.20×10^{6}	0.00190	2.13×10^{6}	3.80×10^{6}	0.00196
18.9	1.05×10^{6}	1.59×10^{6}	0.00184	2.87×10^{6}	5.13×10^{6}	0.00193
21.0	1.16×10^{6}	1.75×10^{6}	0.00182	3.08×10^{6}	5.50×10^{6}	0.00186
33.6	1.83×10^{6}	2.75×10^{6}	0.00180	4.92×10^{6}	8.79×10^{6}	0.00186
33.7	1.83×10^{6}	2.76×10^{6}	0.00179	4.95×10^{6}	8.84×10^{6}	0.00186
37.3	2.06×10^{6}	3.10×10^{6}	0.00182	5.37×10^{6}	9.59×10^{6}	0.00183
46.2	2.69×10^{6}	4.05×10^{6}	0.00192	7.00×10^{6}	1.25×10^{7}	0.00192

Table A.10: Phosphorescence Quantum Yields of Control Monomers

Power Density (mW/cm^2)	**$Ru(dmb)_3$**		
	Phosphorescence Data		
	I	**Corr I**	**QY**
1.12	1.33×10^6	1.45×10^6	0.024
3.71	4.13×10^6	4.49×10^6	0.023
5.85	6.45×10^6	7.01×10^6	0.022
10.3	1.07×10^7	1.17×10^7	0.021
12.3	1.32×10^7	1.43×10^7	0.022
13.8	1.50×10^7	1.70×10^7	0.023
18.9	2.06×10^7	2.24×10^7	0.022
21.0	2.33×10^7	2.53×10^7	0.022
33.6	3.31×10^7	3.60×10^7	0.020
33.7	3.56×10^7	3.87×10^7	0.021
37.3	3.90×10^7	4.24×10^7	0.021
46.2	4.91×10^7	5.33×10^7	0.022

Table A.11: Corrected Intensities of Rhodamine 6G Standards

Power Density (mW/cm^2)	**Rhodamine 6G**			
	Corrected Intensity			
	A	**B**	**C**	**D**
1.12	5.80×10^7	4.10×10^7	1.68×10^8	1.74×10^9
3.71	1.92×10^8	1.36×10^8	5.55×10^8	5.76×10^9
5.85	3.03×10^8	2.14×10^8	8.75×10^8	9.09×10^9
10.3	5.33×10^8	3.77×10^8	1.54×10^9	1.60×10^{10}
12.3	6.37×10^8	4.51×10^8	1.84×10^9	1.91×10^{10}
13.8	7.15×10^8	5.06×10^8	2.07×10^9	2.14×10^{10}
18.9	9.79×10^8	6.93×10^8	2.83×10^9	2.94×10^{10}
21.0	1.09×10^9	7.70×10^8	3.14×10^9	3.26×10^{10}
33.6	1.74×10^9	1.23×10^9	5.03×10^9	5.22×10^{10}
33.7	1.74×10^9	1.24×10^9	5.04×10^9	5.23×10^{10}
37.3	1.93×10^9	1.37×10^9	5.58×10^9	5.79×10^{10}
46.2	2.39×10^9	1.69×10^9	6.91×10^9	7.18×10^{10}
59.2	3.07×10^9			
59.8	3.10×10^9			
81.7	4.23×10^9			
105	5.44×10^9			

Table A.12: Constants Utilized in Quantum Yield Calculations

Species	**OD**$_{532nm}$	**1-10**$^{-OD}$	ϕ_F	ξ	**Area C.F.**	**N**
Rhodamine 6G A	0.26	0.45	0.75		2.014	
Ru(dmb)$_3$ + 16× DPA	0.17	0.33		2.244	1.222	2
Ru(dmb)$_3$ + 48× DPA	0.15	0.30		2.211	1.271	2
Ru(dmb)$_3$ Ph	0.15	0.29		0.915	1.087	1
Rhodamine 6G B, C, D	0.15	0.30	0.75		2.014	
Ru2DPA UC Fl	0.13	0.26		2.399	1.467	2
Ru6DPA UC Fl	0.09	0.20		2.492	1.401	2
Ru2DPA Ph	0.13	0.26		0.946	1.507	1
Ru6DPA Ph	0.09	0.20		0.924	1.785	1

References

[1] Martin A. Green. The path to 25% silicon solar cell efficiency: History of silicon cell evolution. *Progress in Photovoltaics: Research and Applications*, 17(3):183–189, 2009.

[2] Christoph J. Brabec. Organic photovoltaics: technology and market. *Solar Energy Materials and Solar Cells*, 83(2-3):273–292, 2004.

[3] Pavel Schilinsky, Christoph Waldauf, and Christoph J. Brabec. Recombination and loss analysis in polythiophene based bulk heterojunction photodetectors. *Applied Physics Letters*, 81(20):3885, 2002.

[4] Alex C. Mayer, Shawn R. Scully, Brian E. Hardin, Michael W. Rowell, and Michael D. McGehee. Polymer-based solar cells. *Materials Today*, 10(11):28–33, 2007.

[5] M. C Scharber, D. Mhlbacher, M. Koppe, P. Denk, C. Waldauf, A. J Heeger, and C. J Brabec. Design Rules for Donors in Bulk-Heterojunction Solar Cells-Towards 10% Energy-Conversion Efficiency. *Advanced Materials*, 18(6):789–794, 2006.

[6] Bernard Kippelen and Jean-Luc Bredas. Organic photovoltaics. *Energy & Environmental Science*, 2(3):251–261, 2009.

[7] Holger Spanggaard and Frederik C. Krebs. A brief history of the development of organic and polymeric photovoltaics. *Solar Energy Materials and Solar Cells*, 83(2-3):125–146, 2004.

[8] Eva Bundgaard and Frederik C. Krebs. Low band gap polymers for organic photovoltaics. *Solar Energy Materials and Solar Cells*, 91(11):954–985, 2007.

[9] Frederik C. Krebs. Fabrication and processing of polymer solar cells: A review of printing and coating techniques. *Solar Energy Materials and Solar Cells*, 93(4):394–412, 2009.

[10] Amaresh Mishra and Peter Buerle. Small Molecule Organic Semiconductors on the Move: Promises for Future Solar Energy Technology. *Angewandte Chemie International Edition*, 51(9):2020–2067, 2012.

[11] Yaowen Li, Qing Guo, Zaifang Li, Jianing Pei, and Wenjing Tian. Solution processable d-a small molecules for bulk-heterojunction solar cells. *Energy & Environmental Science*, 3(10):1427–1436, 2010.

[12] Brian O'Regan and M. Grätzel. A low-cost, high-efficiency solar cell based on dye-sensitized colloidal TiO2 Films. *Nature*, 353(6346), 1991.

[13] Simon Mathew, Aswani Yella, Peng Gao, Robin Humphry-Baker, CurchodBasile F. E., Negar Ashari-Astani, Ivano Tavernelli, Ursula Rothlisberger, NazeeruddinMd. Khaja, and Michael Grätzel. Dye-sensitized solar cells with 13% efficiency achieved through the molecular engineering of porphyrin sensitizers. *Nature Chemistry*, 6(3), 2014.

[14] Michael Grätzel. Solar Energy Conversion by Dye-Sensitized Photovoltaic Cells. *Inorganic Chemistry*, 44(20):6841–6851, 2005.

[15] Anders Hagfeldt and Michael Grätzel. Light-Induced Redox Reactions in Nanocrystalline Systems. *Chemical Reviews*, 95(1):49–68, 1995.

[16] Kiyoshi C. D. Robson, Paolo G. Bomben, and Curtis P. Berlinguette. Cycloruthenated sensitizers: improving the dye-sensitized solar cell with classical inorganic chemistry principles. *Dalton Transactions*, 41(26):7814–7829, 2012.

[17] H. Gerischer, M. E. Michel-Beyerle, F. Rebentrost, and H. Tributsch. Sensitization of charge injection into semiconductors with large band gap. *Electrochimica Acta*, 13(6):1509–1515, 1968.

[18] William Shockley and Hans J. Queisser. Detailed Balance Limit of Efficiency of p-n Junction Solar Cells. *Journal of Applied Physics*, 32(3):510–519, 1961.

[19] J. de Wild, A. Meijerink, J. K. Rath, W. G. J. H. M. van Sark, and R. E. I. Schropp. Upconverter solar cells: materials and applications. *Energy & Environmental Science*, 4(12):4835–4848, 2011.

[20] Jiye Lee, Priya Jadhav, Philip D. Reusswig, Shane R. Yost, Nicholas J. Thompson, Daniel N. Congreve, Eric Hontz, Troy Van Voorhis, and Marc A. Baldo. Singlet Exciton Fission Photovoltaics. *Accounts of Chemical Research*, 46(6):1300–1311, 2013.

[21] Millicent B. Smith and Josef Michl. Singlet Fission. *Chemical Reviews*, 110(11):6891–6936, 2010.

[22] Hagay Shpaisman, Olivia Niitsoo, Igor Lubomirsky, and David Cahen. Can up- and down-conversion and multi-exciton generation improve photovoltaics? *Solar Energy Materials and Solar Cells*, 92(12):1541–1546, 2008.

[23] Angelo Monguzzi, Riccardo Tubino, Sajjad Hoseinkhani, Marcello Campione, and Francesco Meinardi. Low power, non-coherent sensitized photon up-conversion: modelling and perspectives. *Physical Chemistry Chemical Physics*, 14(13):4322–4332, 2012.

[24] Jianzhang Zhao, Shaomin Ji, and Huimin Guo. Triplet-triplet annihilation based upconversion: from triplet sensitizers and triplet acceptors to upconversion quantum yields. *RSC Advances*, 1(6):937–950, 2011.

[25] Tanya N. Singh-Rachford and Felix N. Castellano. Photon upconversion based on sensitized triplet-triplet annihilation. *Coordination Chemistry Reviews*, 254(21-22):2560–2573, 2010.

[26] A. Jablonski. Efficient Anti-Stokes Fluorescence in Dyes. *Nature*, 131(3319):839–840, 1933.

[27] Michael Kasha. Characterization of electronic transitions in complex molecules. *Discussions of the Faraday Society*, 9(0):14–19, 1950.

[28] Francis Perrin. The fluorescence of solutions: Molecular induction, polarization and duration of emission and photochemistry. *Annales de Physique*, 12:169–275, 1929.

[29] Th Förster. Zwischenmolekulare Energiewanderung und Fluoreszenz. *Annalen der Physik*, 437(1-2):55–75, 1948.

[30] D. L. Dexter. A Theory of Sensitized Luminescence in Solids. *The Journal of Chemical Physics*, 21(5):836–850, 1953.

[31] C. A. Parker. Phosphorescence and delayed fluorescences from solutions. *Advances in Photochemistry*, 2:305–383, 1964.

[32] G. W.; Sternlicht, H; Robinson and G. C. Nieman. Triplet-triplet annihilation and delayed fluorescence in molecular aggregates. *Journal of Chemical Physics*, 38:1326–1335, 1963.

[33] Yoan C. Simon and Christoph Weder. Low-power photon upconversion through triplet-triplet annihilation in polymers. *Journal of Materials Chemistry*, 22(39):20817–20830, 2012.

[34] Paola Ceroni. Energy Up-Conversion by Low-Power Excitation: New Applications of an Old Concept. *Chemistry - A European Journal*, 17(35):9560–9564, 2011.

[35] Jianzhang Zhao, Wanhua Wu, Jifu Sun, and Song Guo. Triplet photosensitizers: from molecular design to applications. *Chemical Society Reviews*, 42(12):5323–5351, 2013.

[36] Tanya N. Singh-Rachford, Alexandre Haefele, Raymond Ziessel, and Felix N. Castellano. Boron Dipyrromethene Chromophores: Next Generation Triplet Acceptors/Annihilators for Low Power Upconversion Schemes. *Journal of the American Chemical Society*, 130(48):16164–16165, 2008.

[37] Tanya N. Singh-Rachford, Animesh Nayak, Maria L. Muro-Small, Sèbastian Goeb, Michael J. Therien, and Felix N. Castellano. Supermolecular-Chromophore-Sensitized Near-Infrared-to-Visible Photon Upconversion. *Journal of the American Chemical Society*, 132(40):14203–14211, 2010.

[38] Fan Deng, Jonathan R. Sommer, Mykhaylo Myahkostupov, Kirk S. Schanze, and Felix N. Castellano. Near-IR phosphorescent metalloporphyrin as a photochemical upconversion sensitizer. *Chemical Communications (Cambridge, United Kingdom)*, 2013.

[39] Gerhard Wegner, Stanislav Baluschev, Frédéric Laquai, and Chunyan Chi. Managing Photoexcited States in Conjugated Polymers. *Macromolecular Symposia*, 268(1):1–8, 2008.

[40] Wanhua Wu, Huimin Guo, Wenting Wu, Shaomin Ji, and Jianzhang Zhao. Organic Triplet Sensitizer Library Derived from a Single Chromophore (BODIPY) with Long-Lived Triplet Excited State for Triplet-Triplet Annihilation Based Upconversion. *The Journal of Organic Chemistry*, 76(17):7056–7064, 2011.

[41] Lianlian Liu, Dandan Huang, Sylvia M. Draper, Xiuyu Yi, Wanhua Wu, and Jianzhang Zhao. Visible light-harvesting trans bis(alkylphosphine) platinum(ii)-alkynyl complexes showing long-lived triplet excited states as triplet photosensitizers for triplet-triplet annihilation upconversion. *Dalton Transactions*, 42(30):10694–10706, 2013.

[42] Tanya N. Singh-Rachford and Felix N. Castellano. Nonlinear Photochemistry Squared: Quartic Light Power Dependence Realized in Photon Upconversion. *The Journal of Physical Chemistry A*, 113(33):9266–9269, 2009.

[43] Alexandre Haefele, Jörg Blumhoff, Rony S. Khnayzer, and Felix N. Castellano. Getting to the (Square) Root of the Problem: How to Make Noncoherent Pumped Upconversion Linear. *The Journal of Physical Chemistry Letters*, 3(3):299–303, 2012.

[44] A. Monguzzi, J. Mezyk, F. Scotognella, R. Tubino, and F. Meinardi. Upconversion-induced fluorescence in multicomponent systems: Steady-state excitation power threshold. *Physical Review B*, 78(19):195112, 2008.

[45] Yuen Yap Cheng, Burkhard Fückel, Tony Khoury, Raphaël G. C. R. Clady, Murad J. Y. Tayebjee, N. J. Ekins-Daukes, Maxwell J. Crossley, and Timothy W. Schmidt. Kinetic Analysis of Photochemical Upconversion by Triplet-Triplet Annihilation: Beyond Any Spin Statistical Limit. *The Journal of Physical Chemistry Letters*, 1(12):1795–1799, 2010.

[46] Yuen Yap Cheng, Tony Khoury, Raphael G. C. R. Clady, Murad J. Y. Tayebjee, N. J. Ekins-Daukes, Maxwell J. Crossley, and Timothy W. Schmidt. On the efficiency limit of triplet-triplet annihilation for photochemical upconversion. *Physical Chemistry Chemical Physics*, 12(1):66–71, 2010.

[47] Yuen Yap Cheng, Burkhard Fückel, Tony Khoury, Raphaël G. C. R. Clady, N. J. Ekins-Daukes, Maxwell J. Crossley, and Timothy W. Schmidt. Entropically Driven Photochemical Upconversion. *The Journal of Physical Chemistry A*, 115(6):1047–1053, 2011.

[48] Josie E. Auckett, Yuen Yap Cheng, Tony Khoury, Raphaël G. C. R. Clady, N. J. Ekins-Daukes, Maxwell J. Crossley, and Timothy W. Schmidt. Efficient upconversion by triplet-triplet annihilation. *Journal of Physics: Conference Series*, 185(1):012002, 2009.

[49] S. Baluschev, T. Miteva, V. Yakutkin, G. Nelles, A. Yasuda, and G. Wegner. Up-Conversion Fluorescence: Noncoherent Excitation by Sunlight. *Physical Review Letters*, 97(14):143903, 2006.

[50] S. Baluschev, V. Yakutkin, G. Wegner, B. Minch, T. Miteva, G. Nelles, and A. Yasuda. Two pathways for photon upconversion in model organic compound systems. *Journal of Applied Physics*, 101(2):023101–4, 2007.

[51] R. P. Steer. Comment on "Two pathways for photon upconversion in model organic compound systems" [J. Appl. Phys. [101], 023101 (2007)]. *Journal of Applied Physics*, 102(7):076102–3, 2007.

[52] S. Baluschev, V. Yakutkin, G. Wegner, B. Minch, T. Miteva, G. Nelles, and A. Yasuda. Response to "Comment on 'Two pathways for photon upconversion in model organic compound systems' [J. Appl. Phys. [101], 023101 (2007)]". *Journal of Applied Physics*, 102(7):076103–2, 2007.

[53] Sunish K. Sugunan, Umakanta Tripathy, Sophie M. K. Brunet, Matthew F. Paige, and Ronald P. Steer. Mechanisms of Low-Power Noncoherent Photon Upconversion in Metalloporphyrin-Organic Blue Emitter Systems in Solution. *The Journal of Physical Chemistry A*, 113(30):8548–8556, 2009.

[54] A. Monguzzi, R. Tubino, and F. Meinardi. Diffusion Enhanced Upconversion in Organic Systems. *International Journal of Photoenergy*, page 684196, 2008.

[55] Jae-Hyuk Kim, Fan Deng, Felix N. Castellano, and Jae-Hong Kim. High Efficiency Low-Power Upconverting Soft Materials. *Chemistry of Materials*, 24(12):2250–2252, 2012.

[56] Frédéric Laquai, Gerhard Wegner, Chan Im, Arne Busing, and Susanne Heun. Efficient upconversion fluorescence in a blue-emitting spirobifluorene-anthracene copolymer doped with low concentrations of Pt(II)octaethylporphyrin, journal = The Journal of Chemical Physics, volume = 123, number = 7, pages = 074902-6, keywords = fluorescence polymer blends spectral line intensity polymer films triplet state, year = 2005.

[57] Radiy R. Islangulov, Joseph Lott, Christoph Weder, and Felix N. Castellano. Noncoherent Low-Power Upconversion in Solid Polymer Films. *Journal of the American Chemical Society*, 129(42):12652–12653, 2007.

[58] Tanya N. Singh-Rachford, Joseph Lott, Christoph Weder, and Felix N. Castellano. Influence of Temperature on Low-Power Upconversion in Rubbery Polymer Blends. *Journal of the American Chemical Society*, 131(33):12007–12014, 2009.

[59] Angelo Monguzzi, Riccardo Tubino, and Francesco Meinardi. Multicomponent Polymeric Film for Red to Green Low Power Sensitized Up-Conversion. *The Journal of Physical Chemistry A*, 113(7):1171–1174, 2009.

[60] Jaclyn A. O'Brien, Sailaja Rallabandi, Umakanta Tripathy, Matthew F. Paige, and Ronald P. Steer. Efficient S2 state production in ZnTPP-PMMA thin films by triplet-triplet annihilation: Evidence of solute aggregation in photon upconversion systems. *Chemical Physics Letters*, 475(4-6):220–222, 2009.

[61] P. E. Keivanidis, S. Baluschev, T. Miteva, G. Nelles, U. Scherf, A. Yasuda, and G. Wegner. Up-Conversion Photoluminescence in Polyfluorene Doped with Metal(II)-Octaethyl Porphyrins. *Advanced Materials*, 15(24):2095–2098, 2003.

[62] Stanislav Baluschev, Josemon Jacob, Yuri S. Avlasevich, Panagiotis E. Keivanidis, Tzenka Miteva, Akio Yasuda, Gabriele Nelles, Andrew C. Grimsdale, Klaus Müllen,

and Gerhard Wegner. Enhanced Operational Stability of the Up-Conversion Fluorescence in Films of Palladium-Porphyrin End-Capped Poly(pentaphenylene). *ChemPhysChem*, 6(7):1250–1253, 2005.

[63] S. Baluschev, P. E. Keivanidis, G. Wegner, J. Jacob, A. C. Grimsdale, K. Müllen, T. Miteva, A. Yasuda, and G. Nelles. Upconversion photoluminescence in poly(ladder-type-pentaphenylene) doped with metal (II)-octaethyl porphyrins. *Applied Physics Letters*, 86(6):061904–3, 2005.

[64] Panagiotis E. Keivanidis, Frédéric Laquai, Joseph W. F. Robertson, Stanislav Baluschev, Josemon Jacob, Klaus Müllen, and Gerhard Wegner. Electron-Exchange-Assisted Photon Energy Up-Conversion in Thin Films of Pi-Conjugated Polymeric Composites. *The Journal of Physical Chemistry Letters*, 2(15):1893–1899, 2011.

[65] Soo Hyon Lee, Joseph R. Lott, Yoan C. Simon, and Christoph Weder. Melt-processed polymer glasses for low-power upconversion via sensitized triplet-triplet annihilation. *Journal of Materials Chemistry C*, 1(33):5142–5148, 2013.

[66] Roberto Vadrucci, Christoph Weder, and Yoan Cedric Simon. Low-power photon upconversion in organic glasses. *Journal of Materials Chemistry C*, 2014. DOI: 10.1039/c3tc32473g.

[67] Philip C. Boutin, Kenneth P. Ghiggino, Timothy L. Kelly, and Ronald P. Steer. Photon Upconversion Via Triplet-Triplet Annihilation in $Ru(bpy)_3$- and DPA- functionalized Polymers. *The Journal of Physical Chemistry Letters*, 4:4113–4118, 2013.

[68] Angelo Monguzzi, Michel Frigoli, Chantal Larpent, Riccardo Tubino, and Francesco Meinardi. Low-Power-Photon Up-Conversion in Dual-Dye-Loaded Polymer Nanoparticles. *Advanced Functional Materials*, 22(1):139–143, 2012.

[69] Christian Wohnhaas, Andrey Turshatov, Volker Mailänder, Steffen Lorenz, Stanislav Baluschev, Tzenka Miteva, and Katharina Landfester. Annihilation Upconversion in Cells by Embedding the Dye System in Polymeric Nanocapsules. *Macromolecular Bioscience*, 11(6):772–778, 2011.

[70] Yoan C. Simon, Shuo Bai, Michelle K. Sing, Hervé Dietsch, Marc Achermann, and Christoph Weder. Low-Power Upconversion in Dye-Doped Polymer Nanoparticles. *Macromolecular Rapid Communications*, 33(6-7):498–502, 2012.

[71] N. J. Ekins-Daukes and T. W. Schmidt. A molecular approach to the intermediate band solar cell: The symmetric case. *Applied Physics Letters*, 93(6):063507–3, 2008.

[72] Jonas Sandby Lissau, James M. Gardner, and Ana Morandeira. Photon Upconversion on Dye-Sensitized Nanostructured ZrO_2 Films. *The Journal of Physical Chemistry C*, 115(46):23226–23232, 2011.

[73] Jonas Sandby Lissau, Djawed Nauroozi, Marie-Pierre Santoni, Sascha Ott, James M. Gardner, and Ana Morandeira. Anchoring Energy Acceptors to Nanostructured ZrO_2 Enhances Photon Upconversion by Sensitized Triplet-Triplet Annihilation Under Simulated Solar Flux. *The Journal of Physical Chemistry C*, 117(28):14493–14501, 2013.

[74] Denis V. Kozlov and Felix N. Castellano. Anti-Stokes delayed fluorescence from metal-organic bichromophores. *Chemical Communications*, (24):2860–2861, 2004.

[75] Radiy R. Islangulov, Denis V. Kozlov, and Felix N. Castellano. Low power upconversion using MLCT sensitizers. *Chemical Communications*, (30):3776–3778, 2005.

[76] Tanya N. Singh-Rachford, Radiy R. Islangulov, and Felix N. Castellano. Photochemical Upconversion Approach to Broad-Band Visible Light Generation. *The Journal of Physical Chemistry A*, 112(17):3906–3910, 2008.

[77] Tanya N. Singh-Rachford and Felix N. Castellano. Low Power Visible-to-UV Upconversion. *The Journal of Physical Chemistry A*, 113(20):5912–5917, 2009.

[78] Tanya N. Singh-Rachford and Felix N. Castellano. Supra-Nanosecond Dynamics of a Red-to-Blue Photon Upconversion System. *Inorganic Chemistry*, 48(6):2541–2548, 2009.

[79] Tanya N. Singh-Rachford and Felix N. Castellano. Triplet Sensitized Red-to-Blue Photon Upconversion. *The Journal of Physical Chemistry Letters*, 1(1):195–200, 2010.

[80] Fan Deng, Jörg Blumhoff, and Felix N. Castellano. Annihilation limit of a visible-to-uv photon upconversion composition ascertained from transient absorption kinetics. *The Journal of Physical Chemistry A*, 117(21):4412–4419, 2013.

[81] Haichun Liu, Can T. Xu, David Lindgren, Haiyan Xie, Diana Thomas, Carsten Gundlach, and Stefan Andersson-Engels. Balancing power density based quantum yield characterization of upconverting nanoparticles for arbitrary excitation intensities. *Nanoscale*, 5(11):4770–4775, 2013.

[82] Wenqiang Zou, Cindy Visser, Jeremio A. Maduro, Maxim S. Pshenichnikov, and Jan C. Hummelen. Broadband dye-sensitized upconversion of near-infrared light. *Nature Photonics*, 6(8):560–564, 2012.

[83] Marta Penconi, Fausto Ortica, Fausto Elisei, and Pier Luigi Gentili. New molecular pairs for low power non-coherent triplet-triplet annihilation based upconversion: dependence on the triplet energies of sensitizer and emitter. *Journal of Luminescence*, 135(0):265–270, 2013.

[84] Xian Cao, Bo Hu, and Peng Zhang. High Upconversion Efficiency from Hetero Triplet-Triplet Annihilation in Multiacceptor Systems. *The Journal of Physical Chemistry Letters*, 4(14):2334–2338, 2013.

[85] Sunish K. Sugunan, Chelsea Greenwald, Matthew F. Paige, and Ronald P. Steer. Efficiency of Noncoherent Photon Upconversion by Triplet-Triplet Annihilation: The C_{60} Plus Anthanthrene System and the Importance of Tuning the Triplet Energies. *The Journal of Physical Chemistry A*, 117(26):5419–5427, 2013.

[86] Stanislav Baluschev, Vladimir Yakutkin, Tzenka Miteva, Yuri Avlasevich, Sergei Chernov, Sergei Aleshchenkov, Gabriele Nelles, Andrei Cheprakov, Akio Yasuda, Klaus Müllen, and Gerhard Wegner. Blue-Green Up-Conversion: Noncoherent

Excitation by NIR Light. *Angewandte Chemie International Edition*, 46(40):7693–7696, 2007.

[87] Vladimir Yakutkin, Sergei Aleshchenkov, Sergei Chernov, Tzenka Miteva, Gabriele Nelles, Andrei Cheprakov, and Stanislav Baluschev. Towards the IR Limit of the Triplet-Triplet Annihilation-Supported Up-Conversion: Tetraanthraporphyrin. *Chemistry - A European Journal*, 14(32):9846–9850, 2008.

[88] Andrew Nattestad, Yuen Yap Cheng, Rowan W. MacQueen, Tim F. Schulze, Fletcher W. Thompson, Attila J. Mozer, Burkhard Fückel, Tony Khoury, Maxwell J. Crossley, Klaus Lips, Gordon G. Wallace, and Timothy W. Schmidt. Dye-Sensitized Solar Cell with Integrated Triplet-Triplet Annihilation Upconversion System. *The Journal of Physical Chemistry Letters*, 4(12):2073–2078, 2013.

[89] Bernhard Nickel. Delayed Fluorescence from Upper Excited Singlet States Sn (n $>$ 1) of the Aromatic Hydrocarbons 1,2-benzanthracene, fluoranthene, pyrene, and chrysene in methylcyclohexane. *Helvetica Chimica Acta*, 61(1):198–222, 1978.

[90] James L. Charlton, Reza Dabestani, and Jack Saltiel. Role of triplet-triplet annihilation in anthracene dimerization. *Journal of the American Chemical Society*, 105(11):3473–3476, 1983.

[91] Andrew J. McLean and T. George Truscott. Efficiency of triplet-photosensitised singlet oxygen generation in benzene. *Journal of the Chemical Society, Faraday Transactions*, 86(14):2671–2672, 1990.

[92] Sergei M. Bachilo and R. Bruce Weisman. Determination of Triplet Quantum Yields from Triplet-Triplet Annihilation Fluorescence. *The Journal of Physical Chemistry A*, 104(33):7711–7714, 2000.

[93] Peter P. Levin, Silvia M. B. Costa, Teresa G. Nunes, Luis F. Vieira Ferreira, Laura M. Ilharco, and Ana M. Botelho do Rego. Kinetics of Triplet-Triplet Annihilation of Tetraphenylporphyrin in Liquid and Frozen Films of Decanol on the External Surface of Zeolite. Fast Probe Diffusion in Monolayers and Polycrystals. *The Journal of Physical Chemistry A*, 107(3):328–336, 2002.

[94] Vygintas Jankus, Edward W. Snedden, Daniel W. Bright, Victoria L. Whittle, J. A. G. Williams, and Andy Monkman. Energy Upconversion via Triplet Fusion in Super Yellow PPV Films Doped with Palladium Tetraphenyltetrabenzoporphyrin: a Comprehensive Investigation of Exciton Dynamics. *Advanced Functional Materials*, 23(3):384–393, 2013.

[95] T. Trupke, M. A. Green, and P. Wurfel. Improving solar cell efficiencies by up-conversion of sub-band-gap light. *Journal of Applied Physics*, 92(7):4117–4122, 2002.

[96] Ashwin C. Atre and Jennifer A. Dionne. Realistic upconverter-enhanced solar cells with non-ideal absorption and recombination efficiencies. *Journal of Applied Physics*, 110(3):034505, 2011.

[97] Viorel Badescu and Alina Mihaela Badescu. Improved model for solar cells with up-conversion of low-energy photons. *Renewable Energy*, 34(6):1538–1544, 2009.

[98] Yuen Yap Cheng, Burkhard Fückel, Rowan W. MacQueen, Tony Khoury, Raphael G. C. R. Clady, Tim F. Schulze, N. J. Ekins-Daukes, Maxwell J. Crossley, Bernd Stannowski, Klaus Lips, and Timothy W. Schmidt. Improving the light-harvesting of amorphous silicon solar cells with photochemical upconversion. *Energy & Environmental Science*, 5(5):6953–6959, 2012.

[99] Tim F. Schulze, Yuen Yap Cheng, Tony Khoury, Maxwell J. Crossley, Bernd Stannowski, Klaus Lips, and Timothy W. Schmidt. Micro-optical design of photochemical upconverters for thin-film solar cells. *Journal of Photonics for Energy*, 3(1):034598–034598, 2013.

[100] Tim F. Schulze, Yuen Yap Cheng, Burkhard Fückel, Rowan W. MacQueen, Andrew Danos, Nathaniel J. L. K. Davis, Murad J. Y. Tayebjee, Tony Khoury, Raphaël G. C. R. Clady, N. J. Ekins-Daukes, Maxwell J. Crossley, Bernd Stannowski, Klaus Lips, and Timothy W. Schmidt. Photochemical Upconversion Enhanced Solar Cells: Effect of a Back Reflector. *Australian Journal of Chemistry*, 65(5):480–485, 2012.

[101] Tim F. Schulze, Jens Czolk, Yuen-Yap Cheng, Burkhard Fückel, Rowan W. MacQueen, Tony Khoury, Maxwell J. Crossley, Bernd Stannowski, Klaus Lips, Uli Lemmer, Alexander Colsmann, and Timothy W. Schmidt. Efficiency Enhancement of Organic and Thin-Film Silicon Solar Cells with Photochemical Upconversion. *The Journal of Physical Chemistry C*, 116(43):22794–22801, 2012.

[102] T. Trupke, A. Shalav, B. S. Richards, P. Würfel, and M. A. Green. Efficiency enhancement of solar cells by luminescent up-conversion of sunlight. *Solar Energy Materials and Solar Cells*, 90(18-19):3327–3338, 2006.

[103] S. Fischer, J. C. Goldschmidt, P. Loper, G. H. Bauer, R. Bruggemann, K. Kramer, D. Biner, M. Hermle, and S. W. Glunz. Enhancement of silicon solar cell efficiency by upconversion: Optical and electrical characterization. *Journal of Applied Physics*, 108(4):044912–11, 2010.

[104] Guo-Bin Shan and George P. Demopoulos. Near-Infrared Sunlight Harvesting in Dye-Sensitized Solar Cells Via the Insertion of an Upconverter-TiO2 Nanocomposite Layer. *Advanced Materials*, 22(39):4373–4377, 2010.

[105] M. Mojiri-Foroushani, H. Dehghani, and N. Salehi-Vanani. Enhancement of dye-sensitized solar cells performances by improving electron density in conduction band of nanostructure TiO_2 electrode with using a metalloporphyrin as additional dye. *Electrochimica Acta*, 92(0):315–322, 2013.

[106] Neeraj Kumar Giri, Concepcion P. Ponce, Ronald P. Steer, and Matthew F. Paige. Homomolecular Non-Coherent Photon Upconversion by Triplet-Triplet Annihilation Using a Zinc Porphyrin on Wide Bandgap Semiconductors. *Chemical Physics Letters*, 2014. DOI: 10.1016/j.cplett.2014.02.057.

[107] Rony S. Khnayzer, Jorg Blumhoff, Jordan A. Harrington, Alexandre Haefele, Fan Deng, and Felix N. Castellano. Upconversion-powered photoelectrochemistry. *Chemical Communications*, 48(2):209–211, 2012.

[108] Weiping Qin, Daisheng Zhang, Dan Zhao, Lili Wang, and Kezhi Zheng. Near-infrared photocatalysis based on YF3 : Yb^{3+},Tm^{3+}/TiO2 core/shell nanoparticles. *Chemical Communications*, 46(13):2304–2306, 2010.

[109] Zhijie Zhang, Wenzhong Wang, Wenzong Yin, Meng Shang, Lu Wang, and Songmei Sun. Inducing photocatalysis by visible light beyond the absorption edge: Effect of upconversion agent on the photocatalytic activity of Bi2WO6. *Applied Catalysis B: Environmental*, 101(12):68–73, 2010.

[110] Tzenka Miteva, Vladimir Yakutkin, Gabriele Nelles, and Stanislav Baluschev. Annihilation assisted upconversion: all-organic, flexible and transparent multicolour display. *New Journal of Physics*, 10(10):103002, 2008.

[111] Feng Wang, Yu Han, Chin Seong Lim, Yunhao Lu, Juan Wang, Jun Xu, Hongyu Chen, Chun Zhang, Minghui Hong, and Xiaogang Liu. Simultaneous phase and size control of upconversion nanocrystals through lanthanide doping. *Nature*, 463(7284):1061–1065, 2010.

[112] Qian Liu, Tianshe Yang, Wei Feng, and Fuyou Li. Blue-Emissive Upconversion Nanoparticles for Low-Power-Excited Bioimaging in Vivo. *Journal of the American Chemical Society*, 134(11):5390–5397, 2012.

[113] Nicholas Kotov. Bioimaging: The only way is up. *Nature Materials*, 10(12):903–904, 2011.

[114] Dev K Chatterjee and Zhang Yong. Upconverting nanoparticles as nanotransducers for photodynamic therapy in cancer cells. *Nanomedicine (New York, NY, United States)*, 3(1):73–82, 2008.

[115] Sunish K. Sugunan, Matthew F. Paige, and Ronald P. Steer. Determination of oxygen permeabilities in thin polymer films using quenching of upconverted fluorescence in porphyrins. *Canadian Journal of Chemistry*, 89(2):195–202, 2011.

[116] Caishun Zhang, Jianzhang Zhao, Shuo Wu, Zilong Wang, Wanhua Wu, Jie Ma, Song Guo, and Ling Huang. Intramolecular RET Enhanced Visible Light-Absorbing Bodipy Organic Triplet Photosensitizers and Application in Photooxidation and Triplet-Triplet Annihilation Upconversion. *Journal of the American Chemical Society*, 135(28):10566–10578, 2013.

[117] Radiy R. Islangulov and Felix N. Castellano. Photochemical Upconversion: Anthracene Dimerization Sensitized to Visible Light by a Ru(II) Chromophore. *Angewandte Chemie International Edition*, 45(36):5957–5959, 2006.

[118] Shaomin Ji, Wanhua Wu, Wenting Wu, Huimin Guo, and Jianzhang Zhao. Ruthenium(II) Polyimine Complexes with a Long-Lived ^{3}IL Excited State or a ^{3}MLCT/^{3}IL Equilibrium: Efficient Triplet Sensitizers for Low-Power Upconversion. *Angewandte Chemie International Edition*, 50(7):1626–1629, 2011.

[119] Shaomin Ji, Huimin Guo, Wenting Wu, Wanhua Wu, and Jianzhang Zhao. Ruthenium(II) Polyimine-Coumarin Dyad with Non-emissive ^{3}IL Excited State as Sensitizer for Triplet-Triplet Annihilation Based Upconversion. *Angewandte Chemie International Edition*, 50(36):8283–8286, 2011.

[120] Giacomo Bergamini, Paola Ceroni, Pierangelo Fabbrizi, and Stefano Cicchi. A multichromophoric dendrimer: from synthesis to energy up-conversion in a rigid matrix. *Chemical Communications*, 47(48):12780–12782, 2011.

[121] Wei Zhao and Felix N. Castellano. Upconverted Emission from Pyrene and Di-tert-butylpyrene Using Ir(ppy)3 as Triplet Sensitizer. *The Journal of Physical Chemistry A*, 110(40):11440–11445, 2006.

[122] Jifu Sun, Wanhua Wu, Huimin Guo, and Jianzhang Zhao. Visible-Light Harvesting with Cyclometalated Iridium(III) Complexes Having Long-Lived ^{3}IL Excited States and Their Application in TripletTriplet-Annihilation Based Upconversion. *European Journal of Inorganic Chemistry*, 2011(21):3165–3173, 2011.

[123] Xiuyu Yi, Jianzhang Zhao, Wanhua Wu, Dandan Huang, Shaomin Ji, and Jifu Sun. Rhenium(i) tricarbonyl polypyridine complexes showing strong absorption of visible light and long-lived triplet excited states as a triplet photosensitizer for triplet-triplet annihilation upconversion. *Dalton Transactions*, 41(29):8931–8940, 2012.

[124] Angelo Monguzzi, F. Riva, R. Tubino, and F. Meinardi. White light generation by sensitized photon up-conversion. *Chemical Physics Letters*, 521(0):17–19, 2012.

[125] Tomoyasu Mani and Sergei A. Vinogradov. Magnetic Field Effects on Triplet-Triplet Annihilation in Solutions: Modulation of Visible/NIR Luminescence. *The Journal of Physical Chemistry Letters*, pages 2799–2804, 2013.

[126] Yoichi Murakami. Photochemical photon upconverters with ionic liquids. *Chemical Physics Letters*, 516(1-3):56–61, 2011.

[127] S. Baluschev, V. Yakutkin, G. Wegner, T. Miteva, G. Nelles, A. Yasuda, S. Chernov, S. Aleshchenkov, and A. Cheprakov. Upconversion with ultrabroad excitation band: Simultaneous use of two sensitizers. *Applied Physics Letters*, 90(18):181103–3, 2007.

[128] S. Baluschev, V. Yakutkin, T. Miteva, G. Wegner, T. Roberts, G. Nelles, A. Yasuda, S. Chernov, S. Aleshchenkov, and A. Cheprakov. A general approach for non-coherently excited annihilation up-conversion: transforming the solar-spectrum. *New Journal of Physics*, 10(1):013007, 2008.

[129] Paul B. Merkel and Joseph P. Dinnocenzo. Low-power green-to-blue and blue-to-UV upconversion in rigid polymer films. *Journal of Luminescence*, 129(3):303–306, 2009.

[130] Stanislav Baluschev, Fang Yu, Tzenka Miteva, Stefanie Ahl, Akio Yasuda, Gabriele Nelles, Wolfgang Knoll, and Gerhard Wegner. Metal-Enhanced Up-Conversion Fluorescence: Effective Triplet-Triplet Annihilation near Silver Surface. *Nano Letters*, 5(12):2482–2484, 2005.

[131] Karl Borjesson, Damir Dzebo, Bo Albinsson, and Kasper Moth-Poulsen. Photon upconversion facilitated molecular solar energy storage. *Journal of Materials Chemistry A*, 1(30):8521–8524, 2013.

[132] J. Mezyk, R. Tubino, A. Monguzzi, A. Mech, and F. Meinardi. Effect of an External Magnetic Field on the Up-Conversion Photoluminescence of Organic Films: The Role of Disorder in Triplet-Triplet Annihilation. *Physical Review Letters*, 102(8):087404, 2009.

[133] P. E. Keivanidis, S. Baluschev, G. Lieser, and G. Wegner. Inherent Photon Energy Recycling Effects in the Up-Converted Delayed Luminescence Dynamics of Poly(fluorene)-Pt(II)octaethyl Porphyrin Blends. *ChemPhysChem*, 10(13):2316–2326, 2009.

[134] A. Monguzzi, R. Tubino, and F. Meinardi. Upconversion-induced delayed fluorescence in multicomponent organic systems: Role of Dexter energy transfer. *Physical Review B*, 77(15):155122, 2008.

[135] Kianoosh Poorkazem, Amelia V. Hesketh, and Timothy L. Kelly. Plasmon-Enhanced TripletTriplet Annihilation Using Silver Nanoplates. *The Journal of Physical Chemistry C*, 2014. DOI: 10.1021/jp412223m.

[136] Wanhua Wu, Jifu Sun, Shaomin Ji, Wenting Wu, Jianzhang Zhao, and Huimin Guo. Tuning the emissive triplet excited states of platinum(ii) Schiff base complexes with pyrene, and application for luminescent oxygen sensing and triplet-triplet-annihilation based upconversions. *Dalton Transactions*, 40(43):11550–11561, 2011.

[137] Wenting Wu, Wanhua Wu, Shaomin Ji, Huimin Guo, and Jianzhang Zhao. Accessing the long-lived emissive ^{3}IL triplet excited states of coumarin fluorophores by direct cyclometallation and its application for oxygen sensing and upconversion. *Dalton Transactions*, 40(22):5953–5963, 2011.

[138] Wanhua Wu, Shaomin Ji, Wenting Wu, Jingyin Shao, Huimin Guo, Tony D. James, and Jianzhang Zhao. Ruthenium(II)-Polyimine-Coumarin Light-Harvesting Molecular Arrays: Design Rationale and Application for TripletTriplet-Annihilation-Based Upconversion. *Chemistry A European Journal*, 18(16):4953–4964, 2012.

[139] Jill Kunzelman, Brent R. Crenshaw, and Christoph Weder. Self-assembly of chromogenic dyes-a new mechanism for humidity sensors. *Journal of Materials Chemistry*, 17(29):2989–2991, 2007.

[140] Andrew J. Tilley, Min Jeong Kim, Ming Chen, and Kenneth P. Ghiggino. Photoinduced energy transfer in ruthenium-centred polymers prepared by a RAFT approach. *Polymer*, 54(12):2865–2872, 2013.

[141] Dorota Kowalska and Ronald P. Steer. Quenching of MgTPP and ZnTPP fluorescence by molecular oxygen. *Journal of Photochemistry and Photobiology A: Chemistry*, 195(2-3):223–227, 2008.

[142] Manisankar Maiti, Brook R. Danger, and Ronald P. Steer. Photophysics of Soret-Excited Tetrapyrroles in Solution. IV. Radiationless Decay and Triplet-Triplet Annihilation Investigated Using Tetraphenylporphinato Sn(IV). *The Journal of Physical Chemistry A*, 113(42):11318–11326, 2009.

[143] Sunish K. Sugunan, Benjamin Robotham, Ryan P. Sloan, Jedrzej Szmytkowski, Kenneth P. Ghiggino, Matthew F. Paige, and Ronald P. Steer. Photophysics of Untethered ZnTPP-Fullerene Complexes in Solution. *The Journal of Physical Chemistry A*, 115(44):12217–12227, 2011.

[144] Jaclyn A. O'Brien, Yin Lu, Emma N. Hooley, Kenneth P. Ghiggino, Ronald P. Steer, and Matthew F. Paige. Aggregation of zinc tetraphenylporphyrin characterized by ensemble and single-molecule fluorescence spectroscopy. *Canadian Journal of Chemistry*, 89(2):122–129, 2011.

[145] Emilia G. Azenha, Arménio C. Serra, Marta Pineiro, Mariette M. Pereira, J. Seixas de Melo, Luis G. Arnaut, Sebastião J. Formosinho, and A. M. d'A Rocha Gonsalves. Heavy-atom effects on metalloporphyrins and polyhalogenated porphyrins. *Chemical Physics*, 280(112):177–190, 2002.

[146] Inoue H. Takagi, S.S. *Molecular and Supramolecular Photochemistry of Porphyrins and Metalloporphyrins*. Marcel Dekker, Inc., New York, 2000.

[147] Jerzy Karolczak, Dorota Kowalska, Adam Lukaszewicz, Andrzej Maciejewski, and Ronald P. Steer. Photophysical Studies of Porphyrins and Metalloporphyrins: Accurate Measurements of Fluorescence Spectra and Fluorescence Quantum Yields for Soret Band Excitation of Zinc Tetraphenylporphyrin. *The Journal of Physical Chemistry A*, 108(21):4570–4575, 2004.

[148] Adam Lukaszewicz, Jerzy Karolczak, Dorota Kowalska, Andrzej Maciejewski, Marcin Ziolek, and Ronald P. Steer. Photophysical processes in electronic states of zinc tetraphenyl porphyrin accessed on one- and two-photon excitation in the soret region. *Chemical Physics*, 331(2-3):359–372, 2007.

[149] Umakanta Tripathy, Dorota Kowalska, Xia Liu, Suresh Velate, and Ronald P. Steer. Photophysics of Soret-Excited Tetrapyrroles in Solution. I. Metalloporphyrins: MgTPP, ZnTPP, and CdTPP. *The Journal of Physical Chemistry A*, 112(26):5824–5833, 2008.

[150] Xia Liu, Umakanta Tripathy, Sheshanath V. Bhosale, Steven J. Langford, and Ronald P. Steer. Photophysics of Soret-Excited Tetrapyrroles in Solution. II. Effects of Perdeuteration, Substituent Nature and Position, and Macrocycle Structure and Conformation in Zinc(II) Porphyrins. *The Journal of Physical Chemistry A*, 112(38):8986–8998, 2008.

[151] Derrick A. Roberts, Burkhard Fückel, Raphaël G. C. R. Clady, Yuen Yap Cheng, Maxwell J. Crossley, and Timothy W. Schmidt. Synthesis and Ultrafast Excited-State Dynamics of Zinc and Palladium Triply Fused Diporphyrins. *The Journal of Physical Chemistry A*, 116(30):7898–7905, 2012.

[152] Andrew M. Crouch and Cooper H. Langford. Photophysical behaviour of zinc tetraphenylporphyrins in solutions and polymer films. *Journal of Photochemistry and Photobiology A: Chemistry*, 52(1):55–64, 1990.

[153] Kuppuswamy Kalyanasundaram. Photochemistry and sensitized evolution of hydrogen from water using water-soluble cationic porphyrins.

Tetrakis(trimethylaminophenyl)porphyrinatozinc and its free base. *Journal of the Chemical Society, Faraday Transactions 2: Molecular and Chemical Physics*, 79(9):1365–1374, 1983.

[154] Anthony Harriman. Luminescence of porphyrins and metalloporphyrins. Part 1.-Zinc(II), nickel(II) and manganese(II) porphyrins. *Journal of the Chemical Society, Faraday Transactions 1: Physical Chemistry in Condensed Phases*, 76(0):1978–1985, 1980.

[155] Anthony Harriman, George Porter, and Aleksandra Wilowska. Photoreduction of benzo-1,4-quinone sensitised by metalloporphyrins. *Journal of the Chemical Society, Faraday Transactions 2: Molecular and Chemical Physics*, 79(6):807–816, 1983.

[156] J. Spadavecchia, R. Rella, P. Siciliano, M. G. Manera, A. Alimelli, R. Paolesse, C. Di Natale, and A. DAmico. Optochemical vapour detection using spin coated thin film of ZnTPP. *Sensors and Actuators B: Chemical*, 115(1):12–16, 2006.

[157] Deidre M. Cleland, Keith C. Gordon, David L. Officer, Pawel Wagner, and Penny J. Walsh. Tuning the optical properties of ZnTPP using carbonyl ring fusion. *Spectrochimica Acta Part A: Molecular and Biomolecular Spectroscopy*, 74(4):931–935, 2009.

[158] S. M. Khan, M. Kaur, J. R. Heflin, and M. H. Sayyad. Fabrication and characterization of ZnTPP:PCBM bulk heterojunction (BHJ) solar cells. *Journal of Physics and Chemistry of Solids*, 72(12):1430–1435, 2011.

[159] Wenqi Zheng, Ning Shan, Lianxiang Yu, and Xingqiao Wang. UVvisible, fluorescence and EPR properties of porphyrins and metalloporphyrins. *Dyes and Pigments*, 77(1):153–157, 2008.

[160] Yutaka Harima, Kazuhiko Takeda, and Kazuo Yamashita. Molecular solid of zinc tetraphenylporphyrin as a model organic semiconductor with a well-defined depletion layer. *Journal of Physics and Chemistry of Solids*, 56(9):1223–1229, 1995.

[161] Tom J. Savenije and Albert Goossens. Hole transport in porphyrin thin films. *Physical Review B*, 64(11):115323, 2001.

[162] Jonathan Rochford and Elena Galoppini. Zinc(II) Tetraarylporphyrins Anchored to TiO2, ZnO, and ZrO2 Nanoparticle Films through Rigid-Rod Linkers. *Langmuir*, 24(10):5366–5374, 2008.

[163] K. Kalyanasundaram, N. Vlachopoulos, V. Krishnan, A. Monnier, and M. Grätzel. Sensitization of titanium dioxide in the visible light region using zinc porphyrins. *The Journal of Physical Chemistry*, 91(9):2342–2347, 1987.

[164] Suman Cherian and Carl C. Wamser. Adsorption and Photoactivity of Tetra(4-carboxyphenyl)porphyrin (TCPP) on Nanoparticulate TiO_2. *The Journal of Physical Chemistry B*, 104(15):3624–3629, 2000.

[165] Javier Roales, Jose M. Pedrosa, Manuel Cano, Maria G. Guillen, Tania Lopes-Costa, Pedro Castillero, Angel Barranco, and Agustin R. Gonzalez-Elipe. Anchoring effect on (tetra)carboxyphenyl porphyrin/TiO2 composite films for VOC optical detection. *RSC Advances*, 4(4):1974–1981, 2014.

[166] Jonathan Rochford, Dorothy Chu, Anders Hagfeldt, and Elena Galoppini. Tetrachelate Porphyrin Chromophores for Metal Oxide Semiconductor Sensitization: Effect of the Spacer Length and Anchoring Group Position. *Journal of the American Chemical Society*, 129(15):4655–4665, 2007.

[167] Christian Bruckner, Paul C. D. Foss, James O. Sullivan, Ryan Pelto, Matthias Zeller, Robert R. Birge, and Guy Crundwell. Origin of the bathochromically shifted optical spectra of meso-tetrathien-2[prime or minute]- and 3[prime or minute]-ylporphyrins as compared to meso-tetraphenylporphyrin. *Physical Chemistry Chemical Physics*, 8(20):2402–2412, 2006.

[168] Jyoti Seth, Vaithianathan Palaniappan, Thomas E. Johnson, Sreedharan Prathapan, Jonathan S. Lindsey, and David F. Bocian. Investigation of Electronic Communication in Multi-Porphyrin Light-Harvesting Arrays. *Journal of the American Chemical Society*, 116(23):10578–10592, 1994.

[169] Ernst S. Schmidt, Thomas S. Calderwood, and Thomas C. Bruice. Synthesis and characterization of a meso-tetrakis(4-ferrocenylphenyl)porphyrin and examination of its ability to undergo intramolecular photocatalyzed electron transfer. *Inorganic Chemistry*, 25(20):3718–3720, 1986.

[170] Gerrit K. Boschloo and Albert Goossens. Electron Trapping in Porphyrin-Sensitized Porous Nanocrystalline TiO2 Electrodes. *The Journal of Physical Chemistry*, 100(50):19489–19494, 1996.

[171] Galateia E. Zervaki, Mahesh S. Roy, Manas K. Panda, Panagiotis A. Angaridis, Emmanouel Chrissos, Ganesh D. Sharma, and Athanassios G. Coutsolelos. Efficient Sensitization of Dye-Sensitized Solar Cells by Novel Triazine-Bridged Porphyrin-Porphyrin Dyads. *Inorganic Chemistry*, 52(17):9813–9825, 2013.

[172] Reza Dabestani, Allen J. Bard, Alan Campion, Marye Anne Fox, Thomas E. Mallouk, Stephen E. Webber, and J. M. White. Sensitization of titanium dioxide and strontium titanate electrodes by ruthenium(II) tris(2,2'-bipyridine-4,4'-dicarboxylic acid) and zinc tetrakis(4-carboxyphenyl)porphyrin: an evaluation of sensitization efficiency for component photoelectrodes in a multipanel device. *The Journal of Physical Chemistry*, 92(7):1872–1878, 1988.

[173] Yasuhiro Tachibana, Saif A. Haque, Ian P. Mercer, James R. Durrant, and David R. Klug. Electron Injection and Recombination in Dye Sensitized Nanocrystalline Titanium Dioxide Films: A Comparison of Ruthenium Bipyridyl and Porphyrin Sensitizer Dyes. *The Journal of Physical Chemistry B*, 104(6):1198–1205, 2000.

[174] Wayne M. Campbell, Anthony K. Burrell, David L. Officer, and Kenneth W. Jolley. Porphyrins as light harvesters in the dye-sensitised TiO2 solar cell. *Coordination Chemistry Reviews*, 248(13-14):1363–1379, 2004.

[175] Brook R Danger, Krysta Bedient, Manisankar Maiti, Ian J Burgess, and Ronald P Steer. Photophysics of Self-Assembled Zinc Porphyrin- Bidentate Diamine Ligand Complexes. *The Journal of Physical Chemistry A*, 114(41):10960–10968, 2010.

[176] Jedrzej Szmytkowski, Toby Bond, Matthew F. Paige, Robert W. J. Scott, and Ronald P. Steer. Spectroscopic and Photophysical Properties of ZnTPP in a Room Temperature Ionic Liquid. *The Journal of Physical Chemistry A*, 114(43):11471–11476, 2010.

[177] Ana Morandeira, Laurine Engeli, and Eric Vauthey. Ultrafast Charge Recombination of Photogenerated Ion Pairs to an Electronic Excited State. *The Journal of Physical Chemistry A*, 106(19):4833–4837, 2002.

[178] Ravikanth M. Gupta, I. Fluorescence Properties of Meso-tetrafurylporphyrins. *J. Chem. Sci.*, 117(2):161–116, 2005.

[179] Md Wahadoszamen, Takakazu Nakabayashi, Soonchul Kang, Hiroshi Imahori, and Nobuhiro Ohta. External Electric Field Effects on Absorption and Fluorescence Spectra of a Fullerene Derivative and Its Mixture with Zinc-Tetraphenylporphyrin Doped in a PMMA Film. *The Journal of Physical Chemistry B*, 110(41):20354–20361, 2006.

[180] Maxim P. Nikiforov, Barry Lai, Wei Chen, Si Chen, Richard D. Schaller, Joseph Strzalka, Jorg Maser, and Seth B. Darling. Detection and role of trace impurities in high-performance organic solar cells. *Energy & Environmental Science*, 6(5):1513–1520, 2013.

[181] W. J. Belcher, K. I. Wagner, and P. C. Dastoor. The effect of porphyrin inclusion on the spectral response of ternary P3HT:porphyrin:PCBM bulk heterojunction solar cells. *Solar Energy Materials and Solar Cells*, 91(6):447–452, 2007.

[182] David W. Thompson, Akitake. Ito, and Thomas J. Meyer. $[Ru(bpy)_3]^{2+*}$ and other interesting metal-to-ligand charge transfer (MLCT) excited states. *Pure and Applied Chemistry*, 85(7):1257–1305, 2013.

[183] C. R. Bock, T. J. Meyer, and D. G. Whitten. Electron transfer quenching of the luminescent excited state of tris(2,2'-bipyridine)ruthenium(II). Flash photolysis relaxation technique for measuring the rates of very rapid electron transfer reactions. *Journal of the American Chemical Society*, 96(14):4710–4712, 1974.

[184] Janet N. Younathan, Stephen F. McClanahan, and Thomas J. Meyer. Synthesis and characterization of soluble polymers containing electron- and energy-transfer reagents. *Macromolecules*, 22(3):1048–1054, 1989.

[185] Laura A. Worl, Geoffrey F. Strouse, Janet N. Younathan, Steven M. Baxter, and Thomas J. Meyer. Production and storage of multiple, photochemical redox equivalents on a soluble polymer. *Journal of the American Chemical Society*, 112(21):7571–7578, 1990.

[186] Janet N. Younathan, Wayne E. Jones, and Thomas J. Meyer. Energy- and electron-transfer shuttling by a soluble, bifunctional redox polymer. *The Journal of Physical Chemistry*, 95(1):488–492, 1991.

[187] Steven M. Baxter, Wayne E. Jones Jr, Earl Danielson, Laura Worl, Geoffrey Strouse, Janet Younathan, and Thomas J. Meyer. Photoinduced electron and energy transfer in soluble polymers. *Coordination Chemistry Reviews*, 111(0):47–71, 1991.

[188] Laura A. Worl, Wayne E. Jones, Geoffrey F. Strouse, Janet N. Younathan, Earl Danielson, Kimberly A. Maxwell, Milan Sykora, and Thomas J. Meyer. Multiphoton, Multielectron Transfer Photochemistry in a Soluble Polymer. *Inorganic Chemistry*, 38(11):2705–2708, 1999.

[189] Cavan N. Fleming, Laurence M. Dupray, John M. Papanikolas, and Thomas J. Meyer. Energy Transfer between Ru(II) and Os(II) Polypyridyl Complexes Linked to Polystyrene. *The Journal of Physical Chemistry A*, 106(10):2328–2334, 2002.

[190] Gerard J. Wilson, Anton Launikonis, Wolfgang H. F. Sasse, and Albert W. H. Mau. Excited-State Processes in Ruthenium(II) Bipyridine Complexes Containing Covalently Bound Arenes. *The Journal of Physical Chemistry A*, 101(27):4860–4866, 1997.

[191] Andrea Cannizzo, Frank van Mourik, Wojciech Gawelda, Goran Zgrablic, Christian Bressler, and Majed Chergui. Broadband Femtosecond Fluorescence Spectroscopy of $[Ru(bpy)_3]^{2+}$. *Angewandte Chemie International Edition*, 45(19):3174–3176, 2006.

[192] Hitoshi Ishida, Seiji Tobita, Yasuchika Hasegawa, Ryuzi Katoh, and Koichi Nozaki. Recent advances in instrumentation for absolute emission quantum yield measurements. *Coordination Chemistry Reviews*, 254(2122):2449–2458, 2010.

[193] Ming Chen, Kenneth P. Ghiggino, San H. Thang, and Gerard J. Wilson. Star-Shaped Light-Harvesting Polymers Incorporating an Energy Cascade. *Angewandte Chemie International Edition*, 44(28):4368–4372, 2005.

[194] Andres F. Olea and J. K. Thomas. Rate constants for reactions in viscous media: correlation between the viscosity of the solvent and the rate constant of the diffusion-controlled reactions. *Journal of the American Chemical Society*, 110(14):4494–4502, 1988.

[195] C. A. Parker and W. T. Rees. Correction of fluorescence spectra and measurement of fluorescence quantum efficiency. *Analyst*, 85(1013):587–600, 1960.

[196] R. Reisfeld, R. Zusman, Y. Cohen, and M. Eyal. The spectroscopic behaviour of rhodamine 6G in polar and non-polar solvents and in thin glass and PMMA films. *Chemical Physics Letters*, 147(2-3):142–147, 1988.

[197] Laurence Perreux, André Loupy, and François Volatron. Solvent-free preparation of amides from acids and primary amines under microwave irradiation. *Tetrahedron*, 58(11):2155–2162, 2002.

[198] Adam A. Colbourne, Gareth A. Morris, and Mathias Nilsson. Local Covariance Order Diffusion-Ordered Spectroscopy: A Powerful Tool for Mixture Analysis. *Journal of the American Chemical Society*, 133(20):7640–7643, 2011.

[199] G. A. Demas, J. N. Crosby. The Measurement of Photoluminescence Quantum Yields. A Review. *The Journal of Physical Chemistry*, 75(8):991–1023, 1971.

[200] Alun T. Rhys Williams, Stephen A. Winfield, and James N. Miller. Relative fluorescence quantum yields using a computer-controlled luminescence spectrometer. *Analyst*, 108(1290):1067–1071, 1983.

[201] Xian-yong Wang, Andre Del Guerzo, and Russell H. Schmehl. Photophysical behavior of transition metal complexes having interacting ligand localized and metal-to-ligand charge transfer states. *Journal of Photochemistry and Photobiology C: Photochemistry Reviews*, 5(1):55–77, 2004.

[202] G. S. S. Saini, Sarvpreet Kaur, S. K. Tripathi, C. G. Mahajan, H. H. Thanga, and A. L. Verma. Spectroscopic studies of rhodamine 6G dispersed in polymethylcyanoacrylate. *Spectrochimica Acta Part A: Molecular and Biomolecular Spectroscopy*, 61(4):653–658, 2005.